Investigating the icy crust and craters of Enceladus

Master Thesis

T.C. Kroes

Technische Universiteit Delft

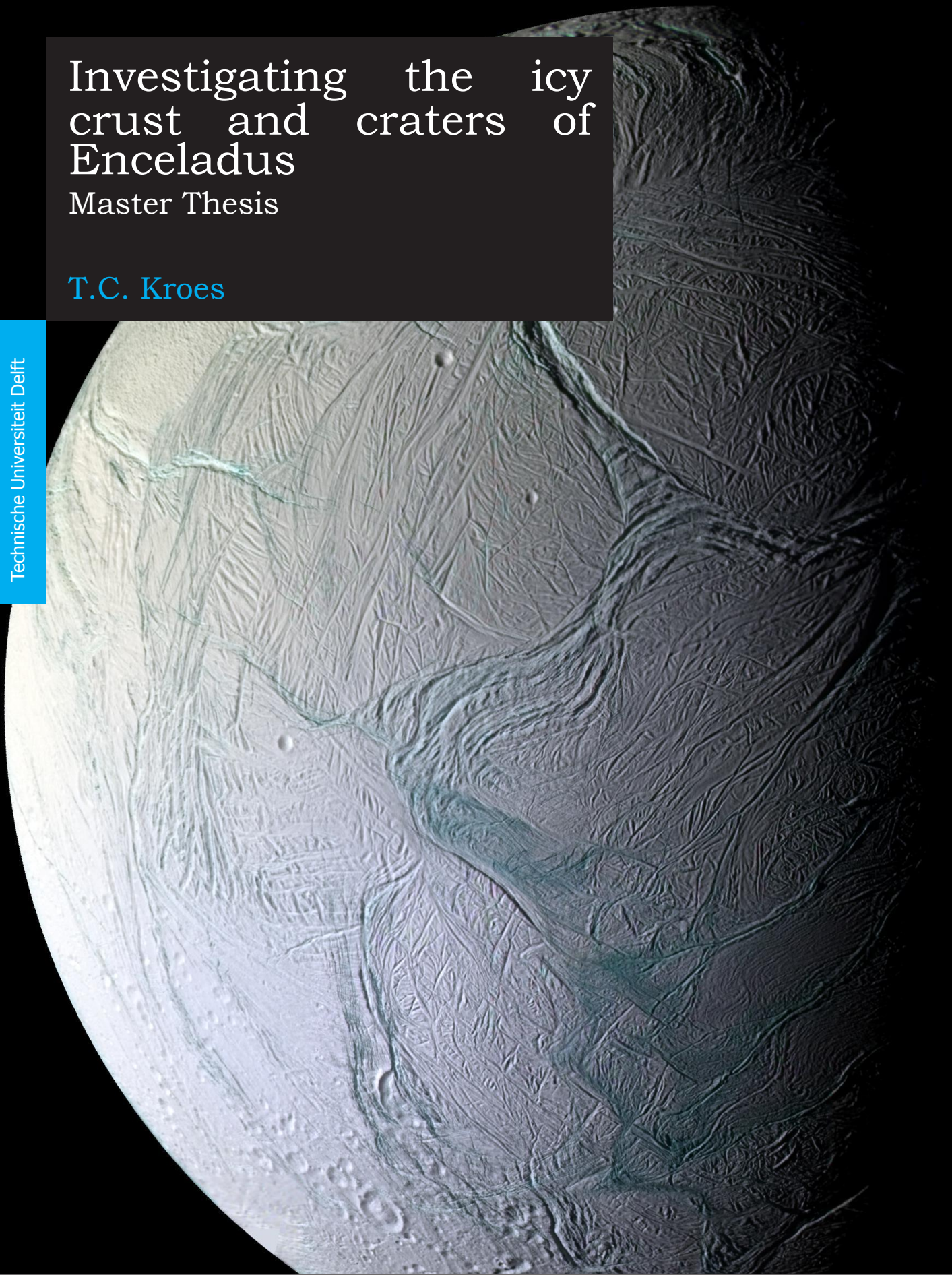

TU Delft Delft University of Technology

Challenge the future

Investigating the icy crust and craters of Enceladus

Master Thesis

by

T.C. Kroes

in partial fulfillment of the requirements for the degree of

Master of Science
in Aerospace Engineering

at the Delft University of Technology,

Supervisor:	dr. S. Cazaux	
Thesis committee:	Prof. dr. B. Vermeersen,	TU Delft
	Dr. A. Menicucci,	TU Delft
	Prof. Dr. B. Brandl,	Leiden University

An electronic version of this thesis is available at http://repository.tudelft.nl/.

TU Delft Delft University of Technology

Acknowledgements

This report represents nearly a full year's worth of research. During this time I've had help from a number of people who have helped me complete this work. First of these is my daily supervisor, dr. Stéphanie Cazaux. Our weekly meetings have been a great help in staying on track, and her suggestion that maybe I should have taken a bit more time off during the summer holidays was, unfortunately in hindsight, an excellent one. I'll try to keep the importance of pacing myself in mind for my future career.

I'd also like to thank everyone else in my assessment committee, and in particular professor Bernhard Brandl, whose advice has been very helpful in getting me to re-asses and vet my methods. I'd also like to thank everyone that has worked on maintaining the Leiden database for ice, which has been an invaluable resource during this study.

Outside of the university, I'd like to thank Stuart Sides at the US Geological Survey centre, who spend a lot of time figuring out an error in the ISIS software that was hampering my ability to process the VIMS cubes. Lastly, I'd like to thank everyone that has taken an interest in my project, from friends and family to random people on the internet that I happened to end up talking with about my study.

Summary

The Cassini-Huygens mission was send to Saturn to perform a wide variety of measurements and experiments in the Saturnian system. Among the mission's goals was the exploration of Saturn's many moons. The Huygens lander was intended to land on Titan, one of Saturn's larger moon's, while the Cassini orbiter itself was equipped with a large variety of instruments including high resolution cameras and spectrometers to record and characterize the surfaces of the moons of Saturn. During this research, images from Cassini's Visual and Infrared Mapping Spectrometer (VIMS) will be the main source of information, which will occasionally be supplemented by images from the Imaging Science Subsystem for additional context.

Enceladus is a small moon orbiting Saturn. Though the moon has been known to exist since the late 18th century, little more than the mass, density and the Albedo was known before the voyager mission's visited the moon. Images from Voyager 1 and 2 revealed that Enceladus had a mixture of old and young terrain, suggesting the moon was geologically active. It wasn't until the first fly-by of the Cassini orbiter that further details of the moon were revealed. This flyby revealed the presence of plumes of water emitting from the moon's south-pole. More flybys have followed this initial observation, and a number of things have since been established about Enceladus, including the presence of a sub-surface ocean across the entire moon. Most research has been focused on Enceladus' south pole and plumes, so the research presented here will aim to create a greater understanding of the rest of Enceladus surface by processing infrared spectra to find non-water ice species and assess the properties of the water ice.

The research is conducted by processing and analyzing infrared spectra from the VIMS instrument. These spectra cover the wavelength range from 0.8 to 5 micron. Of note is that the amount of noise present in the spectra gradually becomes worse with the longer wavelengths. In particular, the section from approximately 3.8 to 5 micron tends to show a lot of noise effects, making analyzing that section of the spectrum a challenge. Initial visual inspection of these spectra suggested the presence of NH_3, CO_2 and CO, so these elements will be the focus for the search for non-water ice species. To find the non-water ice species polynomials will be used to fit the continuum in the areas where features for these species occur. If a feature is present, it will show a clear deviation from the fitted continuum, allowing for a detection.

This study will also look at the degree of crystallinity and crystal size of the water ice. To estimate the crystallinity, the crystallinity dependent 1.65 micron feature's size will be compared with that of the adjacent 1.5 micron water ice feature, which does not change with crystallinity. To make an estimate of crystal size, the instrument values for the post-2 micron water ice feature peak and the 3.5 micron feature will be compared. A relation between these values and the crystal size has been established using based on previous simulations.

Features of all three non-water species have been found using the previously described method, though the detections of CO are uncertain because of the high noise present at 4.68 micron, which is where the CO feature occurs. CO_2 has the most wide-spread detections, matching previous work done on this non-water ice species, though the method in this study provided fewer positive detections than previous work. Finally, some traces of ammonia have been found as well within the trailing hemisphere. Long-range observations using earth-based IR telescopes had led to some speculations about the presence of ammonia on Enceladus, but previous research on VIMS data of the south-polar area had found no traces of the element.

The measurements of crystal sizes mostly match that of earlier studies, with higher crystal sizes detected on the new south-polar terrain, and lower crystal sizes on the older north-polar terrain. The measurements of crystallinity show similar trends, with a rather amorphous south pole due to the constant accretion of new material consisting of flash-frozen particles from the plumes, while other areas have varying degrees of crystallinity. However, in both the measurements for crystal size and crystallinity there are some trends that stand out.

On the crystal size measurements a sizeable region around the equator and 330^o W shows a higher crystal size than the surrounding terrain, suggesting that this section is either newer than expected, is

exposed to less energetic particles than the rest of the surface, or is at a higher temperature than most of the rest of Enceladus. As the crust of Enceladus is expected to be thickest around the equator, the temperature hypothesis can likely be dismissed, leaving the possibility of this zone either being very new, or some quirk of the radiation environment resulting in the area seeing fewer impacts than other zone on Enceladus.

Within the measurements of the crystallinity, craters have been found to stand out from their surroundings in several locations, but in particular in a section from 240^{o}W to 210^{o}W. In this section the craters show a clearly more amorphous floor and more crystalline rim. This is in line with what one would expect from the crater formation process, as the impact instantly vaporizes the ice at the impact size, which will then be flash-frozen shortly afterwards to create amorphous ice. meanwhile, the rim material that is not vaporized will still be heated to some degree, allowing the ice to become more crystalline.

Combining the various measurements reveal a number of further trends. CO_2 tends to be located at or near areas with lower crystallinity and crystal size for the most part, which would suggest hat the presence of CO_2 is linked to plume deposits. However, one of the largest continuous areas of CO_2 detected covers a significant section of the central high-crystal size section. This could be a further clue to the process behind the unusual crystal size in that area, but it is a break from the trend that the CO_2 detections seem to follow in other areas.

This study has brought up several areas of interest for future studies on Enceladus, most notable of which is a potentially young section of terrain at 330^o W. In addition, the way craters appeared to be clearly distinguished when mapping the crystallinity could provide a way for detecting craters other than trying to discern them on visual images.

Contents

List of Figures

List of Tables

List of terms

Several terms related to infrared spectroscopy will be mentioned repeatedly. This section will give a short definition of each for ease of reference.

Absorbance: Absorbance refers to the amount of light absorbed by a sample. A spectral measurement in absorbance will generally show its features as peaks, representing the spectral ranges where light gets absorbed.

Transmittance: Transmittance refers to a technique where light is passed through a sample, and then compared with light that was not. A spectral measurement in transmittance will generally show its features as depressions, representing the areas where light does not pass through the sample because it is either reflected or absorbed.

Rreflectance: A spectral measurement in reflectance evaluates light that has been reflected off a surface. As with transmittance, spectral features in a measurement done with reflection are represented as depressions. The depressions represent spectral ranges where light gets either absorbed or passes through the sample.

1

Introduction

Saturn's moon of Enceladus rocketed to the forefront of scientific interest after the Cassini mission discovered jets of water emerging from its south pole. Since this discovery the Cassini mission has made many more observations of the icy moon and a rather complete set of information of the moon has been created. Now, it is up to researchers to turn this information into knowledge. This research will make use of data from the VIMS infrared spectrometer to obtain a more complete image of Enceladus' surface.

Most research of Enceladus has been focused on the south-polar terrain and the plumes emanating from it. This has led to a wealth of knowledge with regards to Enceladus' internal ocean and south-polar terrain, but it means that far less is known about the rest of the moon. Some work has been performed with regards to particle size and geologic features across Enceladus, as well as a study focused on the non-water ice species in the south-polar terrain and surrounding regions. That particular study found traces of CO and CO_2, though no traces of NH_3, which had been theorized to be present based on measurements from earth-based infrared telescopes. There has also been a recent study mapping the presence of CO_2 across the entire surface of Enceladus.

This study will focus on determining the presence and absence of non-water ice constituents in Enceladus crust, as well as the crystallinity and crystal size of the water ice, in an attempt to increase our understanding of the crust of Enceladus using data from the VIMS instrument on the Cassini mission. By comparing information about non-water ice species and water ice features with previously known information, such as Enceladus' geological features like the craters and tiger stripes larger patterns could become clear that shed light on the way Enceladus' surface has formed and continues to evolve. Such information in turn can be useful for further research into the origins of Enceladus and the other moons around the gas giants, as currently a variety of theories exist explaining how those moons could have come into being. Knowing more about the surface of Enceladus is also useful for the planning of future missions to this potential life-bearing moon.

This report consists of 8 additional chapters. Chapter 2 will discuss the Cassini-Huygens mission. Chapter 3 will introduce the basic concepts of infrared spectroscopy. Chapter 4 will introduce the moon of Enceladus and relevant previous studies of this moon. Chapter 5 will discuss how the data from Cassini's VIMS instrument was chosen, processed and prepared for interpretation. Chapter 6 will detail the methods used during and the results of the hunt for traces of non-water ice species. Chapter 7 will detail the methods used to determine the crystal size and crystallinity of the ice, as well as the results of these methods. Chapter 8 will combine the results of chapters 6 and 7 to determine the presence of patterns and correlations. Finally, chapter 9 will detail the final conclusions of the report. These chapters will aim to answer the following research questions:

1. Which locations on Enceladus surface are representative of the ice shell?
2. Where is VIMS data present with sufficient quality?
3. What outside factors influence the infrared spectra in the chosen locations?
4. What do the infrared spectra in the chosen locations tell us about the ice?

   (a) What is the size of the ice crystals?
   (b) What is the ratio between amorphous and crystalline ice?
   (c) Which non-water elements are present?
   (d) In what amounts are non-water elements present?

5. What do differences, or lack of differences, in ice composition in different locations reveal about the ice shell as a whole?
6. What, if any, is the relation between the presence of non-water elements and other characteristics of the ice.
7. Do craters and other geological features have different ice characteristics than their surroundings?

2

Cassini

This chapter will present a brief overview of the Cassini mission. The Cassini mission was a cooperative venture between the ESA and NASA with the goal of exploring Saturn, its rings and its moons. The data processed in this study originates from Cassini's VIMS instrument, so an understanding of the mission, its goals and the available instruments will be useful. Section 2.1 will detail the Cassini mission and its goals, while section 2.2 will go into more detail on the instrumentation of the Cassini mission.

2.1. the Cassini mission

The Cassini mission was launched in October of 1997 on a mission to Saturn that would end up lasting nearly 20 years. Of these 20 years, the Cassini spent a little over 13 years orbiting Saturn, but during its approach of the ringed planet it made flybys of Venus and Jupiter as well. This section will discuss the goals of the Cassini mission in subsection 2.1.1 and the major milestones achieved during the mission in subsection 2.1.2.

2.1.1. mission goals

The primary goal of Cassini was to conduct an in-depth exploration of the Saturnian system, with mission goals including measurement to determine the structure and composition of Saturn's atmosphere, determining the structure and distribution of the rings, studying Saturn's magnetosphere and it's interactions with satellites and mapping the various icy satellites. To this end it carried a versatile suite of instruments, as well as the Huygens lander which was designed to land on Titan. Titan is of particular interest because its the only known moon with a significant atmosphere, which is the reason it was the moon chosen to be visited by a lander.

Given that the present study focuses on Enceladus, one of Saturn's icy satellites, the Cassini mission's goals with regards to the icy moons are of particular interest. The initial science goals for the icy satellites were[20]:

1. Determine the general characteristics and geological histories of the satellites.
2. Define the mechanisms of crustal and surface modifications, both external and internal.
3. Investigate the compositions and distributions of surface materials, particularly dark, organic rich material and low melting point condensed volatiles.
4. Constrain models of the satellites' bulk compositions and internal structures.
5. Investigate interactions with the magnetosphere and ring systems and possible gas injections into the magnetosphere

During the two extensions on the main mission, a somewhat greater focus was placed on Enceladus because of the discovery of the water plumes emanating from Enceladus south pole. Mission goals during the Equinox and Solstice missions relating to Enceladus include[21]:

1. Study long-term seasonal changes on the mid-sized moons (Enceladus, Rhea, Tethys, Dione, Mimas, Iapetus);

2. Based on new information obtained during the nominal mission, determine whether Enceladus harbours an ocean, and search for possible anomalies in its internal structure;

3. Monitor long-term variability - in particular, seasonal variations in cryo-volcanic activity on Enceladus to help provide new constraints on the mechanism behind plume formation;

4. Study potential temporal variability especially in Enceladus's ocean and interior structure, Dione's activity, Rhea's rings, Tethys's magnetospheric interactions and Rhea's differentiation state;

5. Carry out a comparative study of Saturn's mid-sized satellites (Mimas, Enceladus, Thetys, Dione, Rhea, Hyperion, Iapetus and Phoebe), their cratering and comparative geology and surface composition.

These mission goals focusing on Enceladus have lead to a wealth of information and measurements being available for the icy moon, which will be used in the present project.

2.1.2. mission progress

Cassini's approach to Saturn was far from straightforward. It involved four gravity assist maneuvers, as shown in figure 2.1. Two of these where with Venus, at the 26th of April 1998 and the 24th of June 1999. The gravity assist with earth followed soon after on the 18th of august of 1999. The final gravity assist at Jupiter followed a year and a half later, on the 30th of December of 2000. This complicated flight plan was necessary to get the heavy Cassini mission to Saturn using the rocket technology available at that time.

Figure 2.1: This figure shows the trajectory of the Cassini mission during its journey to Saturn[1].

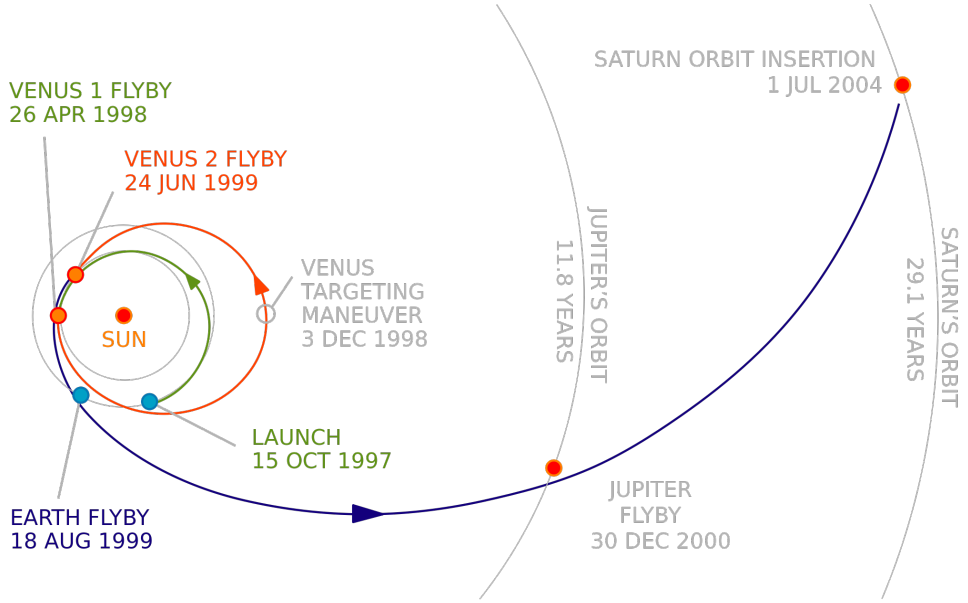

The Cassini orbiter arrived at Saturn the 1st of July 2004, nearly 7 years after its launch in 1997, and shortly afterwards began working towards its science goals. The Huygens probe was deployed at the end of 2004 and entered the atmosphere of Titan in January 2005. The Cassini mission also made several flybys of Enceladus in early 2005, making the first detections of the plumes. Other important milestones in the first mission phase include detecting the presence of methane lakes on Titan and the discovery of a giant storm with an 'eye' similar to that of a terrestrial hurricane at Saturn's north pole.

Cassini's mission at Saturn got extended twice. The initially planned mission phase lasted till 2008, with the mission first getting extended to 2010, and then to 2017. Noteworthy discoveries during this time include the change in colour of Saturn's north-polar storm over the period from 2012 to 2016, in

addition to this discovery the mission also continued performing flybys of Saturn's various moons and taking measurements to help increase our understanding of the icy moons. The Cassini mission ended in September of 2017, when the orbiter was steered into Saturn's atmosphere and was destroyed.

During the mission's life-time, it made over 20 close approaches of Enceladus with altitudes varying between 20 and 1200km. This variety in altitudes in turn results in the wide variety in spatial resolution on the VIMS images as the resolution is, in part, linked to the distance of the approach of the Cassini orbiter to Enceladus. Nasa's Planetary Data System has over 27000 VIMS images from these flybys, which means a selection process to determine which of these images will be of interest to this study is required. This process is discussed in chapter 5.

2.2. Instrumentation

Cassini contains a wide a variety of remote sensing and in-situ instruments for the completion of its mission goals. These instruments include two infrared spectrometers (VIMS and CIRS), a UV spectrometer, a mass spectrometer and a visible light camera, in addition to a suite of instruments for measuring the magnetosphere, cosmic dust and radio waves. Figure 2.2 shows the Cassini orbiter, including its many instruments. Note that many of the remote sensing instruments requiring light are mounted together, which makes using different instruments simultaneously easier. This in turn makes it easier get a compelte understanding of the instrument's target, as in many cases you've got both spectral and visual data from the same target taken under the same circumstances at the same time.

Figure 2.2: This figure shows the Cassini orbiter in full, including the Huygens orbiter. The instruments are split up in a number of separate pallets. The remote sensing pallet contains the IR spectrometers, UV spectrometer and the visible light camera. The fields and particles pallet consists of the plasma spectrometer, the ion and neutral mass spectrometer and the magnetospheric imaging instrument.

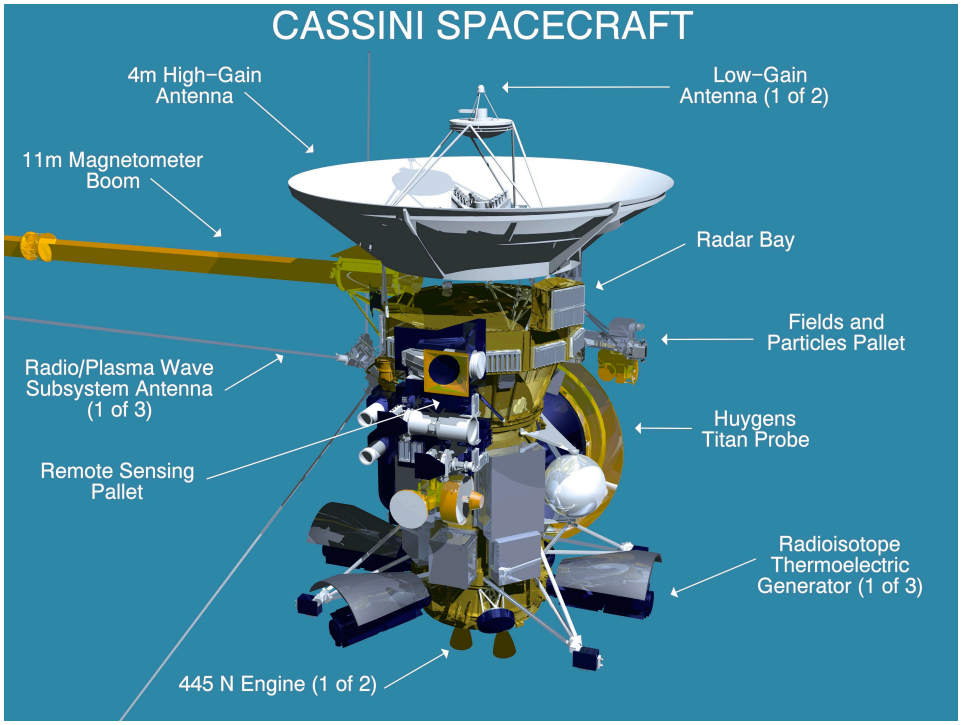

For this study, the two infrared spectrometers are of particular interest, though visible light images from Cassini's high resolution camera, the Imaging Science Subsystem, will occasionally be used to provide additional context. The infrared instruments have been chosen because the main method for determining the composition of the surface is infrared spectroscopy. The two infrared spectrometers are the Visible and Infrared Mapping Spectrometer (VIMS) which records infrared spectra in the near and mid infrared, and the Composite Infrared Spectrometer (CIRS) which measures infrared spectra in the far infrared.

The near infrared data is very useful for the study of the water ice itself and smaller molecules

such as ammonia or carbon-monoxide, while the longer wavelengths from the CIRS instrument can be used to get temperature information, as well as information on larger molecules, such as the longer carbon-chains that have been detected in the plumes[22].

Section 2.2.1 will go into more detail on the VIMS instrument, while section 2.2.2 will go into more detail on the CIRS instrument. Finally, sections 2.2.3 will detail the availability of data from both these instruments.

2.2.1. Visible and Infrared Mapping Spectrometer

The Cassini VIMS instrument is an evolution of the Near-Infrared Mapping Spectrometer (NIMS) instrument carried by Galileo on its mission to Jupiter. It has been designed to fulfill a wide range of scientific goals, both at Saturn as well as Venus and Jupiter, which the Cassini mission passed on its way to Saturn. Figure 2.3 shows what a spectra from the VIMS instrument can look like. This spectra has been taken from Enceladus' south pole and clearly shows the features of water ice at 1.4, 1.5, 2 and 3 microns, as well as a peak associated with CO_2 at 4.26 micron. The data from the VIMS instrument will provide information regarding the water ice itself, as well as other common species, such as CO, CO_2 and NH_3.

Figure 2.3: This figure shows an example of the kind of spectra obtainable from the VIMS instrument[2]. The Y-axis provides the incident flux, while the x-axis gives the wavelength in microns

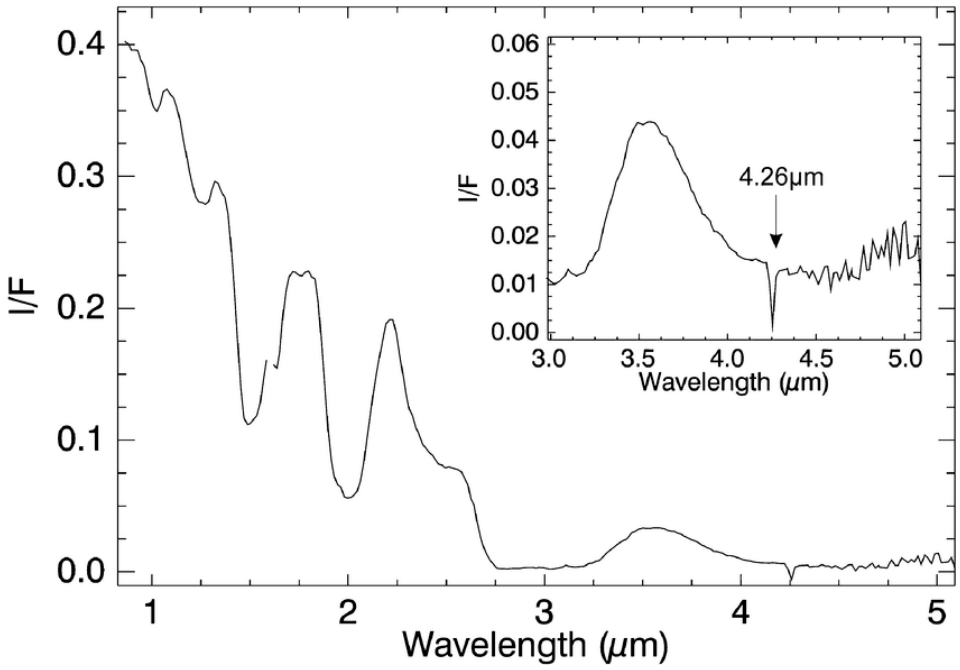

The VIMS instrument has two major sub-assemblies, being the VIMS-VIS for visible light, and the VIMS-IR for infrared light. Though mounted together, each sub-assembly has its own foreoptics and internal systems for processing incoming light. For this study, the VIMS-IR sub-assembly is the most interesting as the IR spectral data can be used to characterize Enceladus' surface.

VIMS instrument optics information

The VIMS-IR instrument foreoptics consists of a 23cm Ritchey-Creitin telescope with a focal ratio of $f/3.5$. From the Ritchey-Creitin telescope the light moves through a slit and a $f/3.5$ Dahl-Krikham collimator into a classic grating spectrometer[3]. After the spectrometer, the light passes into a camera through a set of Cassegrain optics and the spectrograph is recorded[23]. Figure 2.4 shows a wire-frame depiction of the VIMS instrument and the basic optical path.

The VIMS-IR instrument takes measurements in the 11500 to 2000 cm^{-1} region, which means it covers most of the Near Infrared and part of the Middle infrared region. The spectrometer itself is a grating spectrometer with 256 channels, which means that total spectrum is divided over 256 bins

Figure 2.4: This wire-frame shows the Cassini VIMS instrument[3]. It consists of two sub-assemblies, the smaller VIMS-VIS is the section in the top left, while the larger VIMS-IR takes up most of the image. The optical path can be followed, starting at the telescope on the right side, then entering the infrared spectroscope taking up the lower left of the image, before finally passing into the camera in the centre of the image.

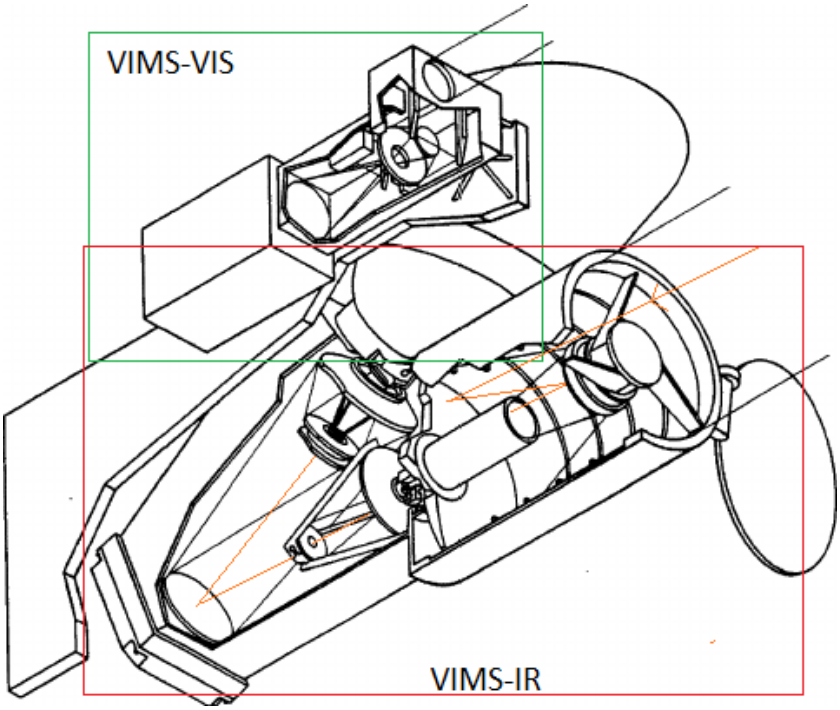

for measurements.[3] The pixel size is 0.5x0.5 mrad when recording images at standard resolution or 0.5x0.25 mrad when recording at high resolution.[23]

2.2.2. Composite Infrared Spectrometer

Unlike the VIMS, which uses a more traditional grating spectrometer, the CIRS instrument makes use of a Fourier transform infrared spectrometer. The CIRS instrument has two separate interferometers, one for the Far Infrared region and one for the Middle Infrared region. Both these interferometers share a single Cassegrain telescope. After the telescope, the light is split and fed into the two different interferometers so the entire spectrum is sampled all at once. The instrument has 3 major detector arrays, known as focal planes 1, 3 and 4. Focal plane 1 is used for detecting the far IR radiation and is a 3.9 mrad FWHM thermopile detector. Focal plane 3 is a 1x10 array of photoconductive detectors which measures the 600 to 1100 cm^{-1} region, while Focal plane 4 is a 1x10 array of photovoltaic detectors sensitive from 1100 to 1400 cm^{-1}[4].

However, the instrument does have some limitations to what it measures at once. While Focal plane 3 and 4 have 10 detectors, they only have 5 amplification channels. This means that only 5 of the 10 detectors can be used at once. The instrument has a number of different modes in which it can switch these detectors on and off, being the even and odd modes, which use every other detector, the centre mode which only uses the central 5 of the detector and the pairs mode, which adds the results from neighbouring pairs of detectors to create a lower-resolution model that covers the entire spectrum. Because of the way the detectors are set up, even mode on one focal plane 3 is generally used with odd mode on focal plane 4, as that will result in the detectors neatly lining up[4].

Figure 2.6 shows a spectra of the atmosphere of Saturn measure with the CIRS instrument[5]. Note that this spectrum shows far more rapid and abrupt changes in the spectra than in figure 2.3. This is because in this case the instrument is measuring gasses, rather than solid materials. The reasons for this will be discussed further in chapter 3. When applied to Enceladus, the main use for data from this instrument will lie in determining the temperature and detecting signs of larger molecules.

Figure 2.5: This figure shows the layout of the CIRS instrument. The left path measures the higher wavelengths, while the right path measures the lower wavelengths.[4].

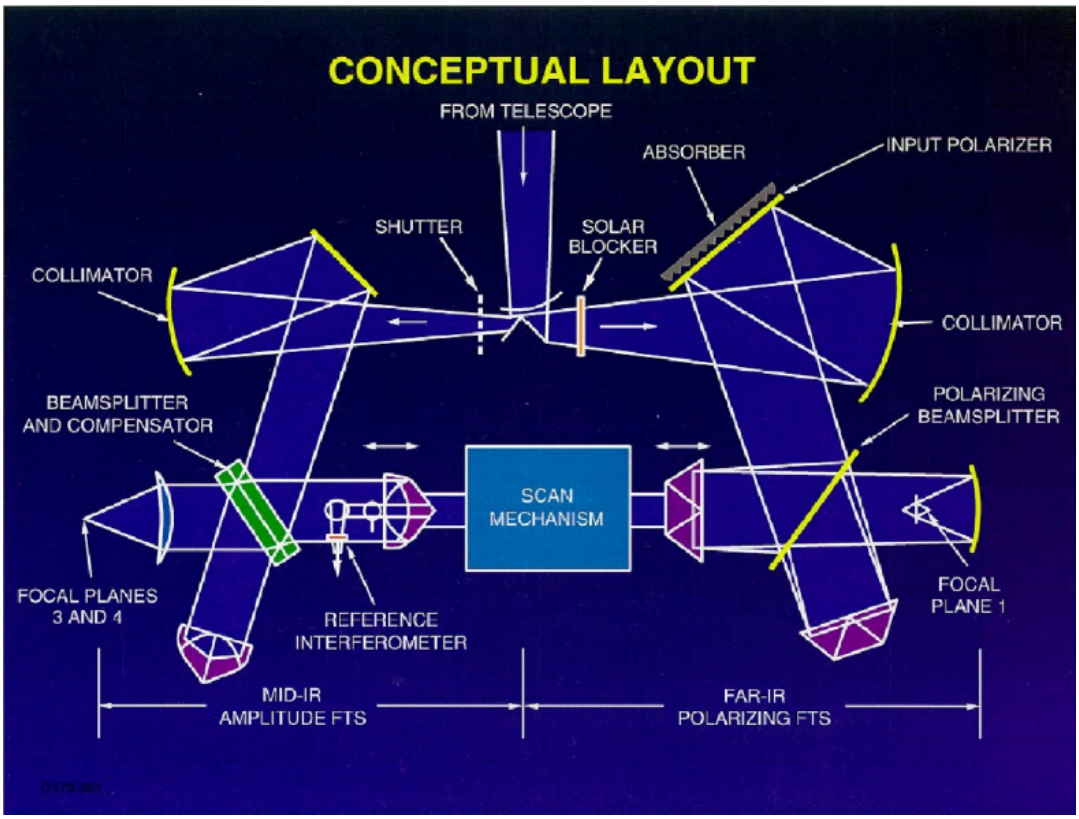

Figure 2.6: This figure shows an infrared spectrum of Saturn created using data from the CIRS instrument[5]. This image has been created by combining data from all three focal planes.

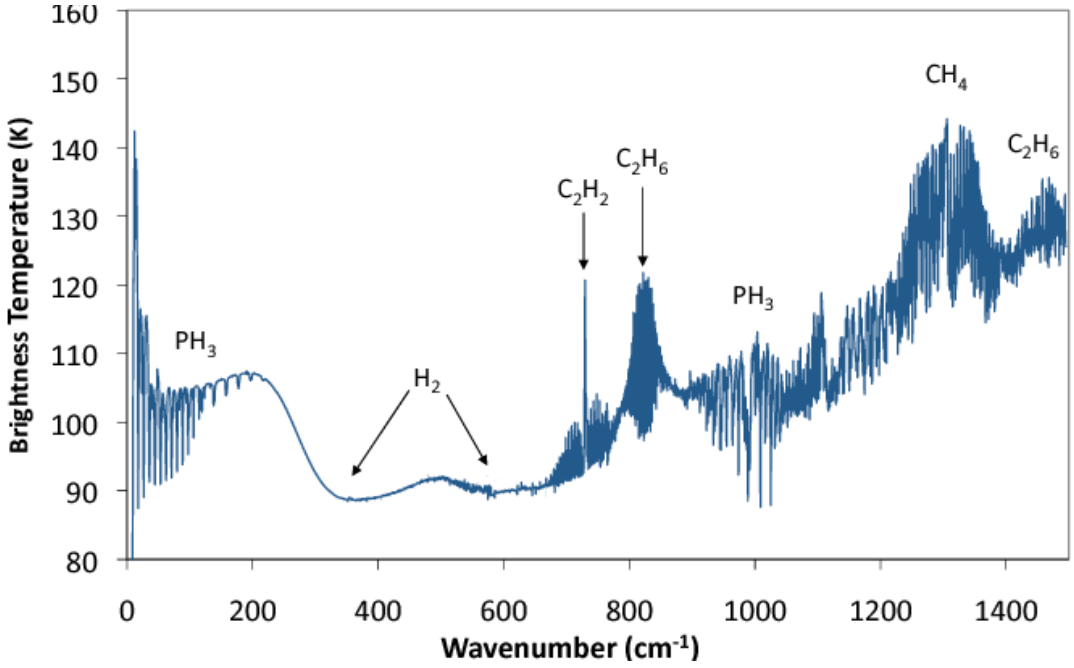

2.2.3. data availability

The data from the VIMS and CIRS instruments are available from NASA's planetary data system. However, for the VIMS data there are pre-existing tools allowing for reading and processing the data, while the same is not true for the CIRS data, so any programs for processing the CIRS data would have to be build up from the very ground, starting at making the data readable. This makes the VIMS data more accessible than the CIRS data. Further information about the data format and processing is provided in chapter 5.

3

Infrared radiation and spectroscopy

This chapter will provide a basic background on infrared radiation and the basics of spectroscopy. As this thesis deals extensively with extracting information from infrared spectra, a basic understanding is necessary to understand the contents of later chapters. Section 3.1 will provide the basics of infrared radiation, while section 3.2 will provide and discuss an example of VIMS spectral data.

3.1. infrared radiation

Infrared radiation is a form of electromagnetic radiation, just like visible light and radio waves. The infrared section of the spectrum is a set of wavelengths that are slightly longer than the visible light, covering the range from 700nm to 1 mm, or 14000 cm^{-1} to 10 cm^{-1}. Figure 3.1 shows how the Infrared region is located within the full electromagnetic spectrum.

Figure 3.1: This image shows the full length of the electromagnetic spectrum[6] based on wavelength. This study will focus on the infrared region.

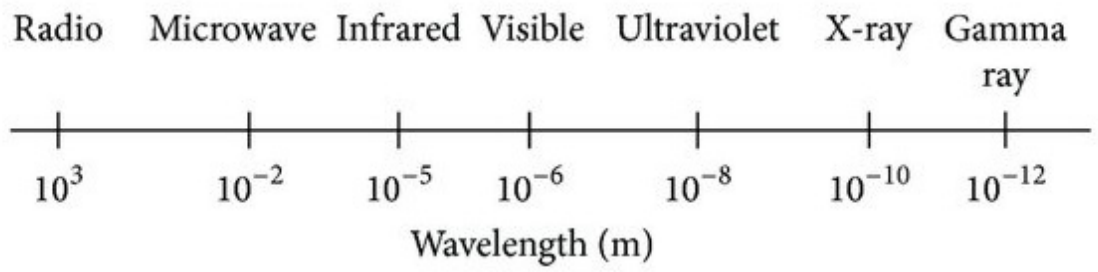

Like all electromagnetic radiation, the energy of a photon in the infrared spectra is a function of its wavelength. Likewise, atoms require discrete input of energy to set them to vibrate, as the mechanism causing the vibrations is the change in energy level and orbit of an electron. As electrons have discrete energy levels rather than a continuous spectrum, electrons generally change levels by either absorbing or emitting light of the appropriate wavelength. This is the base for infrared spectroscopy.

If we observe infrared radiation coming form an object at a particular wavelength, it would be indicative of the object consisting of materials that emit energy in this particular discrete set (or quanta). Likewise, if we notice a lack of light in a particular wavelength, we know that it has passed through an object absorbing this particular quanta of energy. Figure 3.2 shows the emission and absorption spectra of hydrogen in visible light. Note that the bands in the absorption and emission spectra overlap perfectly, showing the two different ways in which these characteristic bands can be detected.

To put it in simpler words: electromagnetic radiation can excite parts of molecules, causing it to vibrate, rotate or flex, but only if the radiation is providing the exact amount of energy necessary to excite the molecule. This causes the characteristic spectra that can be used to analyze an object.

Figure 3.2: This figure shows the absorption and emission bands of Hydrogen

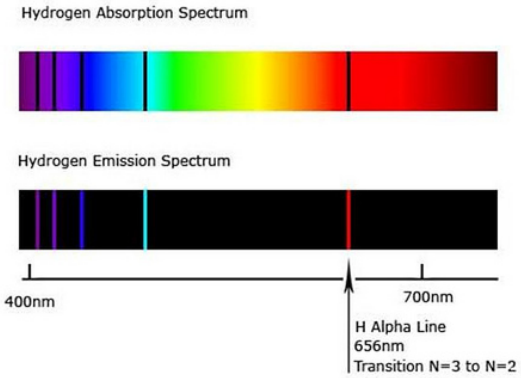

Subsection 3.1.1 goes more in depth on these vibrations, while subsection 3.2 provides an example using a VIMS spectrum from Enceladus.

3.1.1. Molecule vibration

Molecules have a variety of different modes in which they can vibrate, which in turn causes the different bands in an infrared spectrum. The theoretical amount of absorption bands a molecule has is limited by the amount of degrees of freedom of a molecule, which is equal to 3 times the amount of atoms within a molecule. The other limiting factor of the amount of absorption bands is the type of atoms a molecule is built up of. A -C-H bond will absorb on the same wavelengths irrespective of whether there is only 1 or 20 of these bonds in the molecule.

It should be noted that, though bands would theoretically be infinitely narrow, in practice they are not. A number of factors play a role in broadening these bands. In gasses the Doppler effect plays a role as specific molecules could be moving towards or away from the instrument. Collisions between atoms also causes bands to broaden. Furthermore, due to the limited time the molecule states exist, quantum mechanics come into play as well in the form of the Heisenberg uncertainty principle. A relation between the lifetime of the excited state and the bandwidth of the absorption band exists as a consequence of this principle [24].

Another important factor influencing molecule spectra is the state of the molecule. The spectra of CO_2 gas and CO_2 ice are very different, for example. This is caused by the changes in molecule interactions between gas, liquid and solid states. In a solid state, molecules are less free to move individually than in a gas state, with, fro example, no rotation being possible.

3.2. Cassini VIMS example

Pure samples of a molecule provide extremely clear lines such as were shown in figure 3.2. However, making such clean and clear observations generally requires a laboratory set-up and sample preparation, something that is not possible when performing remote sensing on another planet or moon with an instrument like VIMS. Real conditions not only provide a mix of different species, but will also include noise as source of interference, which could obscure features, or make it appear like a feature could b present where none is. Figure 3.3 is an IR spectra taken from the surface of Enceladus, showing many of the features that are typical for such measurements.

This spectra shows measurements in absorption, with the troughs on the spectrum marking the locations of spectral features, such as those at 2 and 3 micron, which are markers associated with water ice. In addition, an overall downward slope is visible, which is caused in part by properties of the surface, such as crystal size, and in parts by properties of the light. The light recorded here is sun-light reflected from the surface of Enceladus, and sun-light itself does not have equal intensity at every wave-length, the spectral energy distribution instead being very similar to that of black-body radiation. Cassini's own IR emissions have little effect in the 1 to 5 micron range of the VIMS. Figure 3.4 shows a comparison between the sun black-body, corrected for the distance it has to travel to be reflected off Enceladus, and a black body with a temperature of 81K, which is the temperature measured at the

Figure 3.3: This figure shows an example of an IR spectrum taken by Cassini's VIMS instrument, taken from the surface of Enceladus. The wavelength is marked in micron.

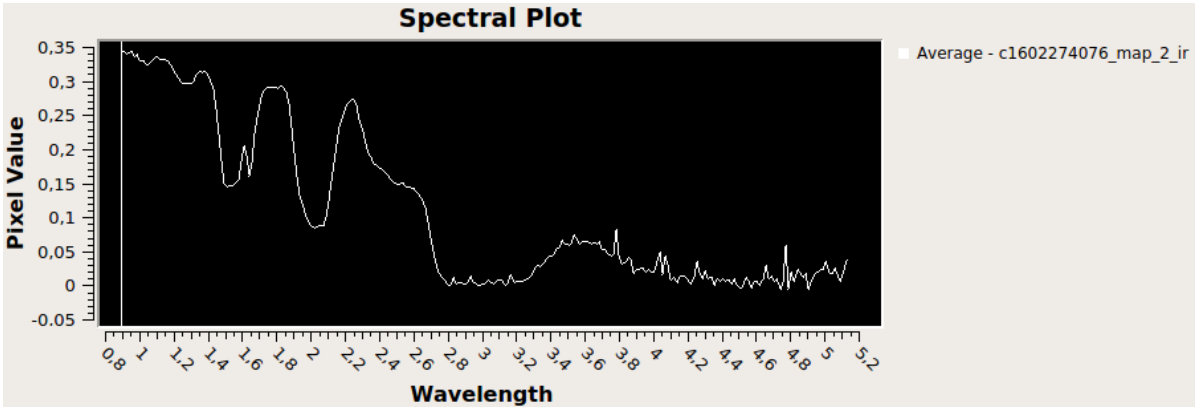

tiger stripes. The 81K blackbody only starts reaching meaningfull values past a wavelength of about 7 micron. At shorter wavelengths the IR radiation of Enceladus does not have a meaningful impact on the IR spectrum of the icy moon.

Figure 3.4: This figure shows an approximation of the reflected energy distribution from the sun and the energy distribution of a black body with a temperature of 81K. Noe that the effect of the 81K blackbody curve is negligible within the 1-5 micron range of the VIMS instrument.

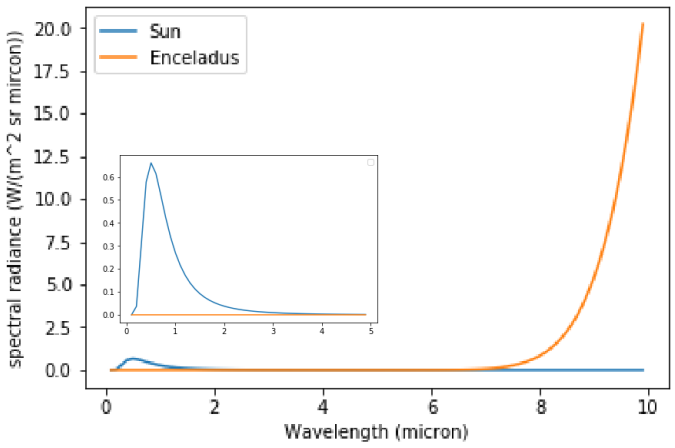

Another notable feature is that the latter portions of the spectrum appear more noisy. This is something that appears to some degree in most VIMS spectra of Enceladus, and is an unfortunate reality of working with remote sensing data. This noise should be kept in mind when processing the spectra and judging the results, but it does not render the data unusable.

4

Enceladus

This chapter will discuss the target of this study, Saturn's icy moon Enceladus. Section 4.1 will provide a basic overview of the surface off Enceladus, while section 4.2 will discuss previous work performed on similar topics as the present study.

4.1. The Enceladus surface

This section will discuss the main features of the surface of Enceladus. Section 4.1.1 will briefly introduce the four main geological areas of Enceladus, while subsection 4.1.2 will discuss the plumes of Enceladus and how they affect its surface. This will provide useful context for identifying trends in the IR spectra across the surface of Enceladus.

4.1.1. Geological areas

Understanding the surface of Enceladus is important, as it provides context to the results of any mapping effort of non-water ice species, water ice crystallinity or crystal size. Enceladus has generally been split up in 4 main geological areas, as shown in figure 4.1, which also shows a further subdivision of the four major terrain types. These are the cratered terrain, trailing hemisphere terrain, leading hemisphere terrain and south-polar terrain[25]. As the names suggest, the trailing hemisphere terrain, leading hemisphere terrain and south polar terrain correspond to distinct geographical regions, while the cratered terrain can be found at the north-pole and as a separating region between the trailing and leading hemisphere terrains. As Enceladus is tidally locked, one hemisphere is always pointed in the direction the moon is travelling. while the other hemisphere is always pointing away from the direction of travel, resulting in the names of leading and trailing hemisphere.

The main differences between the terrain types are a matter of age and geological activity. The cratered terrain is the oldest terrain on Enceladus, as indicated by the large collection of old craters present. The leading and trailing hemisphere terrains are both younger, with less evidence of impacts and more structures associated with geological activity, such as ridges and troughs. The south polar terrain is the youngest terrain on Enceladus and is largely dominated by the 'tiger stripes', which is a group of four parallel fractures from which the south-polar plumes emerge.

4.1.2. Plume contents and accretion

An important factor in the evolution of the surface of Enceladus are the south-polar plumes. The plumes are responsible for creating Saturn's 'E' ring [26], but not all plume material ends up in Saturn's orbit. Plume materials that end up falling back to Enceladus will slowly add to the surface over time. Figure 4.2 shows the results of a simulation of the plumes with likely distribution of particles on Enceladus performed by Kempf et al. [27]. The figure shows that plume material deposition is mainly concentrated in the south-polar regions where the green sections indicate high rates of deposits. However, there are further ares of non-negligible deposits stretching out into the cratered terrain separating the leading and trailing hemisphere areas.

Knowing where on Enceladus plume material is expected to be deposited is important for this study, as it influence what species we expect to find in those areas. The material from the plumes would cover

Figure 4.1: geological regions overlaid on a cylindrical image mosaic of Enceladus made by Cassini. The crosses mark the leading (L) and trailing (T) points of the map[7]. The light purple, green and blue sections around the L marker comprise the leading hemisphere terrain, the dark purple and ice-blue sections at the southern end of the map comprise the south polar terrain, and the green, red, light and dark purple sections around the T marker comprise the trailing hemisphere terrain.

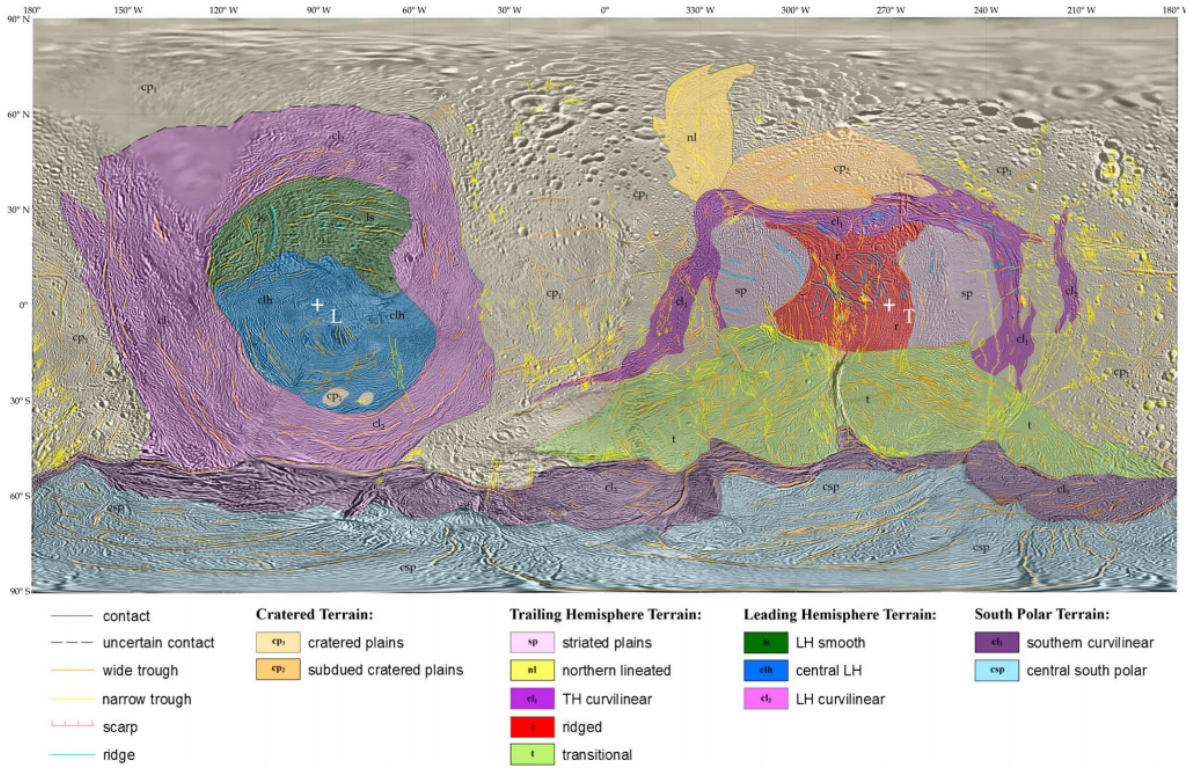

Figure 4.2: The rate of deposition in mm/year of new ice from plume materials. The locations marked in the south-polar terrain are locations of plumes.

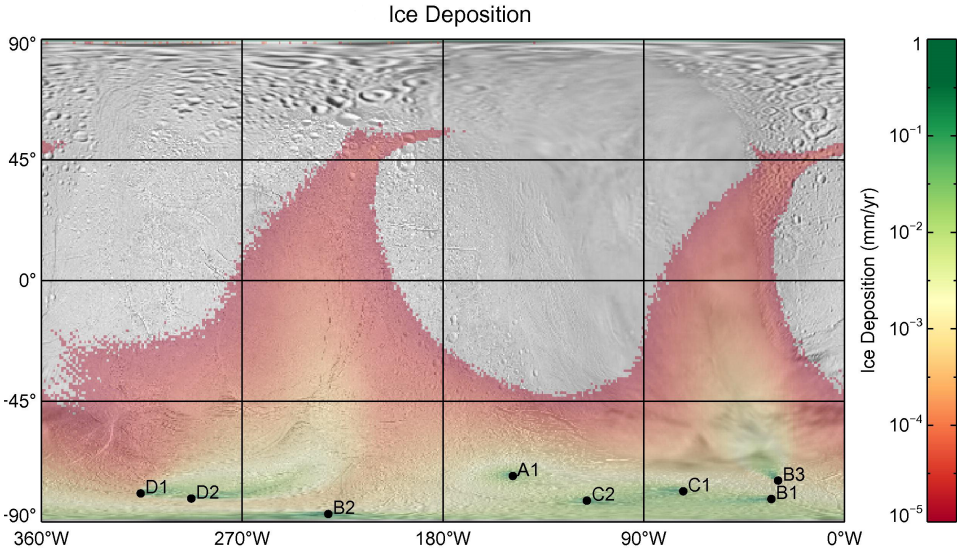

the underlying terrain, so in these areas we would not expect to find any species that are not present in the plumes themselves. Research by McKinnon et al.[28] on data from Cassini's INMS instrument has identified a number of species within the plume, the most abundant of which are listed in table 4.1. Of the non-water species listed here, the most likely to appear in the IR spectra of areas with heavy plume accretion are NH_3, CO_2 and CH_4, though the low abundance of methane might mean that it is not visible within the IR spectra.

Table 4.1: This table contains the species measured by Cassini's INMS instrument. The major species in the first column have been detected without ambiguity, while the minor species listed in the second column are somewhat ambiguous.

Major species (>0.1%)	Minor species (<0.2% and >100ppm)
H_2O (96-99%)	CO
CO_2 (0.3-0.8%)	C_2H_2
CH_4 (0.1-0.3%)	C_2H_4
NH_3 (0.4-1.3%)	C_2H_6
H_2 (0.4-1.4%)	N_2
	HCN
	CH_2O
	NO

4.2. Previous work

A number of studies have focused on Enceladus in the past. While many of these studies have focused on the plumes, there are some that have focused on the icy crust in part or as a whole. This section will discuss the past studies that are relevant to this research.

4.2.1. Surface ice types

Crystallinity

Previous research[29] has been done with regards to the amount of amorphous and crystalline ice that can be found on Enceladus surface. There are three main types of ice, being amorphous, cubic and crystalline ice. Of these 3, cubic is an in-between state for amorphous and crystalline ice, and therefore more difficult to remotely detect as cubic ice will look similar to a mix of amorphous and crystalline ice. Because of the different conditions in which the ice-types are created, knowing which parts of Enceladus are more amorphous, and which are more crystalline helps with shedding light on the processes behind the surface's formation and evolution. Figure 4.3 shows one of the main spectral difference between crystalline and amorphous ice. It shows three different mixes of amorphous and crystalline ices, and the way the 1.5 and particularly the 1.65 micron water ice feature changes under these different circumstances.

The spectra of amorphous and crystalline ice differ in a number of key ways which allows the difference to be seen when looking at a pure sample. In the case of an icy moon each pixel would likely contain a mix of the two, so an algorithm is employed to try to determine the fraction of crystalline ice. The study implements two different approaches. One algorithm functions by comparing the spectra taken from Enceladus to either models or spectra taken from the moon that are representative of semi-pure versions of the two ices to calculate a crystallinity factor for each pixel. The other looks at the 1.65 micron feature in the water ice and detriment the ratio of two of the instrument bands to determine the depth of the feature.

Looking at the crystallinity can tell us several things about Enceladus. Amorphous ice is generally formed by depositing at very low temperatures, but amorphous ice can also be created by bombarding crystalline ice with energetic particles. The study by Newman has encountered this in its analysis of the South pole of Enceladus, as radiation has caused most of the surface to be largely amorphous, but because of the increased temperature around the tiger 'stripes' the ice continually recrystallizes in that area.[29].

Crystal size

Jaumann et al.[9] have performed research on the crystal size of Enceladus, with a focus on the south-polar area. They used a collection of water-ice spectra with different crystal sizes simulated using the

Figure 4.3: This figure shows a simulated model of the albedo, a measurement of reflectance, of one of the main spectral differences between amorphous and crystalline ice [8].

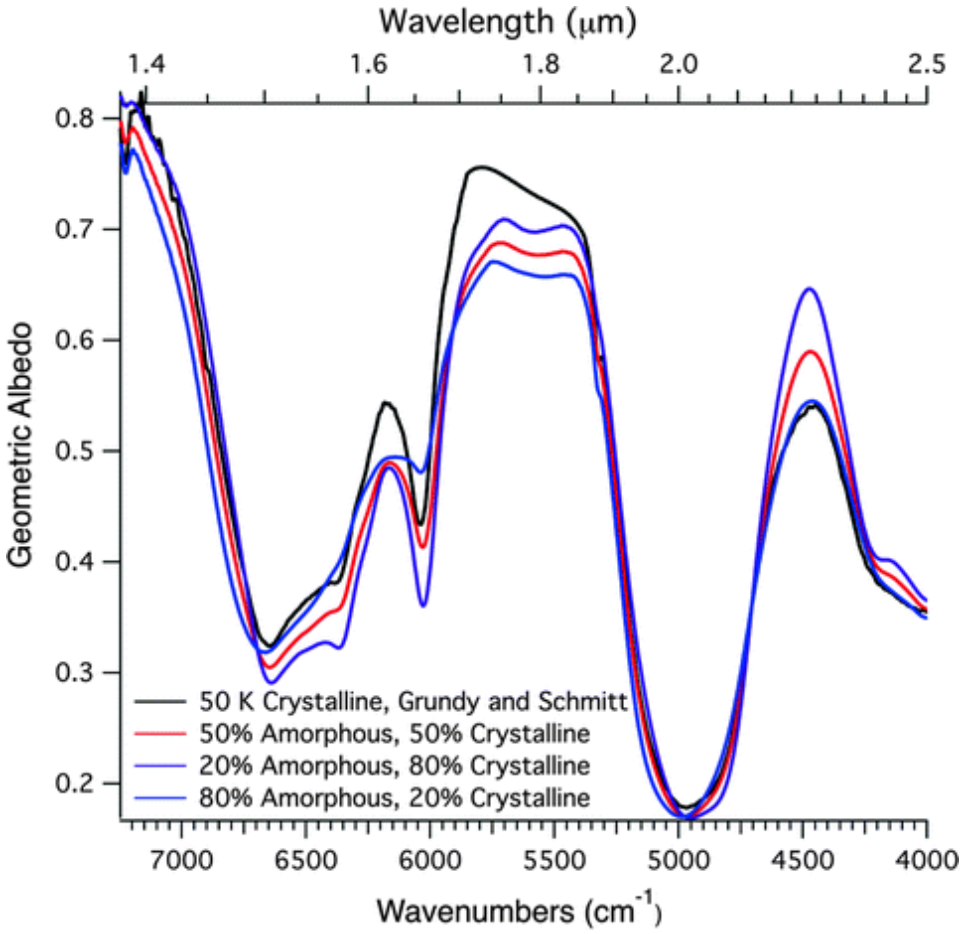

Hapke model to determine a relation between the band depths of the 1.04, 1.25, 1.5 and 2.0 micron water ice features and the crystal size. These relations where then used to determine the crystal size of parts of the surface of Enceladus.

Figure 4.4: This figure shows the crystal sizes as calculated by Jaumann[9], using the 1.5 micron absorption band.

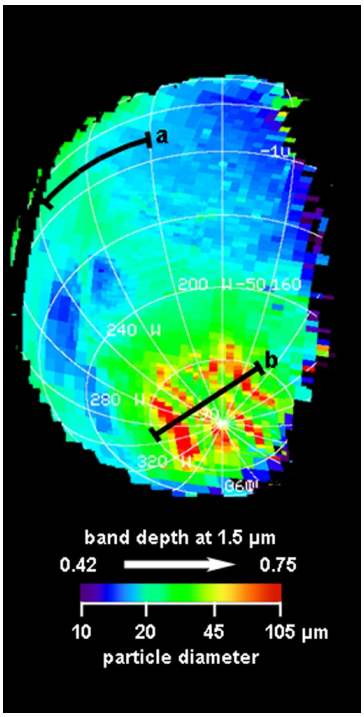

As the research by Jaumann occurred fairly early on in the Cassini mission, no full IR mosaics of Enceladus where available yet, so only a portion of the surface was mapped, as can be seen in figure 4.4. The tiger stripes very clearly stand out as having a higher crystal size than the surrounding terrain, while the areas with lower crystal size correspond to the older cratered terrain.

Crystal size can be used to make an estimate of the age of the different sections of Enceladus, as older sections tend to have lower crystal sizes as there has been more time for environmental effects like impacts by micrometeorites and energetic particles to break down crystals.

4.2.2. Non-water ice species

Only a few studies have concentrated on the non-water ice species in the entire crust of Enceladus, with most researchers focusing on the plumes and south-polar areas instead. However, during the course of this study a paper was published discussing the presence of CO_2 in the ice of Enceladus[10]. This study made use of VIMS images to create a mosaic covering the entirety of Enceladus and then focused on two features of CO_2, at 2.7 and 4.24-4.3 micron, to determine where CO_2 is present on Enceladus.

The study by Combe et al. used a large set of VIMS images, and a relatively simple method for detecting the presence of CO_2. For the feature at 4.24-4.3 micron, the channels between 4.18 and 4.22 micron and between 4.32 and 4.36 micron where used to determine the shoulders of the feature by taking the average of each of these two sets of channels. This was then used to to determine a continuum to which the depths of the wavelength channels at 4.24, 4.26, 4.28 and 4.30 micron could be compared. Figure 4.5 gives a basic overview of this method. The feature at 2.7 micron is narrow enough that it only occupies a single wavelength channel, so its depth is established by using the two neighbouring channels to establish a linear continuum from which the depth at 2.7 micron can then be determined.

This fairly simple method can work well if the data is clean, with only small artifacts or noise, which this study accomplishes by using a very large dataset, with multiple spectra for each location. Averaging the spectra of the same location together should reduce noise without losing spatial resolution. They

Figure 4.5: This figure shows one of the 4.24-4.3 micron features of CO_2 found by Combe [10]. The green lines indicate the bound between which the left shoulder is determined, while the blue line indicates the same for the right shoulder. The orange line is an approximation of what the determined continuum from these two shoulders would look like. The red zone then indicates where a band depth is detected.

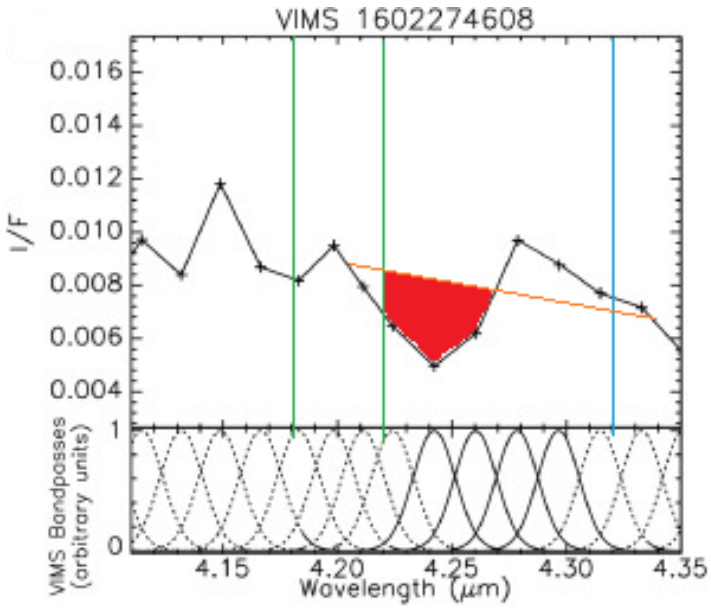

did this by selecting VIMS pixels that covered areas smaller than 20 km^2 and images based on signal-to-noise ratio measured by looking at the standard deviation of the dark current. They then projected and merged the data that met the above criteria and re-sampled it into a mosaic with pixels with a length of 4.4 km on each side.

Figure 4.6: This figure shows the band depths of the 4.24-4.3 micron (top) and 2.7 micron (bottom) features of CO_2 on Enceladus as determined by [10].

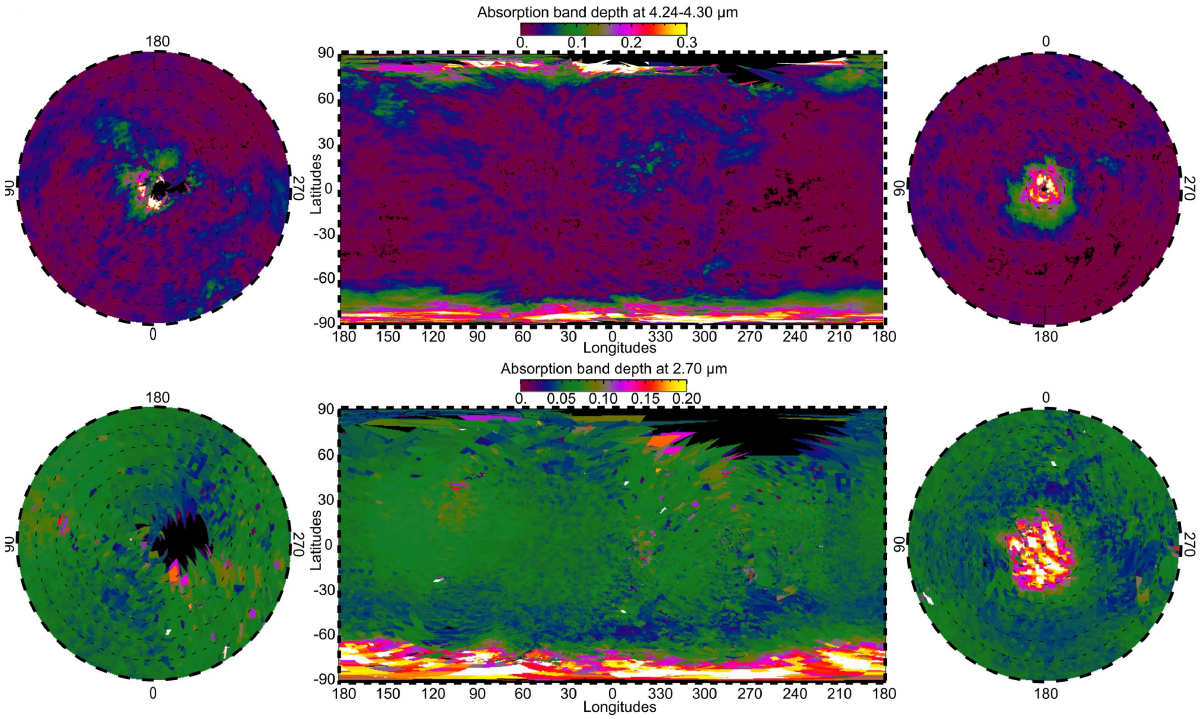

The results of Combe's approach can be found in figure 4.6. At both wavelengths there are fairly deep bands at the south pole, while at the north pole only the 4.24-4.3 micron feature stands out. The paper suggest that this is due to the presence of a number of different types of CO_2 compounds, with a kind with a strong 2.7 micron feature and a peak at 4.26 micron predominantly present at the south pole, while at the north there are CO_2 compounds with a weak 2.7 micron feature and the 4.24-4.3 micron feature varying over the entire range.

In addition to the information about the distribution of CO_2, the paper also provided insight into the amount of VIMS observations across the surface of Enceladus, as shown in figure 4.7. Of note is the bias towards the southern hemisphere, with some parts of the north pole having only 1 image, while most parts of the south-pole have several.

Figure 4.7: This figure shows the amount of observations at different locations across Enceladus that met Combe's requirements of how high spatial resolution and signal-to-noise ratio [10].

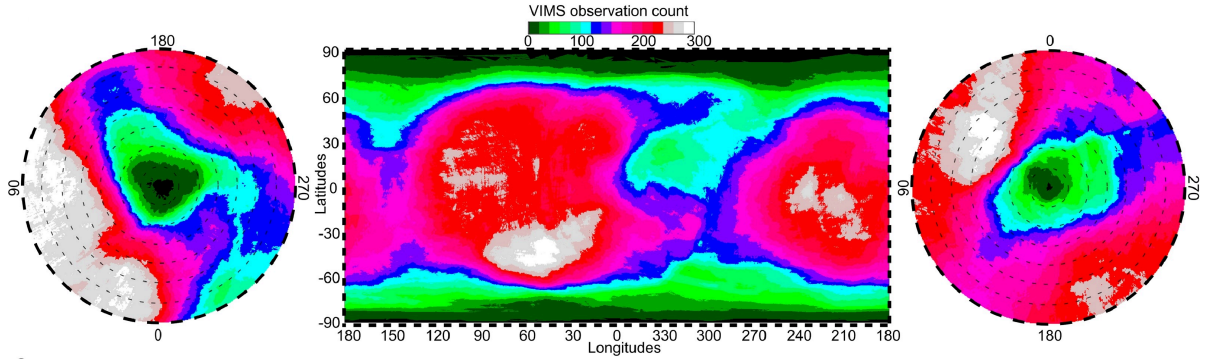

5

Data selection and processing

This chapter will discuss the method used for selecting the data and the initial round of processing to make the data readable. Section 5.1 will provide a short note on the decision to only use data from the VIMS instrument, and not from the CIRS instrument. Section 5.2 will provide information on the selection of the data while section 5.3 will detail the initial round of processing to make the data readable.

5.1. instruments

The VIMS instrument provides the core of the information necessary for this thesis, with the CIRS instrument providing some ancillary measurements at a lower spatial resolution. However, during the initial forays into processing the data of the VIMS and CIRS, the data from the CIRS instrument proved to require a far larger time investment for building the necessary tools to be able to extract the spectra, without accounting time for processing and extracting information from the data. Because of time constraints, the decision was eventually made to focus solely on the data from the VIMS instrument.

5.2. Selection

Cassini has taken over 25,000 measurements of Enceladus using its VIMS instruments. Using all of this data is impractical with the relatively limited computational and data storage facilities and time available for this thesis, so a selection has been made. To make this selection possible, a limited set of locations of interest have been chosen across the Enceladus surface, and only measurements including these locations will be used. For these locations, a further selection from the available images will then be made for pictures with high spatial resolution.

5.2.1. Location criteria

The chosen locations need to meet a number of requirements. First of all, both relatively smooth terrain and terrain with craters, canyons or similar features need to be included. The 4 major terrain types of Enceladus are the south polar terrain, cratered terrain, leading hemisphere terrain and trailing hemisphere terrain. In addition, recent mapping efforts of Enceladus [7] have subdivided these major types into smaller units. For the initial sample of locations, 2 will be chosen from each of the 12 distinctive regions identified in figure 5.1. One of these locations will be located in relatively smooth terrain, while the other will be located in a crater or in another deep terrain feature. In addition to these, 4 more locations will be placed in the larger craters in the cratered terrain area, as these are some of the largest and oldest terrain features on Enceladus

The intended goal of using these criteria for the measurement locations is to get as varied and complete an image of Enceladus as possible. By choosing locations in deeper geological features some information about the subsurface layers of the icy crust will hopefully be revealed.

Figure 5.1: geological regions overlaid on a cylindrical image mosaic of Enceladus made by Cassini. The crosses mark the leading (L) and trailing (T) points of the map[7].

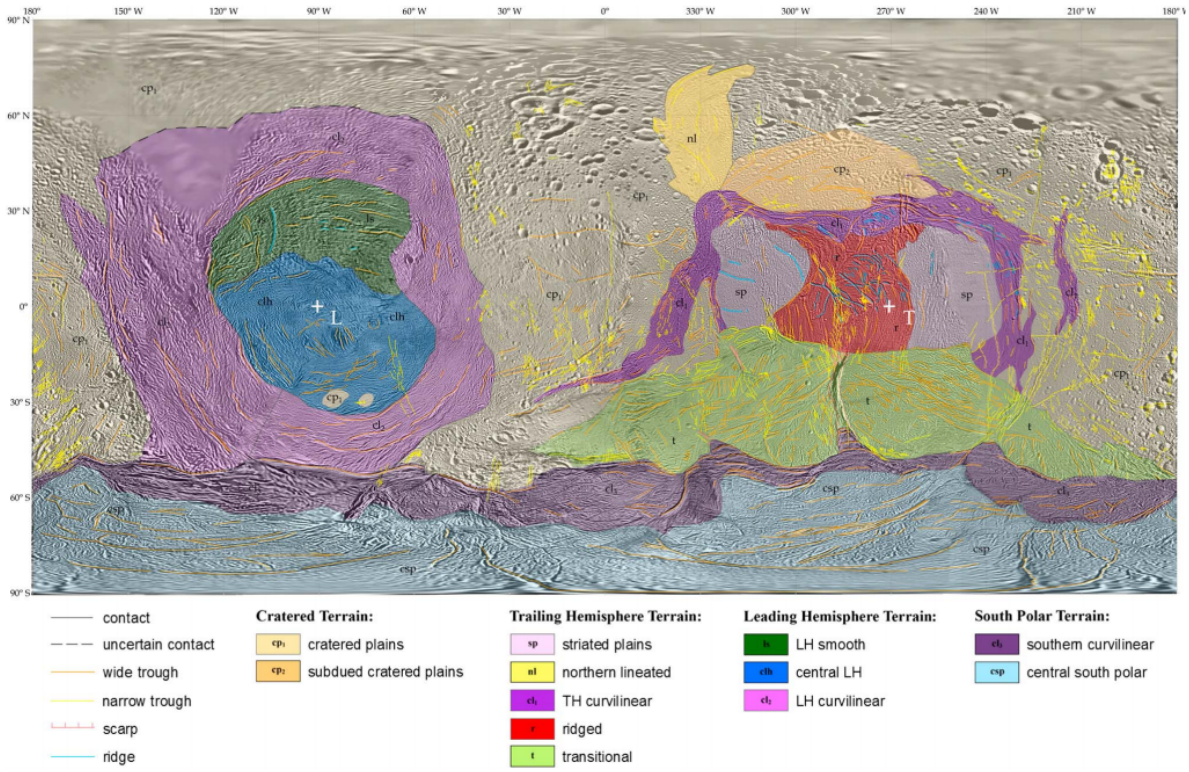

5.2.2. Initial locations

The initially chosen locations are shown in figure 5.2. Of these, several stand out. The eastern most striated plains (the light purple area within the trailing hemisphere terrain in figure 5.2) seem to contain a mostly smooth section with a single prominent crater. The region's smoothness suggest a relatively recent resurfacing event, so the single crater is most likely very fresh. Because of this, both the crater and a section of the smooth-appearing plain is chosen as a measurement location, so that any differences between the smooth terrain and the crater can be detected

Another clearly visible feature is the large canyon in the transitional terrain (the light green area within the trailing hemisphere terrain in figure 5.2). This crevasse is one of the largest terrain features on Enceladus and so including it in the area studied night reveal some differences between the crevasse and the surrounding terrain.

5.2.3. Data comparison and final chosen locations

NASA's planetary Data System (PDS) database contains many thousands of VIMS images of Enceladus. However, many of these have been taken from long distances with resolutions in the tens of kilometers per pixel, which makes them less ideal for precise location-bound analysis.

The sharpest VIMS IR images have a resolution of about a kilometer per pixel, but there are only a handful of these images, and most of them are focused on the south polar terrain. For any given location, the database does contain images with resolutions of 10-30 km per pixel, which should still provide a decent overview, though information about smaller features will unfortunately be lost. The crater in the striated plains area is fortunately located on one of the highest resolution pictures available, which will be a big boon for analyzing this seemingly very fresh crater.

Table 5.1 gives the precise coordinates of the 31 chosen locations, as well as the approximate resolution of VIMS-IR images at these locations. As mentioned in the table, the resolution of the data differs significantly per location, though it should be noted that the differences are almost always only significantly longer along one side of the pixel, with the other side generally being in the order of 8-10

Figure 5.2: The red crosses mark the initially chosen locations

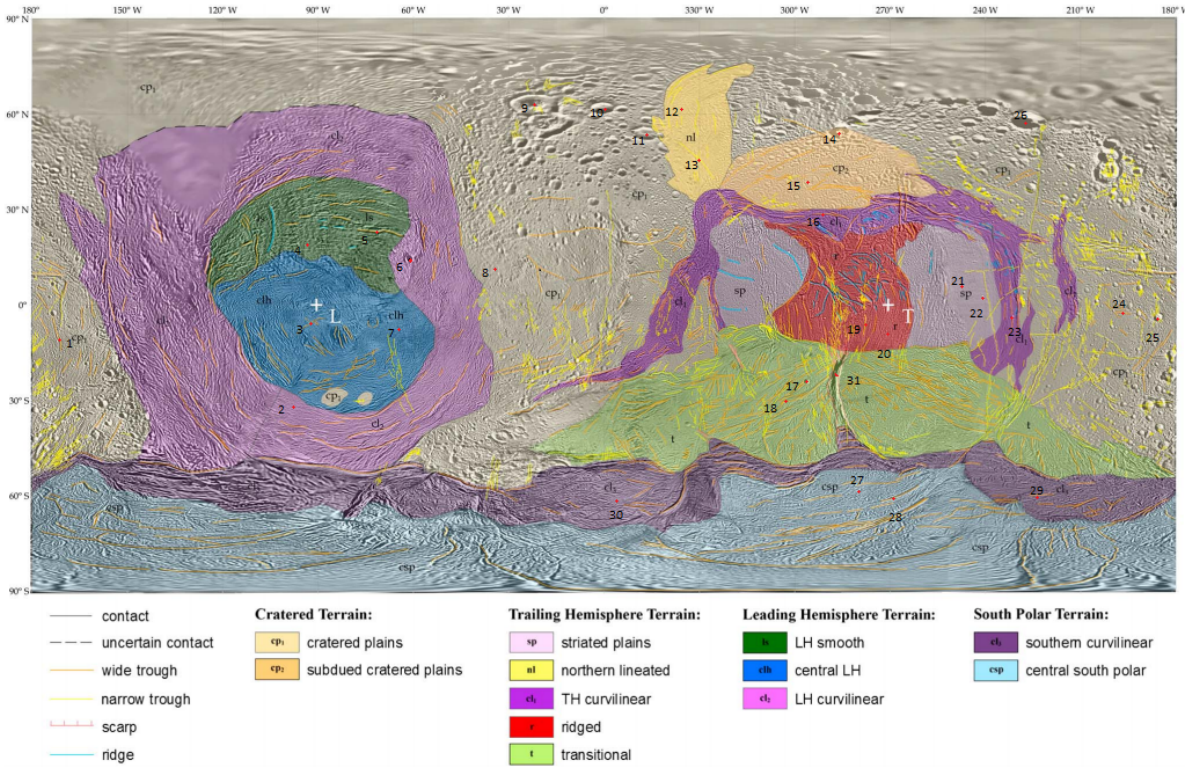

km. This means that the overall area differences per pixel are less than an order of magnitude.

5.3. Processing

The VIMS data available from NASA's PDS database consists of so-called data cubes. This refers to the fact that the data could be represented as a cube, with two axes mapping to the locations of the pixels in the image, and the third dimension being the bins of the spectrometer.

The data on the PDS database is mostly unprocessed. Artifacts due to communication errors have been removed before the data was made available on the database, but the data itself hasn't gone through any further calibration and processing yet. The methods used for this further processing is described in section 5.3.1.

5.3.1. The ISIS3 toolbox

The VIMS data can be read using the USGS Integrated Software for Imagers and Spectrometers (ISIS). This software suite contains tools for calibrating, orthorectifying and processing the spectral information.

Calibration and Orthorectification Pipeline

Calibration of the VIMS images requires several steps. The first step is to split the VIMS spectral cubes between an image holding the visual spectral information and the IR spectral information. This is both required for further processing by ISIS and isolates the IR spectral information from the Visual spectral information, allowing the IR data to be processed in isolation, reducing the storage overhead that would be present if the Visual data was included as well, as the visual spectrum information is not of interest to this study.

The next step is to add information from NASA's spice kernels to the data cubes. These kernels contain a wealth of information that is necessary for the calibration and orthorectification of the data, including spacecraft attitude and positioning data, instrument information and information on the location and shape of the target, which in this case is Enceladus.

Table 5.1: This table contains the locations of the 31 points. The final columns gives a rough indication of the best spatial resolution of the location available. The pixels are often rectangular in shape, with one side being less than 10 km, and the other side being significantly longer. Here, the rough length of the longer side is given.

location number	Latitude	West Longitude	Best VIMS-IR resolution
1	-10.93	171.26	20 km
2	-32.06	97.65	20 km
3	-5.83	92.19	30 km
4	18.95	93.28	30 km
5	22.96	71.42	50 km
6	14.21	61.21	30 km
7	-7.65	64.49	10 km
8	11.30	34.25	20 km
9	63.04	21.86	30 km
10	61.58	359.64	30 km
11	53.56	346.52	30 km
12	61.58	335.22	40 km
13	45.55	330.12	20 km
14	53.93	286.03	30 km
15	38.62	295.87	30 km
16	28.42	291.13	50 km
17	-24.05	296.23	20 km
18	-30.24	302.79	20 km
19	-6.19	277.65	10 km
20	-9.11	270.73	20 km
21	5.83	247.41	10 km
22	2.19	240.85	10 km
23	-4.01	231.74	10 km
24	-2.55	196.76	10 km
25	-5.83	185.83	10 km
26	57.21	227.37	30 km
27	-58.66	279.84	10 km
28	-60.85	268.91	10 km
29	-60.49	223.72	10 km
30	-61.58	355.99	10 km
31	-22.23	287.49	10 km

After the Spice kernels have been added, the data can be calibrated to remove the effects of dark current and apply a flat field correction to account for differences in sensitivity between pixels. These are some of the most common errors in imaging, and accounting for them is a necessary step to making the data usable.

After the data has been calibrated, it can be projected to a map format, which in turn makes it possible to determine which pixels correspond to the locations detailed in section 5.2. Map projection also makes the image as a whole more legible and easier to understand, as the deformation caused by different pixel resolution and camera movement are removed.

The process of orthorectification, or map projection, functions by employing the spice kernels to precisely determine the position and orientation of the Cassini spacecraft and the VIMS instrument with respect to Enceladus over the time it took to take the specific image. This in turn allows the position on Enceladus' surface of every pixel to be determined.

Figure 5.3: The image on the left is the calibrated and orthorectified image, while the image on the right is the uncalibrated raw image.

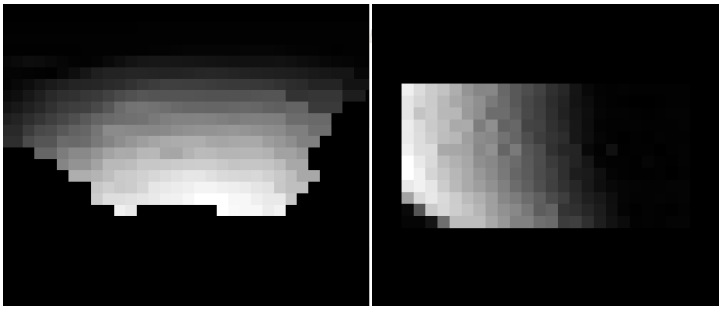

Figure 5.3 shows an example of an uncalibrated and calibrated and mapped VIMS image of part of Enceladus north-polar region. This image in particular shows off the importance of orthorectification, as it is necessary to understand the image by placing it in the proper context. In particular, a crater can just about be made out in the centre of the orthorectified image, while it cannot be made out in the raw image.

5.3.2. Data and mosaicing

From the PDS database a set of high resolution VIMS images covering the chosen locations have been chosen. Around the south-pole, as well as select areas around the equator resolutions better than 1 km^2 per pixel can be reached, but in other areas pixels would be between 5 and 10 km per side. The list below contains all the VIMS images that have been used. The numbers identifying each image relate to the time at which the picture was taken.

- v1487302144
- v1489049916
- v1489050098
- v1489050265
- v1489050426
- v1489050584
- v1500060239
- v1500060456
- v1500061406
- v1597180162
- v1597180327
- v1602274076
- v1604167764
- v1604167799
- v1604167943
- v1637464787
- v1637465327
- v1637465438
- v1637466003
- v1652859600
- v1696174411
- v1711571239
- v1829240892
- v1829241298
- v1858923149
- v1858923675

To make large-scale comparison easier, these files have all been collated in a single mosaic covering a significant part of Enceladus. Where overlap between multiple images exists, the pixels have been averaged to create the new pixels. Given the diverse set of images used, some clear brightness differences are visible in figure 5.4. This brightness is caused by different levels of illumination the instrument received, which could be due to some images being taken while the imaged part was turned towards the sun, and other images being taken while that section was partly or wholly in shadow. These

differing brightness levels necessitates measures during processing to ensure that brightness does not play an important role when presenting the results. This can be achieved easily by scaling the spectra individually before processing, or by focusing on relative differences within the spectra, rather than absolute values.

Figure 5.4: The IR mosaic of Enceladus. The differences in pixel brightness are based on the total light received across the spectrum for each pixel. The fully black areas of the mosaic are not covered by any of the pixels fo the component images. Most other areas are covered by at least two overlapping images, with the north polar area between 180^o and 120^o west and between 270^o and 180^o west being an unfortunate exception. Only one image covers these areas, and images of the north pole often have very low resolution as most of the passes of Cassini by Enceladus have been focused on the southern hemisphere. Because of this, measurements in these two areas should be treated with some caution.

6

Spectra interpretation - Non water ice species

Determining the presence of non-water ice species is done in two steps. First a visual inspection of the spectra of the predetermined locations is performed. This will provide a first estimate of the presence of non-water ice species based on the spectral absorption features present. This can then be expanded on by using computer processing to confirm the presence of the detected species and determine how wide-spread the absorption features are. Section 6.1 will detail the approach and results of the visual inspection, while section 6.2 will detail the results of the identification of non-water ice species.

6.1. Visual inspection

This section will provide details on the visual inspection of the spectra at the locations identified in chapter 5. Subsection 6.1.1 will explain the methods used during the visual inspection, while subsection 6.1.2 presents the overall results.

6.1.1. Approach

For interpreting the spectra, the first step will be to simply determine the location of all the features in the spectra. In an ideal spectra this would be relatively easy, but in real measurements noise will play a role, making identifying smaller features more difficult. For excessively noisy spectra, taking the average of several pixels could aid in reducing the noise, but this will result in a reduction in spatial resolution. Alternatively, a Gauss filter could be applied, which will allow for the original spatial resolution to be kept. Depending on the size of the Gauss filter, it could end up suppressing small localized features by adding in contributions from pixels that do not have that feature, or alternatively end up spreading out a very strong feature present in one pixel over a larger collection of pixels.

Once the locations of possible features within the spectrum have been determined the identification process can begin. Some features will obviously belong to water ice, but others are less obvious, and it is in features such as these that the more interesting compositional information lies. Though in a clean sample determining which features belong to which species can be fairly simple, the potential presence of noise or other artifacts within the remote sensing data means that each feature needs to be approached with a degree of caution to avoid identifying a spike of noise as a feature, or vice-versa. This can become an issue in the 4 to 5 micron range in particular, where noise effects seem to become more significant.

To aid in the deciphering of the infrared spectra, its helpful to first establish what species are expected. For this, the comparison with the species found in cometary and interstellar ices is useful, with the main non-water species being CO, CO_2, NH_3 and CH_4. Each of these species has characteristic lines in the 0.8 to 5 micron range of the VIMS data, as shown in table 6.1.

Figures 6.1, 6.2 and 6.3 show the spectra for CO, NH_3 and CO_2 respectively. The figures for CO_2 and NH_3 also include the spectra for water ice as well. Note that in each case the features of the non-water ice species are very sharp when compared to the water ice species, which should make

Table 6.1: The absorbance lines of CO, CO_2, NH_3 and CH_4

Specie	**Centre of absorbance lines (in micron)**	**vibration mode**
CO	4.68[16]	CO stretching
CO_2	2.13, 2.7 and 4.24-4.30[13][10]	Asymmetric stretching overtone, symmetric+asymmetric stretching and asymmetric stretching
NH_3	2 and 2.2[12]	Symmetric bend+symmetric stretch and symmetric bend+degenerate bend
CH_4	2.22 and 2.38[30]	Degenerate stretch+degenerate bend and Symmetric stretch+degenerate bend
H_2O	1.5, 2.02 and 3[31]	symmetric stretch+asymmetric stretch, symmetric stretch+bend+asymmetric stretch, symmetric stretch

them fairly easy to identify if they are present. Lastly, figure 6.4 shows the 4.24-4.30 feature of CO_2 ice. Note how the band centre of that feature changes depending on different circumstances.

Figure 6.1: This spectra taken from the Leiden database for ice and part of a study on interstellar surface chemistry [11] shows the main feature of CO ice at 4.68 micron in absorption. There is also a smaller feature around 3 micron, but this feature will not be visible in VIMS images because of the depth of the water feature at 3 micron.

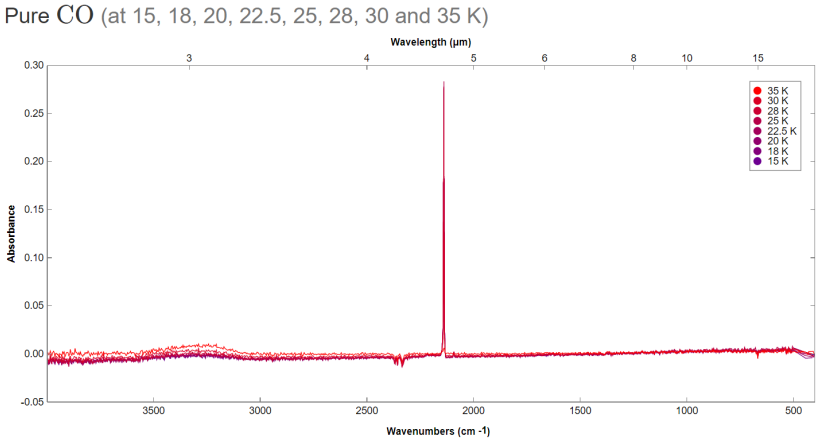

Using these species as a starting point should reduce the number of unknown features. The presence or absence of these different species can also already provide some clues to the evolution of Enceladus' surface and the origin of the moon as a whole. Some theories regarding the icy moon's formation would require the moon's makeup to be similar to that of comets, so the presence or lack off certain species could confirm or deny that theory[32][33]. Furthermore, the presence of certain materials could contain information about the moon's thermal history as certain temperatures might cause certain species to be evaporate away from the surface.

6.1.2. Initial inspection

The first round of inspection of the spectra was done purely visually. An example of this can be seen in figure 6.5, which is a spectra taken at location 27. The various water features, marked by the white dotted lines are all clearly visible. The same is not the case for CH_4, which is marked by the yellow lines, nor for CO and CO_2, which are marked by the purple and red lines respectively. There is a potential feature at the 2.2 micron location for NH_3, but since there is no accompanying feature at 2 micron ammonia is most likely not present in this spectrum either.

Closer inspection revealed the potential presence of NH_3, CO and CO_2 in some spectra. The signatures of these species are extremely small compared to the signals of the water ice, which leaves the possibility of them merely being the result of noise in the signal, in particular where CO is concerned, as the spectra tend to get noisier in the longer wavelength 'tail' after the 3 micron water feature. To

Figure 6.2: These spectra from[12] show the features associated with ammonia in absorption. This thesis focused on the 2 features within the 2 micron feature, as the larger feature in the 3 micron region is drowned out by the large 3 micron water feature.

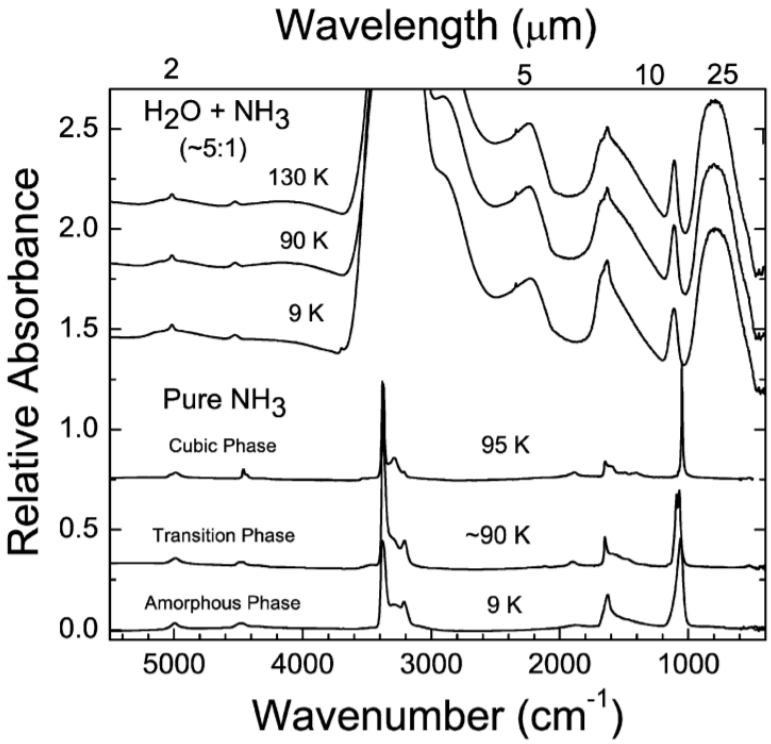

ascertain their presence, further processing of the signal is necessary.

6.2. Non-water ice mapping

This section will detail the methods and results used for the automated detection of non-water ice species. Section 6.2.1 will provide the basic overview of the 2 micron water ice feature, within which a number of features for non-water ice species occur. Section 6.2.2 provides an overview of the possible methods for automated detection, while section 6.2.3 goes into more detail on the past uses of the chosen method. Section 6.2.4 details the implementation of the chosen approach, while section 6.2.5 provides details on the quality of the fits. Finally, sections 6.2.6, 6.2.7 and 6.2.8 provide the results regarding detections of CO, CO_2 and NH_3.

6.2.1. The 2 micron water ice feature.

As established in section 6.1, two of the non-water ice species that are potentially present, CO_2 and NH_3, have features within the 2 micron feature of water ice. To find these features, the overall properties of this water feature need to be taken into account. Unfortunately, the 2 micron feature is not a simple feature, but rather consists of three separate components, centered on 1.99, 2.02 and 2.06 micron respectively[14]. These components are most likely created by bending and stretching effects.

The compound nature of the feature has a number of effects, which can be seen in figure 6.6. Most notable is the way the shape of the feature changes as a function of temperature. Figure 6.6 Shows the spectra at different temperatures, with steps of 50K between each spectrum. The 2 micron feature changes with temperature, with the longer wavelength contribution becoming more pronounced as the temperature decreases, resulting in a flatter bottom of the feature. Fortunately, temperature differences on Enceladus are overall fairly small, with only about 30 to 40 kelvin difference between the warmest and coldest areas, which means changes in the feature should remain fairly small. Nevertheless, this is something that needs to be kept in mind when processing the 2 micron feature.

The surface temperature on Enceladus varies between about 40 and 80 Kelvin [34], which means that the 2 micron feature on Enceladus would resemble one of the two coldest spectra in figure 6.6,

Figure 6.3: This spectrum shows a 5:1 mixture of H_2O and CO_2 at 15 Kelvin[13] in transmittance. The 2.13, 2.7 and 4.26 features are all marked. Note how sharp these features are with respect to the surrounding water features and continuum.

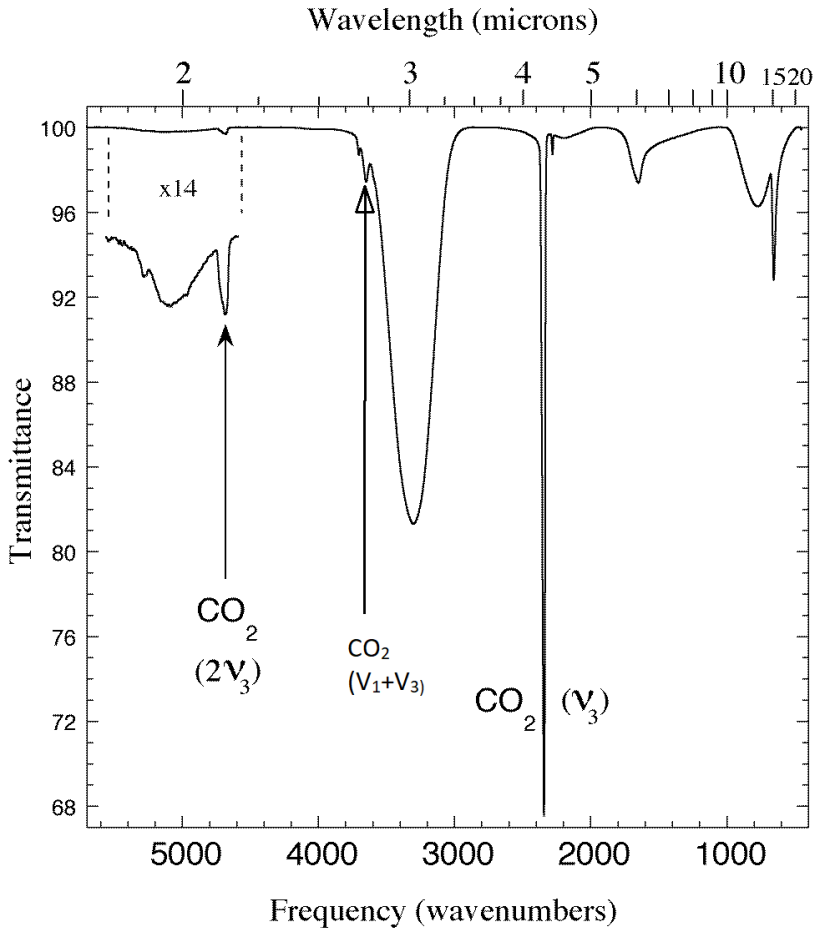

Figure 6.4: These spectra shows a closer look at the 4.26 micron feature of CO_2 ice in absorption [10]. Note how the band centre shifts between 4.24 and 4.30 micron depending on factors like crystallinity and temperature.

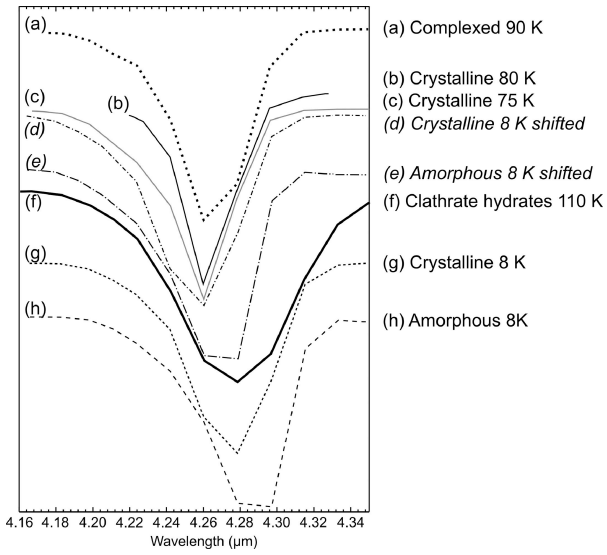

Figure 6.5: The spectra of location 27, from VIMS cube 1500061406. The wavelength is given in micron. The pixel value is the light intensity reaching the instrument, with a value between 0 and 1.

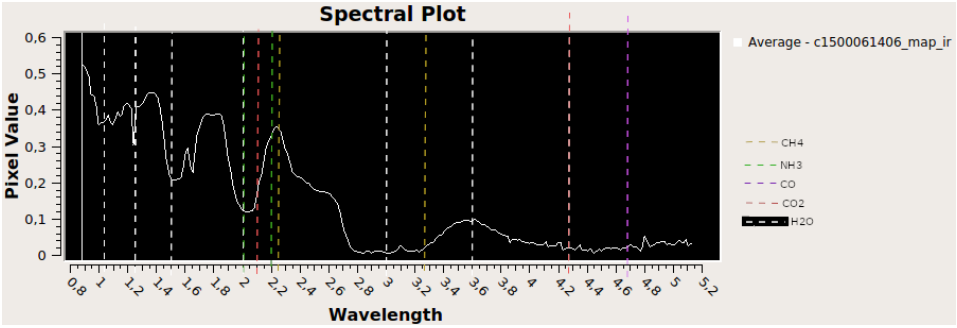

Figure 6.6: The spectra of water ice from 1.2 to 2.8 micron[14].

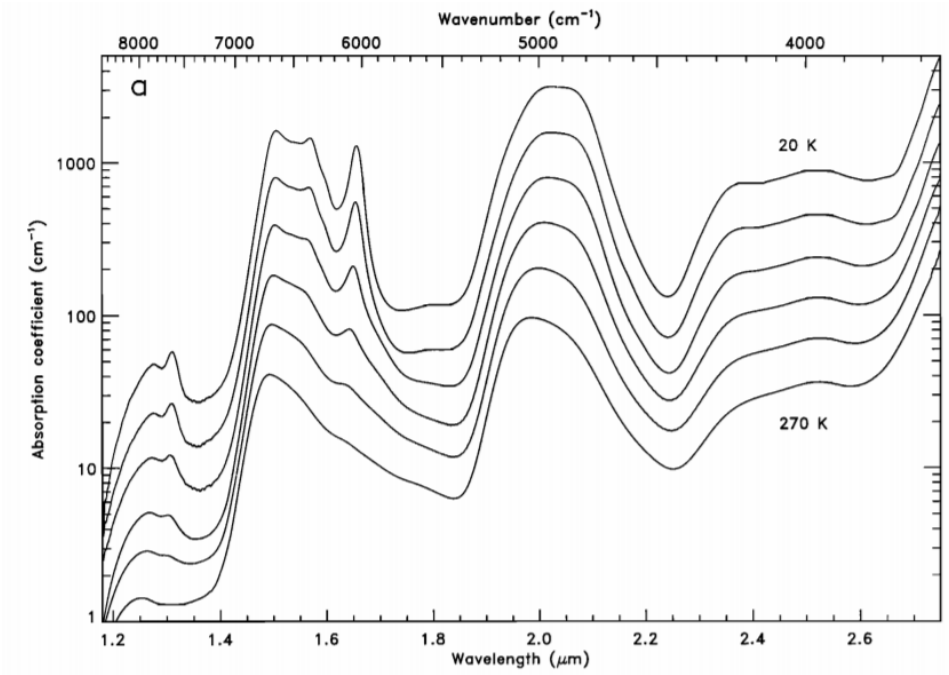

with the feature itself being mostly symmetrical with a rather broad flat top.

6.2.2. General overview of the possible methods

Any method for automated searches for non-water ice species needs to be able to handle 2 distinct sections of the water ice spectra. The first is the 2 micron feature detailed in section 6.2.1. The second is the 3.6-5 micron 'tail' of the spectrum, which tends to be very noisy. There are a couple of approaches that could be taken.

Figure 6.7: The black line shows a VISM spectra of Saturn's moon Rhea, while the red line provides a Hapke model made based on VIMS data of Rhea[15].

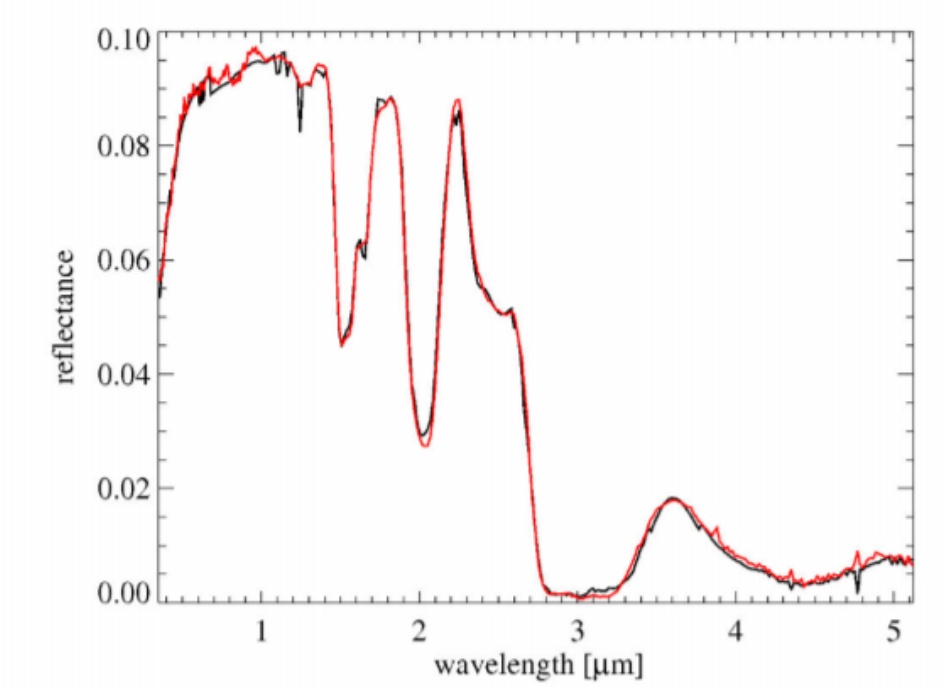

First, the entire water ice spectrum could be simulated with a model such as the Hapke model[35]. Figure 6.7 provides an example of a Hapke model created using VIMS data for another of Saturn's moons, Rhea. The red line provides a fairly good approximation of the data presented in black, with only minor deviations. Some of tehse deviations, such as the difference in shape of the crystallinity dependant 1.65 micron feature, can likely be attributed to inputs in the model that don't quite match reality. Such models can provide very accurate simulations of the spectrum of the infrared spectrum of water or other species under real conditions, but to do this they require a large variety of input data ranging from the temperature of the ice to the characteristics of the illumination to the angle of the camera with respect to the ice during the observation to the size of the ice crystals themselves. Some of these inputs, such as the crystal size of the ice, are currently unknown and can have significant impacts on the model, as can be seen in figure 6.8 which shows how water cie spectra change for different crystal sizes. Because of this and the complexity of the model, building such a model is considered outside of the scope of this thesis.

Alternatively, one could use the results of laboratory measurements to remove the features of water ice from the spectra, leaving only the features of the non-water ice species. Such measurements have the opposite problem of using a sophisticated model like the Hapke model, as such a measurement needs adjusting before they fit the real-life measurements, and such adjustments will be different for every spectrum. The most readily available database of ices also does not include the 2 micron feature of water ice, which is where a number of the major markers for non water ice species can be found.

The third option is to fit the spectra using more basic equations such as polynomials or Gaussians. Polynomials are commonly used for determining the continuum in sections of the spectrum[17], with the most common sue being to fit the continuum over a larger feature to establish a baseline. An example of this can be found in figure 6.9, which shows two possible fits for the continuum across a feature of

Figure 6.8: This figure shows IR spectra for water ice for a number of different crystal sizes, as modelled using the Hapke model[9].

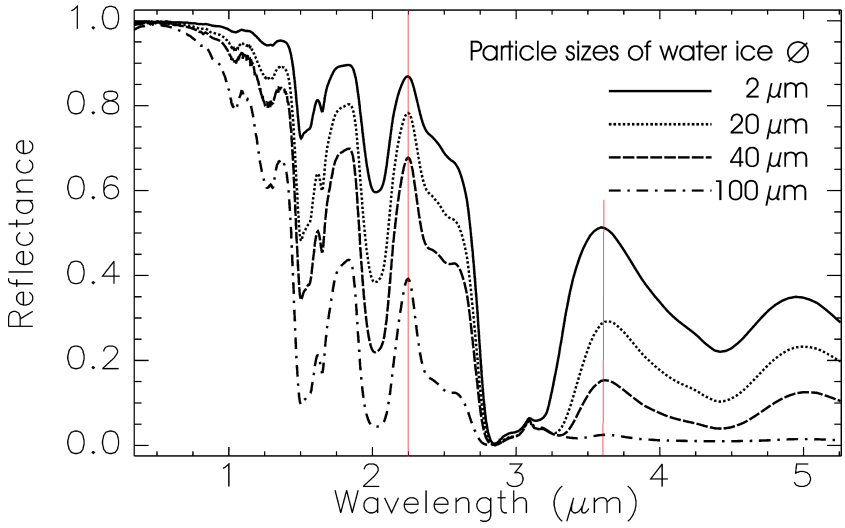

Figure 6.9: This figure shows the 13 micron feature of CO_2 in water ice, with a 1st and 2nd order polynomial fitted to establish the continuum due to the influence of water ice across the feature[16].

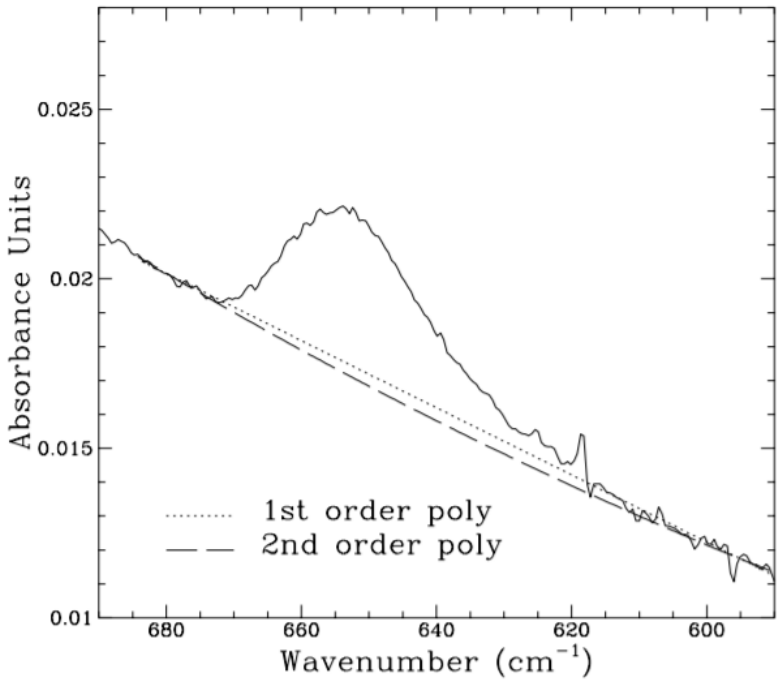

CO_2 in absorption, one using a 1st order, and one using a 2nd order polynomial. In addition to fitting the continuum, polynomials have also been used to fit the lower sections of features to determine the exact band minima independently from the spectrometers spectral resolution[36]. Polynomials have also been used smooth and reduce noise in spectra[37] by fitting larger sections using series of partially overlapping low order polynomials. Polynomials would be a particularly good solution for processing the tail, while they could be used for determining the presence of non-water ice species in the 2 micron feature by making use of the relatively sharp peaks. A low order polynomial would not fit these narrower features. Figure 6.10 shows an impression of the way a low-order polynomial fit would behave on a mixture of water ice and CO_2 ice. This makes polynomials suitable for initial detection of non-water ice species, and processing the 3.6-5 micron tail. However, the accuracy would most likely not be high enough for accurately determining band strengths, which in turn would mean little information could be gleaned about the abundance of non-water ice species using this method.

Figure 6.10: This spectrum shows a 5:1 mixture of H_2O and CO_2 at 15 Kelvin[13]. The red curves show how a low order polynomial fit on parts of this spectrum is expected to look.

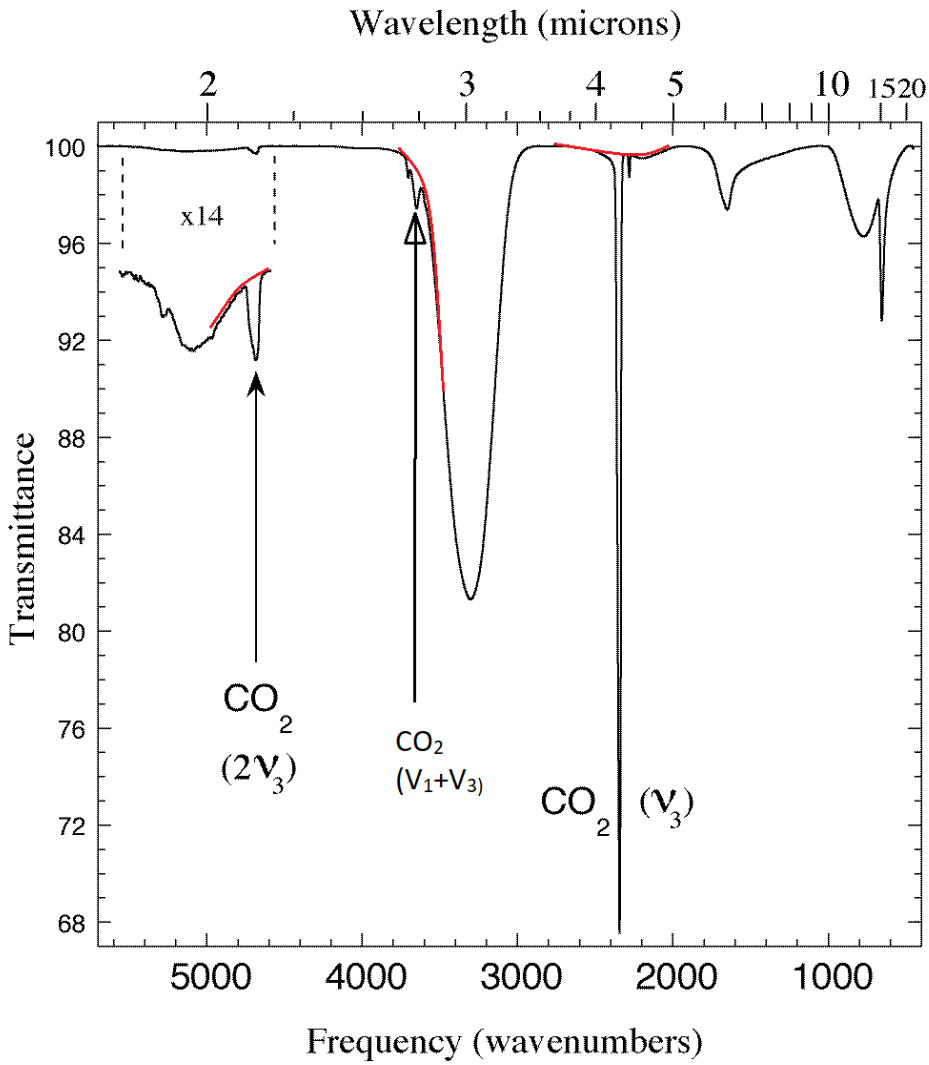

Gaussians are commonly used for a process known as curve deconvolution, where an IR feature is broken down in its component parts represented as Gaussian curves of varying size. This allows for more accurate assessment of the quantities present of non-water ice species, but is far more computationally intensive, as a deconvolution of the 2 micron feature for Enceladus would require 6 Gaussains (3 for the water feature itself, 2 for the 2 ammonia features and 1 for the carbon monoxide feature), in addition to a polynomial fit for the continuum. Figure 6.11 shows a Gaussian deconvolution

for the water ice spectrum from 1 to 2.7 micron. Note that the 2 micron feature itself consists of 3 Gaussians, with several neighbouring features also impacting the 2 micron feature.

Figure 6.11: The top line shows an IR spectrum of water ice ine mission, while the lines below that show a Gaussian deconvolution of the spectrum[14].

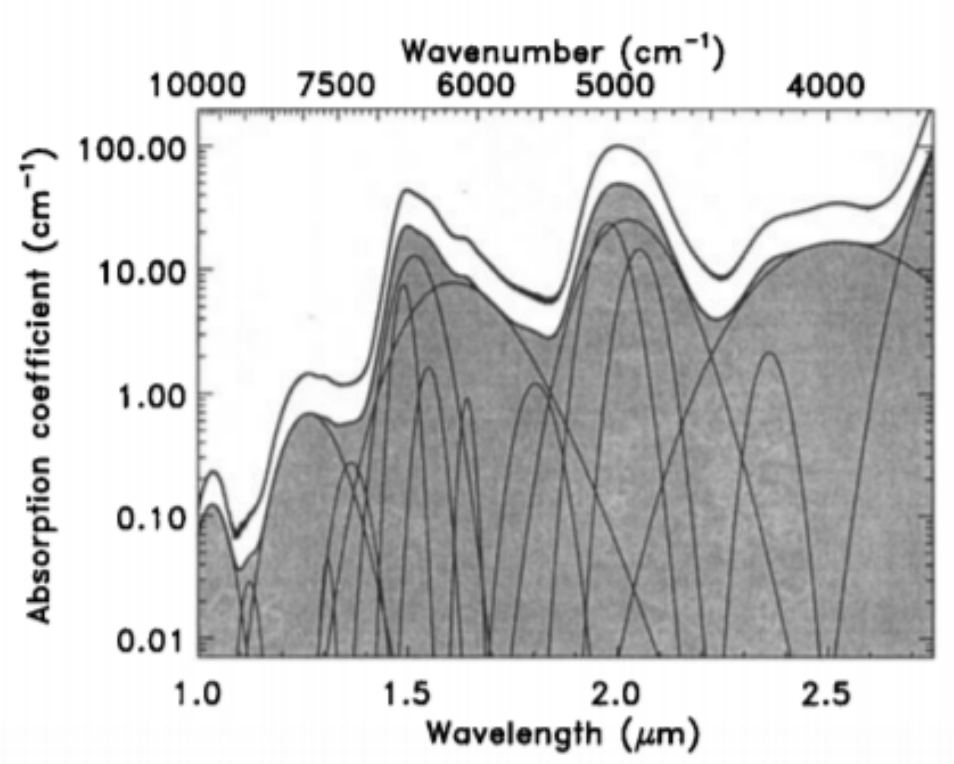

Gaussians are also less useful for the features in the 3.6-5 micron tail. The features themselves would be rather sharp, covering only about a 1-3 bins area making a fit very difficult. The Gaussian fitting method would also not be very useful for finding the features in the first place.

Because of the large volume of available infrared spectra, the polynomial method was selected over the Gaussian method to keep computational times manageable. The consequence of this is that detections will be considered in a binary present-or-not state, rather than going into more detail with regards to abundances based on band strengths, as the polynomial method will not be accurate enough for estimating abundances.

6.2.3. Previous use of polynomials

Plynomials have been used in past spectroscopic studies for a number of purposes. The most common uses are for determining the continuum[17], determining band-minima and band-centres[36] and for more general interpolation between data points [38], but the technique of fitting polynomials has been used to smoothe out spectra and reduce noise as well[37].

The use of fitting polynomials for determining band minima and for interpolation share a large overlap. Without further processing the band minima or wavelength of the lowest point of an absorption feature can be approximated by simply taking the location of the lowest measurement in the range in which the band minimum is expected to lie. However, interpolation using a cubic spline, or a 2nd order polynomial can be used to determine where the true band minimum would be located. The robustness of this method can then be further increased by re-sampling the spectra using random noise or measuring errors and making additional polynomial fits, using the average band minima of these fits to determine a true minimum[36].

The Use of polynomials to establish a continuum is of greater interest to this study. The continuum is generally what a spectrum would look like if there where no absorption bands present, and can be considered a combination of curves, such as the black-body curves of the reflected light and emitted radiation from the target body, as well as other factors and optical effects [39]. Removing the continuum

Figure 6.12: This figure from [17] showcases the use of a polynomial continuum to enable a gaussian fit of a feature on real data.

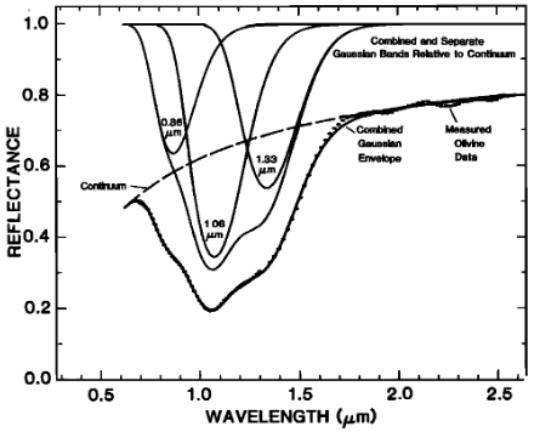

from a measurement allows for more precision with advanced fitting techniques like curve deconvolution using Gaussian fits, as shown in figure 6.12. This figure shows a mineral example at 1 micron, but it can be applied to other species in other parts of a spectrum just as easily. This part of the technique is used in this study in the 3.6-5 micron tail, where makers of CO_2 and CO could be present. By determining the continuum in this section, areas that deviate can be detected and analyzed. An example of this can be found in figure 6.13. Note how the blue line shows a clear peak at 2 micron, while the polynomial fit in orange only follows the overall shape of the curve, leaving the peak visible as a clear deviation.

Figure 6.13: This figure shows two polynomial fits on the 2 micron feature. The lines in red and orange are the polynomial fits, while the lines in blue and green are the data.

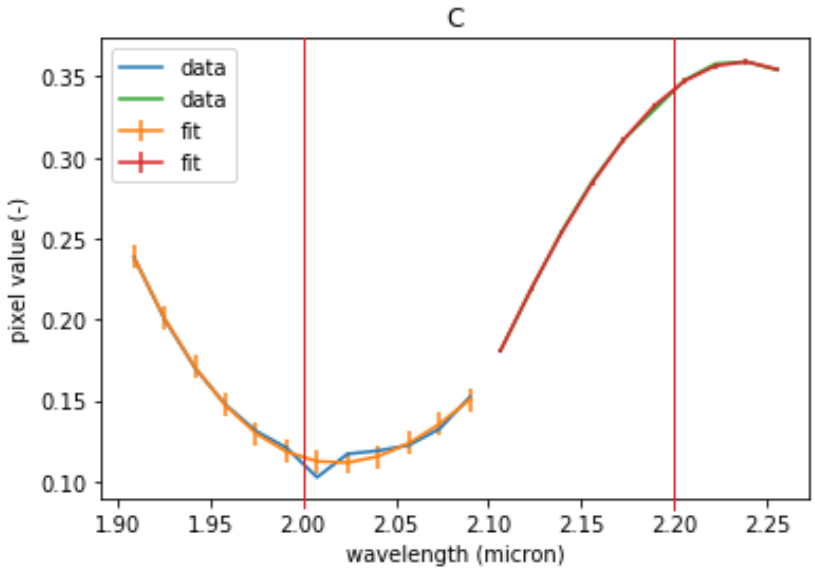

For processing the 2 micron feature, a process similar to the one used in[37] will be used. 2 or 3 third order polynomials will be used to fit the 2 micron feature. The low order of the polynomials ensures a smooth rendition of the feature, with smaller features such as those associated with NH_3 not being fit. These smaller features will then stand out when subtracting the smooth fit from the actual measurements, which in turns allows for automatic detection.

It should be noted that polynomial fitting is not a replacement for other techniques, such as curve matching with laboratory data and curve deconvolution using Gaussians. Rather, it is a tool suitable for first order estimates and qualitative detections. It also has the advantage in that it is computationally

less demanding than curve deconvolution, allowing for large data-sets to be processed in short amounts of time. Finally, the method is very repeatable[39]. When using the same data with a similar order polynomial and similar size of the fitted area, the fit itself should be the same, as there is only one possible solution to converge towards. If polynomials of a far higher order are used then issues could arise, as the polynomial would also fit the far smaller features, but as long as polynomials of relatively low orders are used, this will not be a problem.

6.2.4. Approach

Python will be used for the fitting procedure. To make the data-cubes readable for python, they are converted to an ASCII format using the ISIS suite. The code for extracting non-water ice species will have three variations. One variation is designed for the 2 micron feature, where the markers for NH_3 are present, one focuses on the 3.6 to 5 micron 'tail' where a feature for CO_2 and the feature for CO are present and the final variation will focus on the left side of the 3 micron water ice feature, where another feature of CO_2 is present.

Figure 6.14: This figure shows a spectrum from the same area of VIMS image 150061406. The upper spectrum has not been processed with a Gauss filter, while the lower spectrum has been.

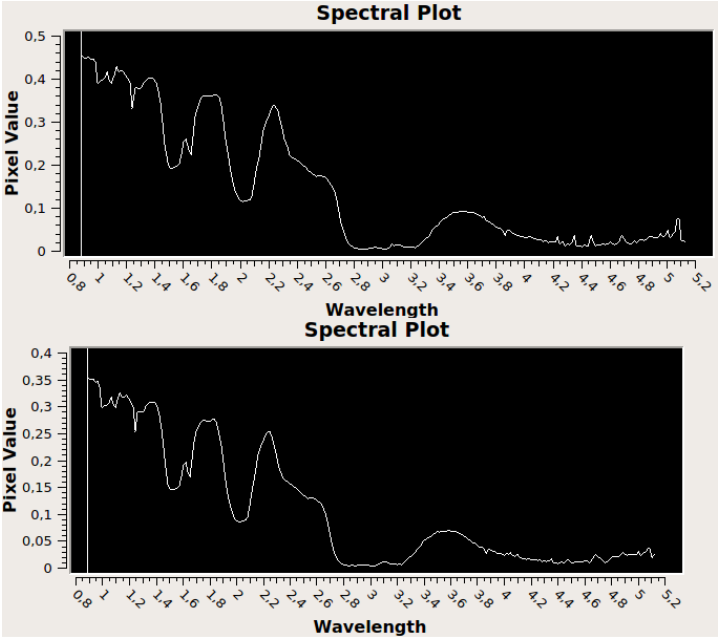

The first step is to extract the spectra from the ASCII files. The data imported from ISIS for the two programs will also be slightly different, with the programs dealing with the longer wavelength tail using data that has been processed using a 3x3 Gauss filter. This might remove or shrink features present in only 1 pixel, but it will reduce the overall noise. Figure 6.14 shows a spectrum from one of the VIMS images to demonstrate the differences between an pixel that has been processed using the Gauss filter, and one that has not been processed using the filter. The most notable differences are the reduction in noise in the tail area, and the overall reduction in the pixel values, or brightness, of the spectrum.

The fitting for the 3.6-5 micron tail is done in two steps. First a global fit of the tail is made using the relevant portion of all the spectra in the VIMS image at once. This method should ensure that the fit is a good match for the water features and doesn't include any deviations from the non-water ice species unless those are omnipresent, which has been established to not be the case by manual inspection. The global fit is then matched to the individual spectra by moving the spectra up or down and scaling it to the range of the data to account for individual differences.

Fitting the 2 micron feature is done in a single step, using 2 3rd degree polynomials to fit each spectrum individually. Making the two fits in a single step has several disadvantages, but it is necessary because factors like crystallinity and to a lesser degree temperature can change the shape of the 2 micron feature. It would be difficult to determine whether a difference between the fit and the data

would be due to differences caused by crystallinity or the presence of a non-water ice feature if a global fit was made first. The major downside of fitting each spectrum individually is that the fit will attempt to shape itself to account for non-water species as much as the low order of the polynomial allows, which will reduce the amount of positive detections as both the difference between any features and the main fit decreases, while the total error in the fit increases, which raises the thresh-hold necessary for a certain detection. The left slope of the 3 micron feature is fitted similarly to the 2 micron feature, but uses only a single 3rd order polynomial.

For the best polynomial fits, a range for the fit needs to be chosen that only contains a major curve. For example, for fitting the entire 2 micron feature, 3 polynomials would be needed at least. One to fit the bottom curve, and one each for the left and right 'wing'. Figure 6.15provides an example of two of the three fits for the 2 micron feature, with one polynomial for the bottom curve, and another on the right wing. Fitting too large an area can worsen the fit as the polynomial tries to adapt to too many curves, while fitting too small an area could lead to over-fitting. Generally speaking, a section 0.15-2 micron wide, containing around 10 data points centered on the feature location provides good results for fitting the 2 micron feature.

Figure 6.15: An example fit on the 2 micron spectra. The blue line is the data, the red line is the fit. The fit consists of 3 third order polynomials.

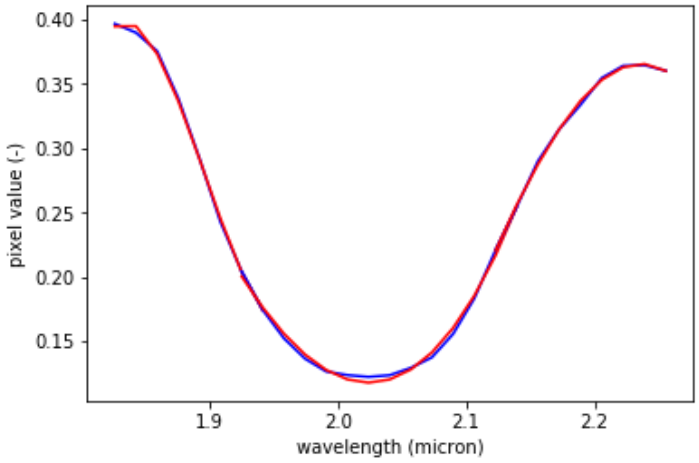

Once the fit is known, the size of the deviation in the area associated with the non-water ice species can be calculated. A 3-5 bin sample centered on the location of the expected deviation is subtracted from the fit and any negative differences in the area are set to 0, as a negative value would indicate part of the data being located above the fit, suggesting that they are not part of the feature. The largest remaining difference is then taken and compared with a value equal to 3 times the standard deviation of the residuals, and only if the difference is greater than that is the feature considered a detection. Once all spectra are processed, the results are plotted as an image indicating the locations in which detection have occurred. Figure 6.16 shows a typical spectrum fora non-detection. The data and the fit do no differ much at any location within the spectrum. Compare this with the spectra in the sections 6.2.6, 6.2.7 and 6.2.8, which show spectra where detections were made.

6.2.5. Fit quality

To assess the quality of the fits, the root mean square error has been calculated. This value represents the standard deviation of the residuals and therefore gives a representation of how closely the fitting method is representing the data. The RMSE has been normalized using the range of the data to allow for comparison between different spectra.

$$RMSE = \sqrt{\Sigma_{i=1}^{n}\left(\frac{OBS_i - fit_i}{n}\right)^2} \tag{6.1}$$

$$NRMSE = \frac{RMSE}{OBS_{max} - OBS_{min}} \tag{6.2}$$

Figure 6.16: A fit on the two sections of the spectra used for finding NH_3 features. In this fit, no detection was made. The data does not differ from the fit by more than 3 sigma in any of the locations where NH_3 features could be present. Contrast this with the spectra in figure 6.23 where detections where made.

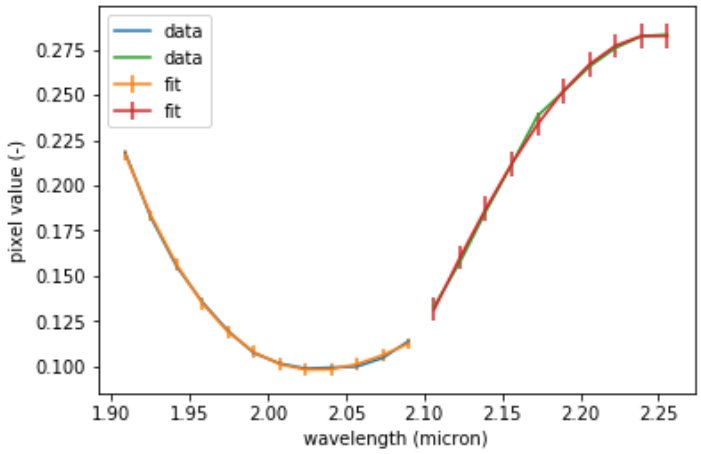

Equation 6.1 provides the equation for calculating the root mean square error (RMSE), with OBS_i the values of the data, fit_i the values for the fit, and n being the total number of data points in the fitted part of the spectrum. Equation 6.2 provides the equation for normalizing the RMSE, with OBS_{max} being the maximum value for the data and OBS_{min} being the minimum value. The OBS_{max} and OBS_{min} values for the data along each individual fitting segment are used for normalization.

Table 6.2: This table contains the mean, median, minimum and maximum RMSE for the fits. The RMSE has been normalized using the range of each individual data-set to allow for comparison. This normalization means that the error can be seen as a percentage of the total range in most cases.

Specie	NH3		CO2		CO
fit-section(micron)	1.9-2.1	2.1-2.25	2.62-2.77	3.8-4.5	3.8-5.0
RMSE mean	0.01953	0.01146	0.01993	0.1265	0.1217
RMSE median	0.01679	0.009015	0.01267	0.1258	0.1179
RMSE max	0.1563	0.1777	0.2557	0.3031	0.2491
RMSE min	0.002289	0.001287	0.003499	0.03696	0.0411

Table 6.2 Displays the mean, median, maximum and minimum RMSE values for all fits made for determining the presence of non-water ice species, split up by the individual segments fitted. These four values are chosen as they give a clear indication of both the mean fitting error, as well as the range of values the fitting error occupies. The inclusion of the median also shows whether the error of any given fit is more likely to be larger or smaller than the mean.

A couple of factors stand out clearly. First of these is the large difference between the fits of the 2 micron feature and the left slop of the 3 micron feature and of the 3.8-5 micron tail. Given the differences in noise that are visible when inspecting the spectra visually, this difference in RMSE is as expected, but it does indicate that care needs to be taken with detections based solely on spectra in this area.

In the 2 and 2.7 micron features, the RMSE is generally small, in the order of 1-3% of the total range. Furthermore, the median RMSE is smaller than the mean RMSE, indicating that that more than half the fits have a better RMSE than the mean, suggesting that the fit is a close match of the data most of the time. This also confirms that the high maximum values of the error sitting around 15% are significantly more rare than the low minimum values in the order of fractions of a percent.

Overall, this suggests that the fits for the 2 and 2.7 micron features are fairly close to the data, while the results from fits for the 3.6-5 micron tail should be approached with more caution.

6.2.6. CO

Within the infrared spectra measured by Cassini's VIMS, carbon monoxide has only one major feature, located at 4.68 micron. This poses a problem, as the spectra become steadily more noisy as the wavelength increases. The amount of noise present makes certain detection of CO more difficult, even when applying measures to reduce noise, such as averaging together adjacent spectra or applying a Gauss filter to the image. The final set of measurements was taken from images prepossessing a 3x3 standard Gauss filter to reduce noise as much as possible without running the risks of losing actual signal.

Figure 6.17: The red pixels indicate areas where the CO feature exceeded the 3-sigma detection threshold.

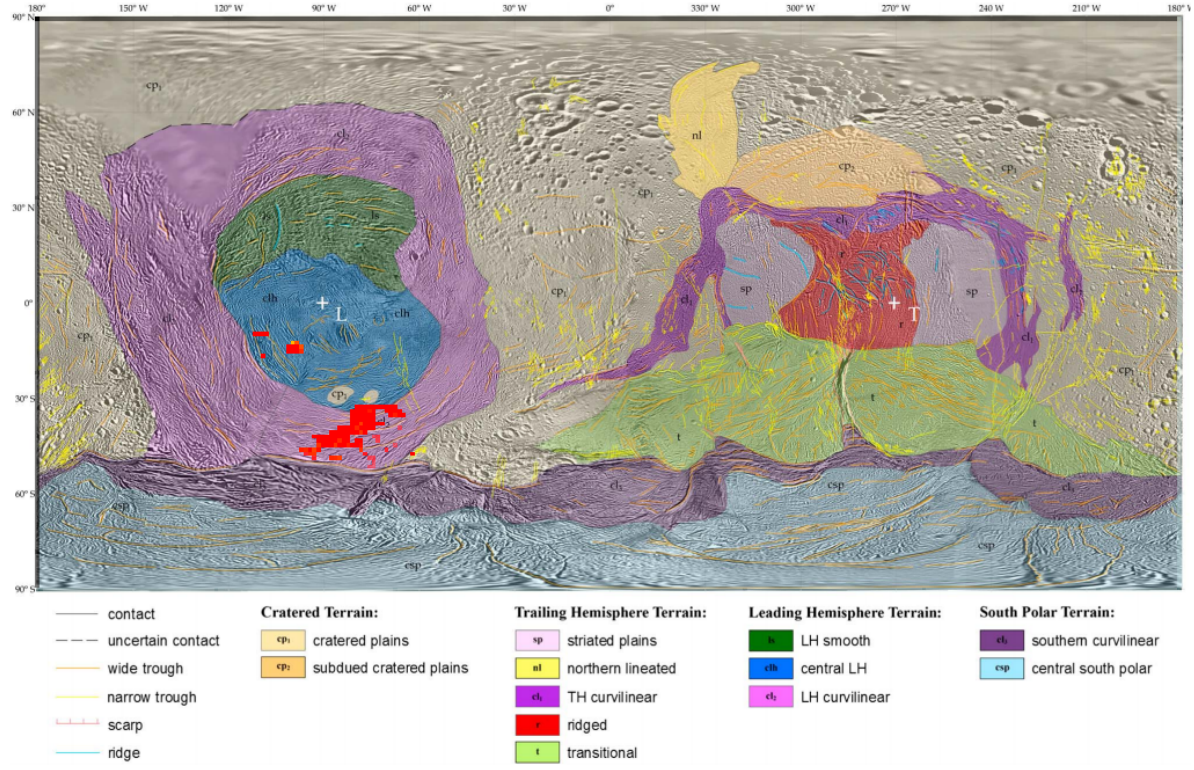

Sporadic detections on a number of the available images where made, with the most widespread set occurring in band running from -20 to -50 degrees latitude, and 97 to 66 degrees western longitude,as shown in figure 6.17. Figure 6.18 presents a typical spectra for a possible detection. Though the feature occurs in the expected place, it is generally not much stronger than some of the other artifacts present in the spectra, making it difficult to ascertain whether CO is present. As noted in section 6.2.5, the error in the residuals is still very high in this section. This means that though detections that exceed the thresh-hold of 3 standard deviations have been made, the quality of the data in this section is such that even with such a high thresh-hold, these detections can not be considered certain.

6.2.7. CO_2

There are three main features for CO_2 in water ice, located at 2.13, 2.7 and 4.26 micron. The 2.13 micron feature however is not visible in pure CO_2 ice, only in instances where CO_2 and water ice are thoroughly mixed, as shown in figure 6.19. Because of this, the 2.13 feature will not be included in this analysis. The 2.7 and 4.26 micron features are both present no matter the composition of the CO_2 ice. The feature at 4.26 micron is generally far stronger. However, the overall signal strength in that section of the spectra is far weaker, with the presence of strong noise effects, making positive detection of the 4.26 micron feature more difficult than detecting the smaller 2.7 micron feature. As with the processing of the CO feature, a Gauss filter has been used to reduce the noise and increase the likelihood of positive secure at the 4.26 micron feature.

Figure 6.18: A spectra typical for a possible CO detection. The X axis has the wavelength in microns, while the Y axis contains the strength of the light at the wavelengths as detected by the VIMS instrument. The blue line represents one set of measurements, while the orange line is the fit. The orange lines perpendicular to the fit show the 1-sigma uncertainty. The red line is the expected location of the CO feature.

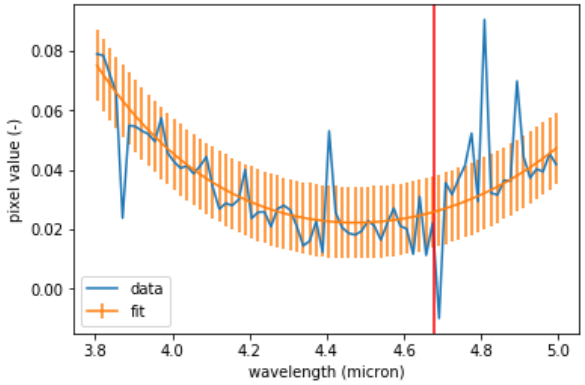

Figure 6.19: This figure shows the 2.13 micron feature of CO_2 The two top spectra shows the absence of this feature in pure CO_2 and H_2O, while the lower spectra show the feature's presence in various mixes of water and CH_3OH [13]

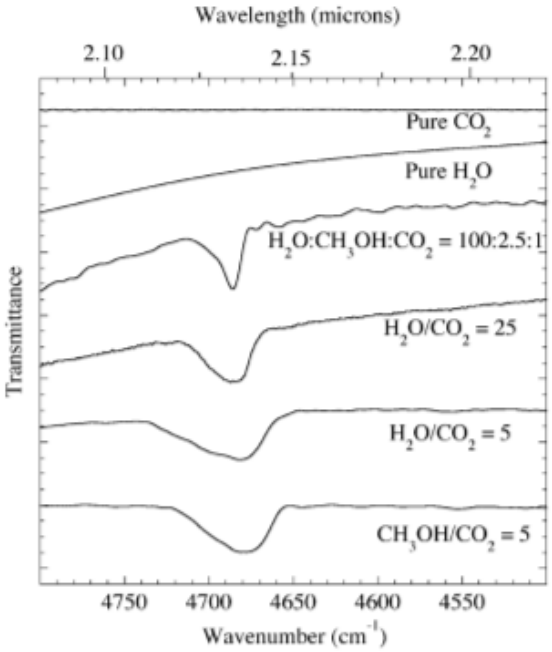

Figure 6.20: The blue pixels indicate areas in which only the 2.7 micron feature has been detected.The green pixels indicate areas where only the 4.26 micron feature has been detected, while turquoise pixels indicate areas where both features have been detected. The markers A, b, C, D and E indicate locations for which sub-spectra have been provided in figure 6.21

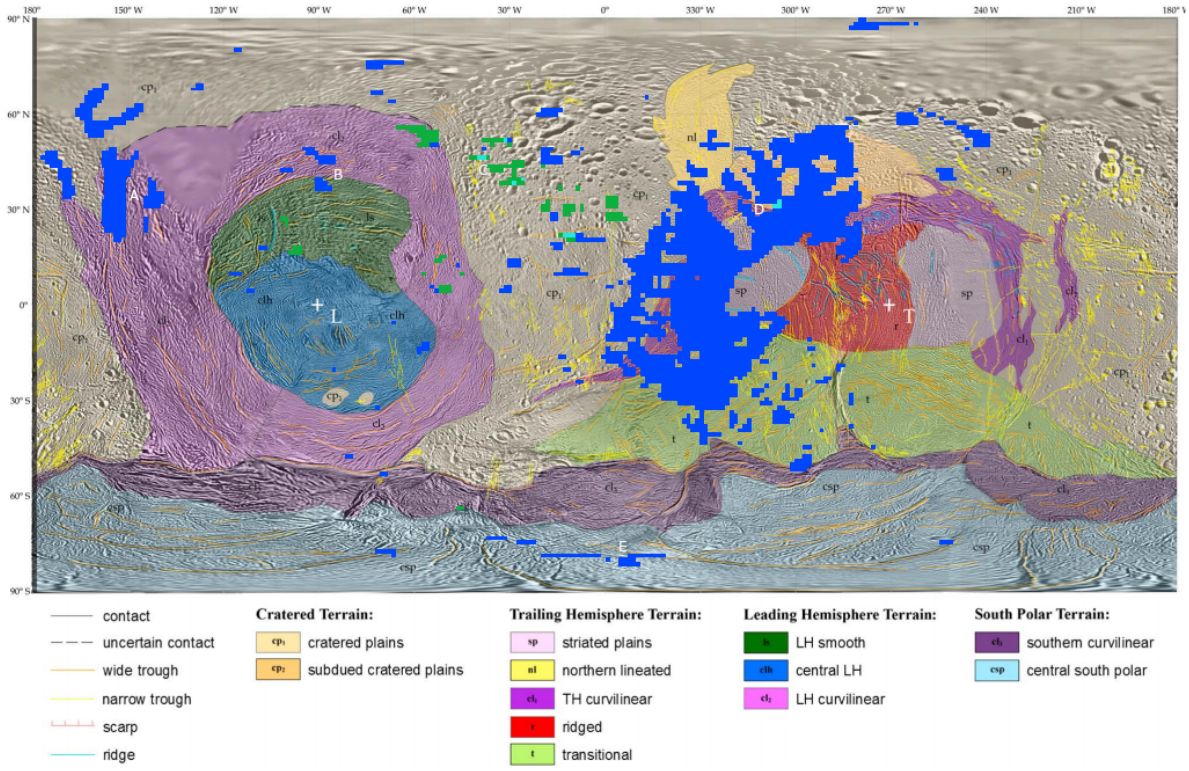

Figure 6.20 shows the detections on a mosaic of the used VIMS images overlaid on a visual map of Enceladus. The mosaic itself is represented in section 5.3.2. It does not cover the surface of Enceladus entirely, but it does cover enough so that Enceladus varied terrain and features are well represented. The detections seem to occur mostly on the trailing hemisphere, with sporadic detections on the leading hemisphere and south pole. The east end of curve of the large area of detections on the trailing hemisphere also seems to correspond to an area where accretion of surface materials due to plume material increases. The plumes themselves consist of mainly water, but some CO_2 has been measured as well[40]. The lack of detections in the zones where heavier plume accretion takes place suggests that the plume material is lower in CO_2 than the surrounding terrain. The relatively low amount of detection's in the south pole are also noteworthy, as other studies have found CO_2 in the south-polar area's using the 2.7 and 4.26 micron band[10].

Figure 6.21 shows spectra for detections in the five different locations indicated in figure 6.20. Note that the code only considers potential features located below the fit. Deviations above the line of the fit are ignored. There are a couple of things of note. First of these are the 2.7 micron features at A, B, C and D. In all four cases the data itself is noise-free and the small deviation itself is clearly visible, suggesting that these are all solid detections. The 2.7 micron feature at location E is somewhat less clear-cut, with either a noise effect or a feature at 2.64-2.65 micron appearing. The spectrum for location E is fairly typical for the south-polar area, which might explain why there are less detections than expected in this area, as the presence of either noise or an additional feature increases the detection thresh-hold.

The 'tail' spectra at 4.26 micron show the distinctive noisiness of that part of the Enceladus spectra. Sizeable dips are seen in the 4.24-4.26 micron region, with the deepest point closer to 4.24 micron. If the tails where not as noisy, the band centre could be used to determine information about the CO_2 ice's structure, Unfortunately, the data in this section is too noisy to be able to draw any definite conclusions based on these peaks apart from the likely presence of CO_2 ice.

6.2.8. NH_3

NH_3 in water ice has a number of features within the IR spectra. of these, the 2 and 2.2 micron features are the clearest within the VIMs spectra. As both these features are present within the 2 micron feature, noise end fitting errors should be a smaller factor than they would be for features in the 3.6-5 micron tail.

The detections that have been made are shown in figure 6.22. The detections are sporadic, occurring mostly in newer terrain. This is in line with expectations, as ammonia is susceptible to being snowed under by plume material, which does not contain much ammonia. As accretion of the plume material occurs mainly between 0^o to 90^o west and 180^o to 270^o degrees west[41] it is natural that no ammonia is detected in these areas. The majority of detections have been made on the trailing hemisphere.

Figure 6.23 provides 4 spectra from ammonia detections in different locations. A couple of factors of note can be seen. First of these is the 2.2 micron feature in spectra A, B and D. At first glance, the features seems oddly shaped, with part of it located below the fit, and part of it above. This is a consequence of the limitations of the fitting procedure. as the polynomial tries to fit the entire feature it uses a least–squares algorithm to minimize the residuals. This leads to the fit trying fora mid point between the two edges of the feature. The true water feature would likely follow a slightly different trajectory. The sky-blue line in spectrum A shows the expected curve of the true water feature. This tendency of the fitting procedure would be a problem if more quantitative information about the non-water ice features was sought. However, it does not obscure the feature from sight or prevent it from being picked up by the code, so of or this qualitative analysis it is not a problem.

Somewhat more worrisome is the extremely small size of the 2.2 feature in comparison with the 2 micron feature in C. and the small size of the 2.0 micron feature in A when compared with the 2.2 micron feature. The 2.2 micron feature is generally a bit smaller than the 2 micron feature as can be seen in figure 6.2[12, 42], but within the same order of magnitude. This is not the case in A, where the 2 micron feature is barely present, or at C, where the 2.2 micron feature is barely present. In the case of C, that particular combination of a large 2 micron feature and a negligible 2.2 micron feature seems characteristic for most of the detections in that part of Enceladus. This in turn suggests that that set of detections are false positives. In the case of both B and D, whoever, the two features seem to be at the right proportions, suggesting that the detections there are correct. C

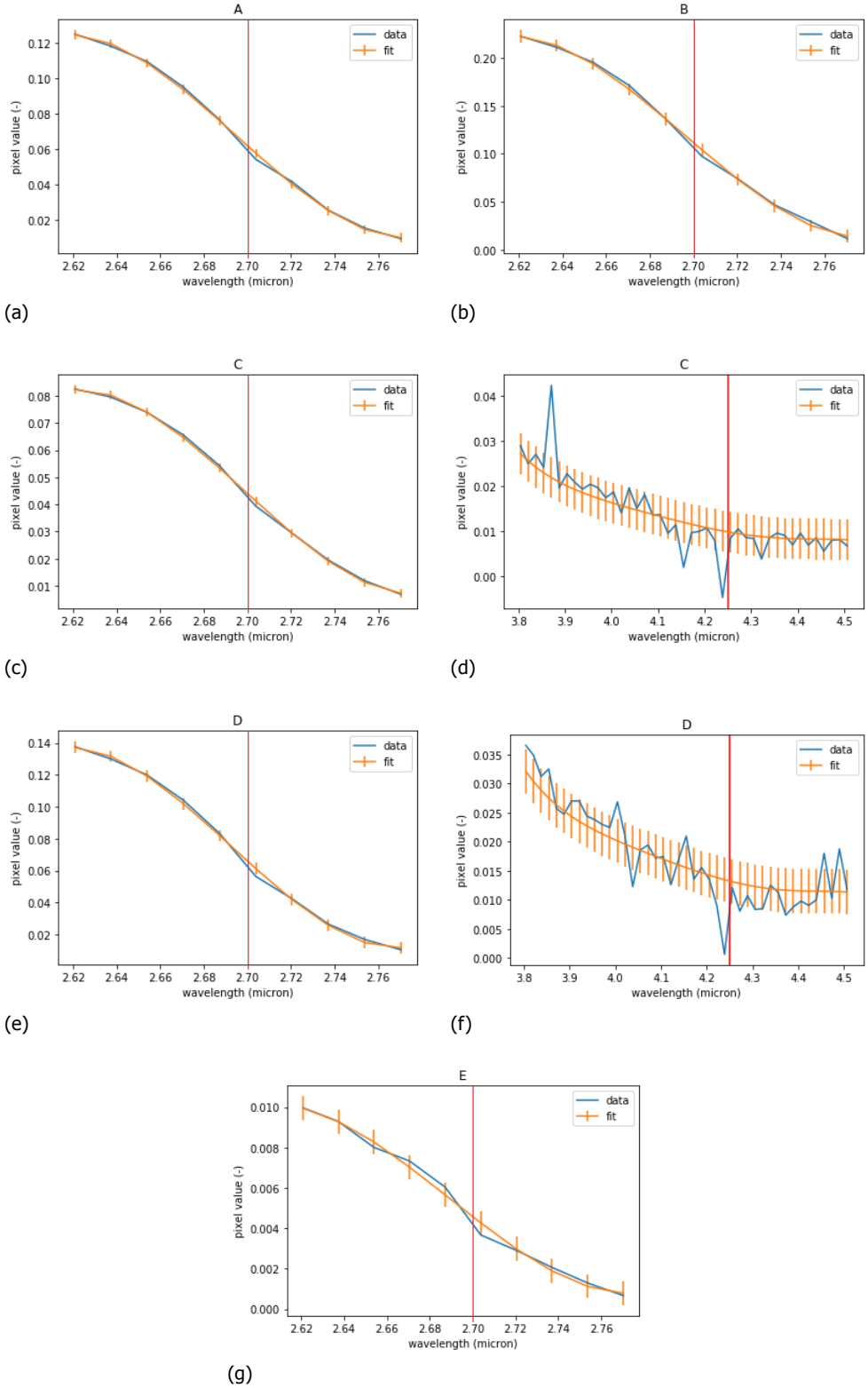

Figure 6.21: The four spectra corresponding to the locations marked in figure 6.20. The Y axis presents the instrument pixel value, which is normalized on a scale from 0 to 1 with respect to the minimum and maximum intensities possible for the instrument to measure. The orange line is the polynomial fit, while the blue line represents the data. The orange lines perpendicular on the fit represent the 3-sigma uncertainty for the 2.7 micron features, and the 1-sigma uncertainty for the 4.26 micron feature.

Figure 6.22: The green pixels indicate locations where the features of NH_3 exceeded the 3-sigma detection threshold. The letters A, B, C and D indicate areas from which spectra have been taken for further discussion. These spectra can be found in figure 6.23.

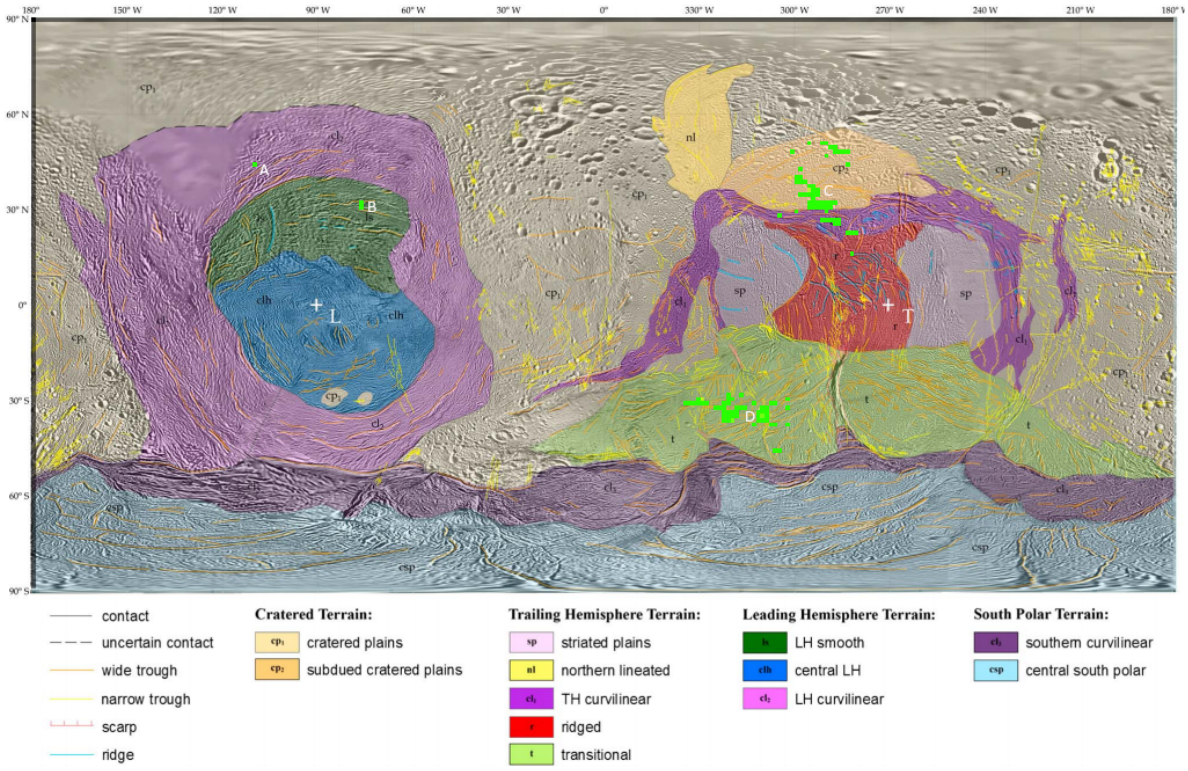

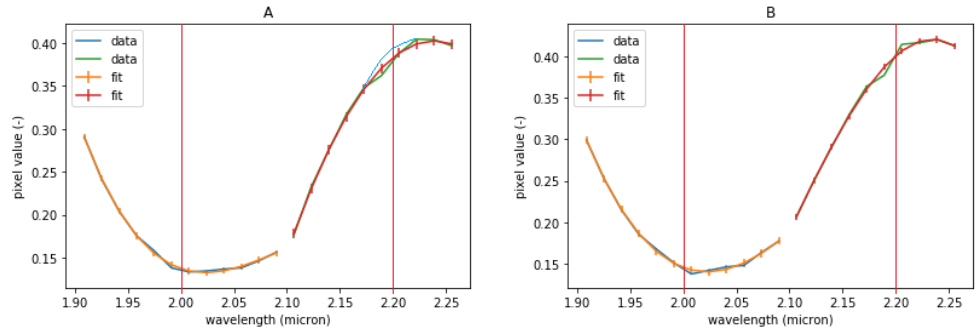

(a) (b)

(c) (d)

Figure 6.23: The four spectra corresponding to the locations marked in figure 6.22. The Y axis presents the instrument pixel value, which is normalized on a scale from 0 to 1 with respect to the minimum and maximum intensities possible for the instrument to measure. The blue and green lines represent data, while the orange and red curves are the fits. The vertical bars on the fit lines represent the 3-sigma range for detection.

7

Spectra interpretation - Crystallinity and Crystal size

The presence or absence of non-water ice species is not the only information about Enceladus' icy crust that can be extracted from the VIMS spectra. Information regarding the make-up of the water ice itself is also of interest. There are two major factors of interest regarding the morphology of water ice, being the degree of crystallinity and the crystal size.

The degree of crystallinity refers to how much of the ice is crystalline as opposed to amorphous, and can provide some clues to the circumstances under which the ice has been formed and the environment in which it exists, as factors like temperature, radiation and formation process can all influence whether ice is amorphous or crystalline. This is discussed further in section 7.1.

Crystal size, meanwhile, can provide clues towards the age of the surface. Effects like impacts by high energy particles and micro-meteoroids can cause the ice crystals on the surface to break up, so the overall crystal size gives an indication about the time period to which this surface has been exposed to these weathering effects. This characteristic is further discussed in section 7.2.

Finally, section 7.3 will discuss the craters of Enceladus and how cratered locations are visible by looking at the crystallinity and crystal size.

7.1. Crystallinity mapping

The presence of crystalline and amorphous ice can provide some insight into the way the surface of Enceladus has evolved. Crystalline and amorphous ice come into existence under different circumstances. Crystalline ice is the most stable form of ice and is formed by a gradual freezing process, while amorphous ice is generally the result of a liquid or vapour flash-freezing. Bombardment by high radiation, such as ultraviolet radiation, can cause crystalline ice to become amorphous, while amorphous ice at higher temperatures, in the order of 100-150K, will become crystalline over time as the ice settles into a crystalline configuration [43].

Because of these properties, the presence of crystalline and amorphous ice will shed some light on the processes by which the ice is formed, as well as the external circumstances to which the ices are subjected. This section will describe the crystallinity properties of Enceladus in two parts. Subsection 7.1.1 will describe the approach used to numerically determine the crystallinity of the surface based on the VIMS spectra, while the result of this method will be described in subsection 7.1.2

7.1.1. Approach

There are a number of markers in the infrared spectra of water ice that can be used to make estimates regarding how crystalline the ice is. The clearest marker is the peak at 1.65 micron which is very pronounced in crystalline ice and not present at all in amorphous ice, as shown in figure 7.1. It should be noted that this peak also tends to be less prominent when the ice is at higher temperatures. However, the temperatures on Enceladus are low enough that this peak will always be present in crystalline ice [14] [34]. This temperature dependence does mean that colder areas will show stronger features than warmer areas of the same degree of crystallinity.

Figure 7.1: This figure shows the difference between crystalline and amorphous ice at the same temperature, as well as the differences between low and high temperature crystalline ice[18]. The spectra are presented in absorption rather than the reflection seen in the VIMS spectra. The upper two spectra have been shifted upwards by 40 cm^{-1} to avoid overlap making the figure more difficult to read.

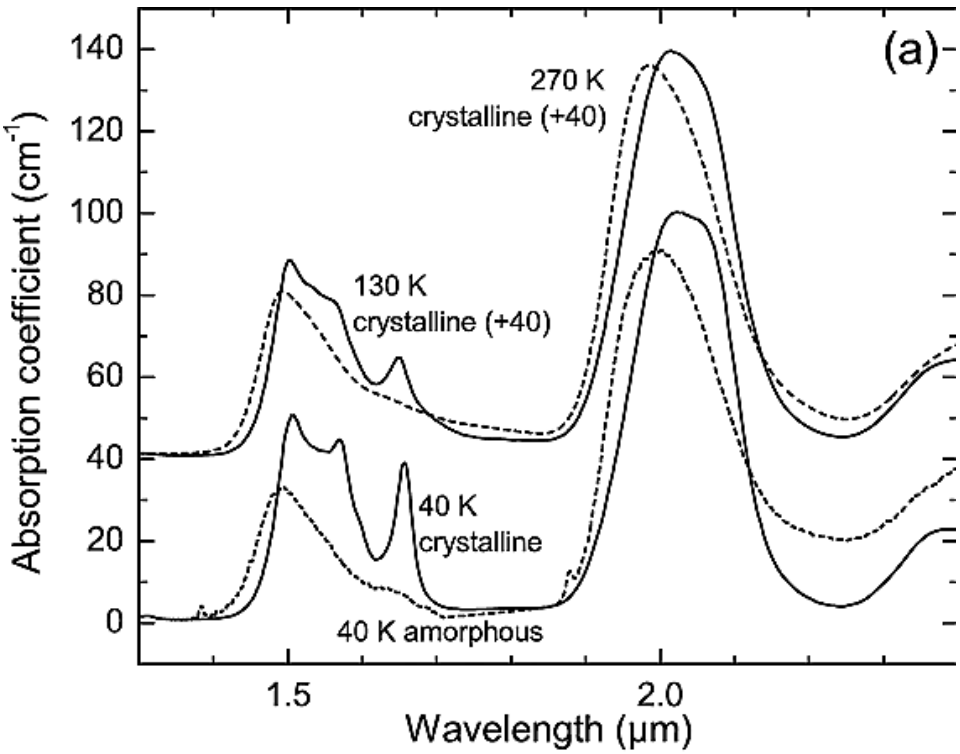

First, the spectra are read in from an ASCII-format data cube. Then the 1.2-1.8 micron region is selected, which contains the 1.65 micron peak, as well as the 1.5 micron peak. The bounds of the 1.5 and 1.65 micron features are established by finding the highest point at the edges and in the middle of this part of the spectra. These edges and the fairly constant height of the dividing peak are then used to determine the total size of the two features, as shown in figure 7.2. The area of the 1.65 micron feature is then divided by the area of the 1.5 micron feature as this feature is not affected by crystallinity. Taking a ratio, rather than looking only at the band-depth of the 1.65 micron feature allows for a fairly good comparison between different samples that might differ in other ways than just crystallinity, such as brightness or crystal size,a s such effects tend to impact both features equally. The results of this comparison can then be plotted in a heat-map format to give an idea of the relative crystallinity of different parts of Enceladus.

Figure 7.2: The green line marks the baseline from which the sizes of the 1.5 and 1.65 micron features are determined. The red area is the area of the 1.5 micron feature, while the blue are is the area of the 1.65 micron feature. The areas are computed by simply summing the differences between the data values and the height of the green line for each data-point within the two features.

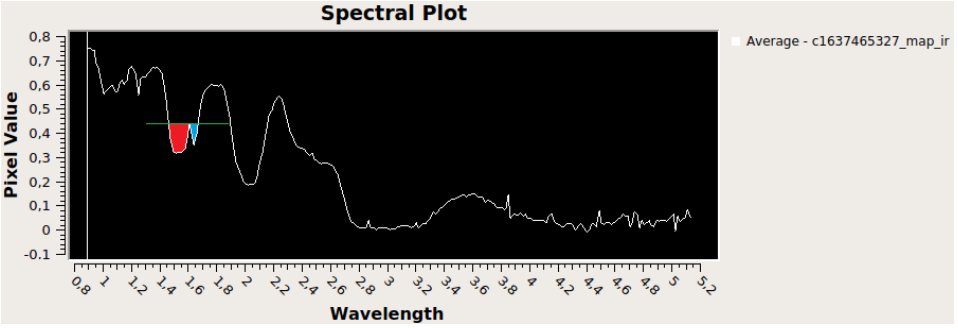

One thing to keep in mind with this approach is that it will only allow for comparison of relative crystallinity on different parts of Enceladus, rather than giving an indication of the absolute degree of crystallinity of the ice on Enceladus. For comparisons between different locations of Enceladus, this is not a problem, however.

7.1.2. Results

Figure 7.3 shows the full crystallinity map of Enceladus. There are a couple of large-scale trends that clearly stand out. Most notable is that the south-polar area is generally darker. This can most likely be attributed to the south-polar plumes. The water being ejected from these plumes would most likely flash-freeze in a way that is will result in the formation of amorphous ice, and plume material accretes fastest in the south-polar area, with areas in the 270 to 180 and 90 to 0 degrees longitude getting steadily less accretion of plume materials as you move further north on the Enceladus surface [27].

Figure 7.3: This figure shows the relative degrees of crystallinity for the IR mosaic of Enceladus. The pure black areas are areas not covered by the mosaic. The axis shows the ratio between the 1.65 and the 1.5 micron feature.

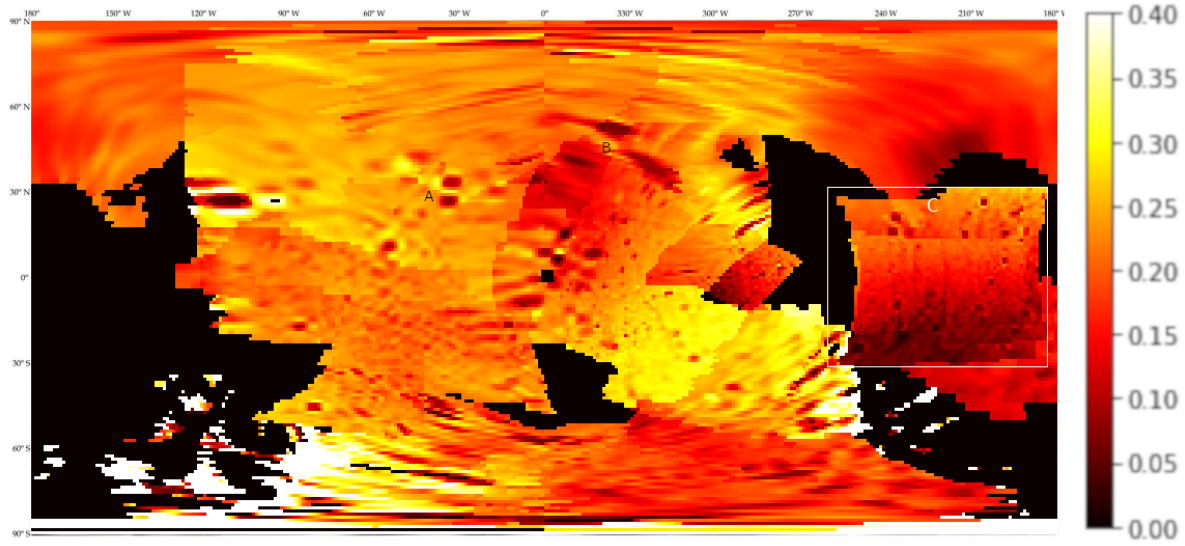

Among the other features of interest are the darker spots in the northern hemisphere, such as the pair of spots at 30^o N, 30^o W and the circle-shaped feature at approximately 60^o N, 330^o W, which are marked with an A and B respectively.. These features do no line up with any features on the full-surface visual mosaic of Enceladus, and are large and regularly shaped enough that they can not be attributed to instrument or measuring errors, to which the extremely bright area in the south pole between 150^o and 90^o W can be attributed.

There are a couple of potential explanations for these features. The first one is temperature. Those locations being at a higher temperature to their surroundings would not explain the difference in size of the 1.65 micron peak for the temperature ranges expected for Enceladus, but a consistent lower temperature could result in an area remaining more amorphous as there is not enough energy present to allow the transition to crystalline ice.

Alternatively, the amorphous ice at these locations could be impact sites of sorts. Though they do not overlap with any impact sites, they are located fairly close. Faults in the orthorectification software could result in the drift visible here. Craters having a more amorphous crater-bottom is also well within the line of expectations. The violence of the impact even would result in the ice vaporizing, but the overall cold temperature of the moon would then see the water vapor flash-freezing again, resulting in a more amorphous ice. This effect can be seen in the area indicated with a C covering 30^oN to 30^oS and 260^oW to 180^oW, where the typical shapes of craters can be seen in the heat-map which largely match up with visible craters, as can be seen in figure 7.8 further in this chapter. The bottom of the craters tend to be darker, indicating a more amorphous ice, while the rims at times seem to be slightly brighter. The slightly brighter color indicating more crystalline rims could be explained by the

crater impact causing a temporary increase in temperature in the areas surrounding it without melting or vaporizing the ice, allowing the ice to crystallize further.

7.2. Crystal size mapping

Crystal size is another factor that can shed light on the ways ice has evolved. Larger particles are indicative of active crystal growth mechanics or a continuous deposition of new surface ice, while smaller particles are indicative of older surfaces with weathering effects, such as impacts by micrometeorites and energetic particles.

This section will go into detail on determining the crystal size for different areas of Enceladus. Subsection 7.2.1 will describe the approach taken for determining the crystal size based on the spectra, while subsection 7.2.2 will describe the results of this approach.

7.2.1. Approach

There are a number of ways to estimate the crystal sizes based on the infrared spectrum of water ice. One could simulate the spectral behaviour of the ice using Mie scattering or a model like the Hapke model. Though such models could give very accurate results, they are computationally intensive if you need to create a separate model for each measurement and require a very large set of inputs.

Figure 7.4: This figure shows IR spectra for water ice for a number of different crystal sizes[9].

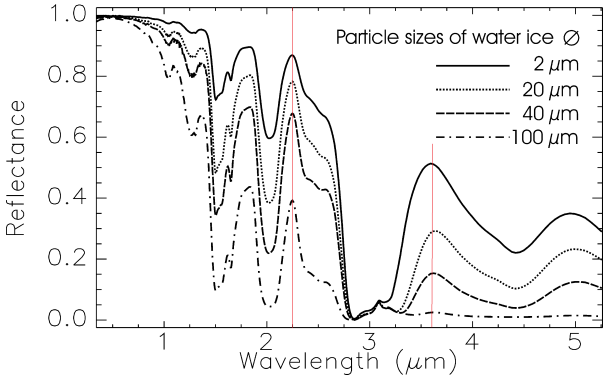

A simpler method is chosen for the present study that can be used for the purposes of comparison between different areas on Enceladus. This method is based on previously modelled data, represented in figure 7.4. This models has used optical constants for ice at temperatures below 110K and has been used for the study of Enceladus surface before by [9]. The model is used to identify some of the markers indicating crystal size and use those to determine an estimate of the crystal size in the VIMS spectra. In this case, the height of the spectra directly after the 2 micron feature and the height of the 3.6 micron reflectance peak would serve the general purpose of determining crystal size. The relative heights of the peaks in this set can be used to create an exponential relation between crystal size and the height of the 3.6 micron peak divided by the height of the post 2 micron feature plateau. These two comparison points where chosen over the comparison points used by Jaumann for two reasons. First, this method automatically scales with the spectra. To use Jaumann's method, all spectra first need to be normalized, and then the continuum for all four comparison points need to be removed to determine the individual band-depths. Secondly, the features at 1.04 and 1.25 micron have occasional noise spikes that would mean the features would have to be fitted. The 2 micron feature has the ammonia feature that could also change the measured band-depth. This would leave the 1.5 micron feature as the sole comparison point. Instead, the approach used here is less likely to be affected by non-water ice species and noise.

The exponential relation is of the shape $y = a * exp^{b*x}$, with y being the crystal size in microns, and x being the value of the 3.5 micron feature divided by the value for the post 2-micron plateau. The calculated values for a and b where 187.7 and -6.5 respectively.

As with the approach for determining crystallinity, an ASCII cube generated using ISIS is loaded into python, which then allows each individual spectra to be read in and processed to find the location and height of the post 2 micron feature plateaus and the 3.6 micron features, the ratio of which is then

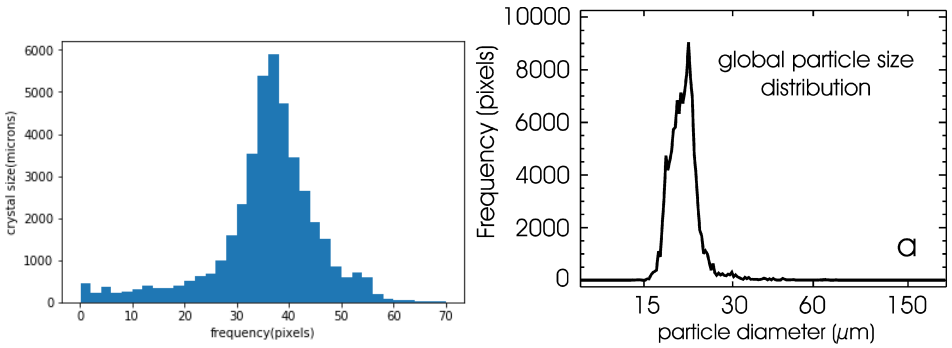

Figure 7.5: This figure shows the histogram for the size distributions of figure 7.6 on the left, and for the study done by Jaumann on the right[9].

processed to form a heat-map.

7.2.2. results

Figure 7.6 shows the results of the method described in section 7.2.1. There are a couple of things to be noted in the figure. First, the overall distribution is in line with current estimates of the crystal size, with the south polar terrain having the largest crystal size, and the older cratered terrain having a far lower crystal size. The estimate for the crystal size in the south polar areas matches that of previous research at estimates at about 75 microns as well, but the peak measurements are lower than the 105 micron from Jaumann et al.[9]. The estimate for the crystal size in the cratered terrain is higher than in other sources, with values in the 20-30 micron range as opposed to the 10 micron range. This could be due to varying temperatures skewing the accuracy of the Hapke model values used from figure 7.4, as that model has been based on a single temperature benchmark, or due to the different method used.

Another way to compare with the results from previous work is to compare the size distribution diagrams of figure 7.6 with that of previous work, as shown in figure 7.5. Distributions overall are similar, though the histogram for this study has a higher centre than that for the work by Jaumann This could, in part be explained by the larger area covered in this study, but is also an indication that the method used here might be biased towards overestimating sizes when compared to previous work. The overall shape is similar, with a single fairly narrow peak. The presence of a longer tail towards 0 micron could be explained by the inclusion of the north pole within this work, as that region is the oldest and is therefore expected to have the lowest crystal sizes, but this area was not included in the work by Jaumann et al.

The most noteworthy feature in this map is the large brighter area around the equator between 300^o and 330^o W. This area corresponds largely to a section of the trailing hemisphere curvilinear terrain, as well as a section of older cratered terrain and a largely more amorphous area as can be seen in figure 7.3. This correspondence to older terrain in particular stands out, as it goes against the established pattern of the smaller crystal sizes in the older and less active terrain. The area is one with little accretion of new surface area due to the plumes, so the higher crystal size could be the result of a past event causing crystal growth, rather than a currently ongoing process.

This region could be fairly new, though that seems unlikely given the presence of craters visible in visual images of the area. Still, the overall surface seems smoother than that of the neighbouring zone to the west, so it's not impossible. This would suggest that the area has undergone a rather large-scale resurfacing event in the not-too distant past.

It should also be noted that the large smooth area noted around 240^o W does not really stand out in terms of crystal size form its surroundings, suggesting that it is not as new as it appears to be.

7.3. Cratering

The possibility of certain markers visible within the crystallinity maps being the result of impact craters has been raised in section 7.1.2. This section will go into a bit more detail on this topic. First, to

Figure 7.6: This figure shows the crystal size on Enceladus. The crystal size scale gives the crystal diameter in micron.

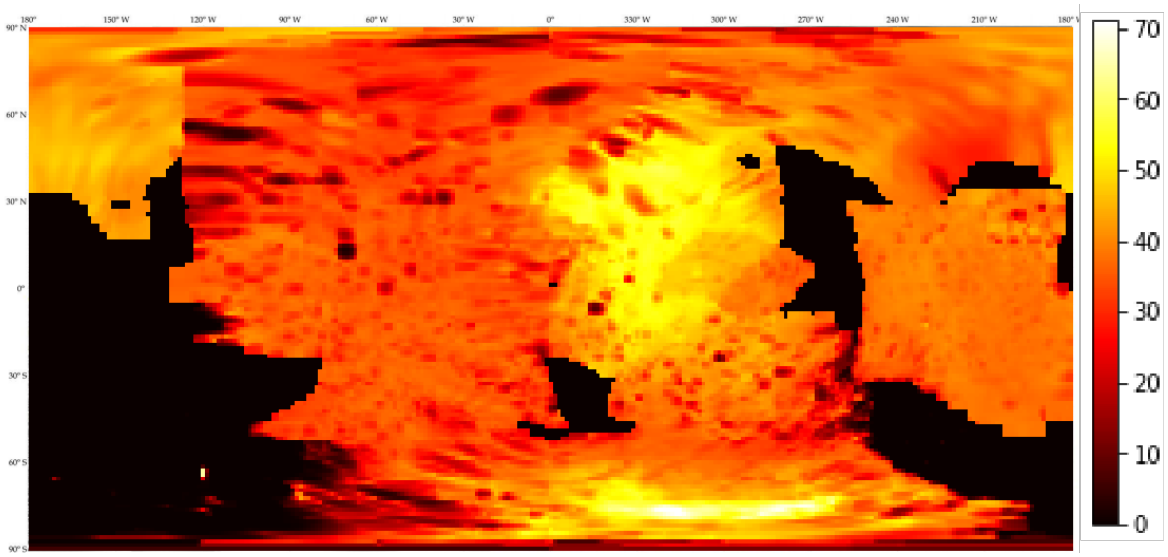

understand the measurements, some background on the crater formations process is needed.

Figure 7.7 shows the formation process for a crater on earth. The crater formation process generally consists of 3 steps. First is the impact step, where the impactor hits the surface and the initial shockwave is transmitted into the surface and starts compacting it downwards ,as shown in panels b and c. This step is followed by the excavation step, where loose materials, which first where pushed downwards and away from the impact location are now forced up and out of the crater by their velocity, as shown in panels d and e. Lastly, there's the modification stage, in which particles that did not leave the craters settle back in, and the crust that was initially compacted starts slowly rising up again, as shown in panel f.

The formation process for a crater on Enceladus would go through similar steps, though the cold and icy environment would react differently. First of all, at the pressures on Enceladus, the ice would either remain solid during the impact, or turn to water vapor, there is not enough atmospheric pressure to facilitate a liquid stage. This means that during the impact a large amount of water ice would be instantly turned to vapor. The extreme cold of the Enceladus environment would see this vapor flash-frozen back into ice shortly after. The rapid nature of this freezing would most likely result in amorphous ice. Meanwhile the solid ejecta and crater floor, while not vaporized, will still have been heated to some degree. This input of heat will result in the crystallization of the ice while the elevated temperature lasts. When the vaporized material settles back to the surface it will settle within the crater itself and on surrounding terrain, leaving the more crystalline rim visible above the amorphous ice.

The results of this process can be seen within the crystallinity, and in particular in the section shown in figure 7.8. Both the dark crater floors and lighter crater rims can be clearly distinguished.

Craters don't really stand out in the map looking at crystal size. This not too surprising, however. A recent impact even could cause a crater to stand out from its surroundings in terms of crystal size as the same influx of heat that causes the rim to increase in crystallinity could also promote crystal growth for a very short period of time. However, as time goes by crystals get worn down and get smaller, making any difference harder to spot. Recent craters could be visible when looking at crystal size in a way similar to how they appear in the crystallinity map, with a brighter rim of larger crystals and a crater floor with smaller crystals. However, no such features are apparent in figure 7.6, so the visibility of craters on Enceladus when looking at crystal size is only hypothetical based on this data.

Figure 7.7: This figure shows the crater formation process for a crater on earth[19]. A crater forming on an icy moon will go through similar steps during the formation process, though the materials involved will be different.

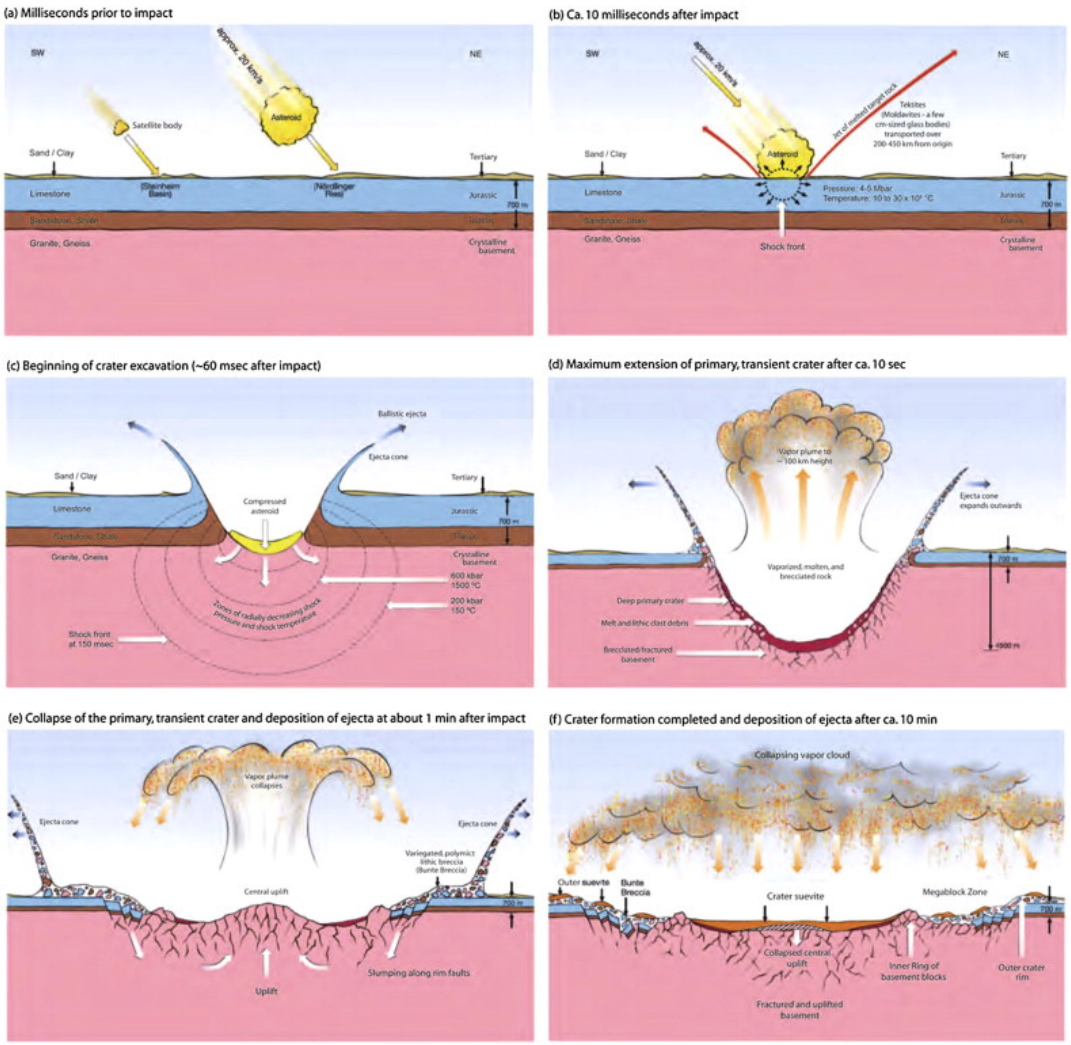

Figure 7.8: This figure shows a section of the figures 7.3 and 7.6, containing a number of craters. The middle section shows crystallinity, the right-most section shows crystal size. Note that the craters themselves tend to have rather amorphous floors, but more crystalline crater rims. In the section showing crystallinity, but do not stand out in the section showing crystal size.

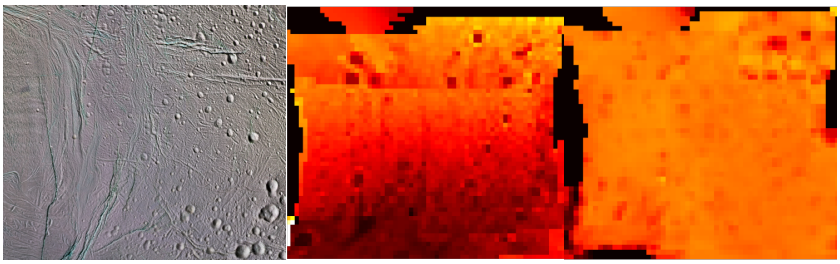

8

Synthesis

This chapter will combine the individual observations from chapters 6 and 7 to allow for more in-depth analysis and conclusions to be made by combining them. Section 8.2 will detail the relative positions of the different non-water ices, while section 8.3 will combine the crystallinity and crystal size observations with the locations of the non-water ice species.

8.1. CO_2 comparison

The availability of the paper by Combe et al.[10] allows for a comparison with the results of this study. Both the study by Combe and this research used the 2.7 and 4.26 features to identify CO_2. Combe's study used the expected shoulders of the feature and a linear continuum to validate the presence of such a feature, while in this study a larger continuum was established using a 3rd order polynomial, against which the presence or absence of a feature can be determined. This more complicated method was necesary as this study used a far smaller dataset than the study by Combe, which made noise a far larger issue. The results by Combe can be found in figure 4.6, while the results of this study can be found in figure 6.20. For this comparison, we'll mostly focus on the results for the 2.7 micron feature, as the higher noise levels in the data used by this study makes detecting the 4.27 micron feature very difficult.

In this study, most detections of CO_2 are focused on the trailing hemisphere, with more sporadic detections in the south-polar area and leading hemisphere. This stands in Sharp contrast to the study by Combe, where the strongest detections are in the south-polar area, while the band-depth across the rest of the moon is fairly uniform, with the exception of a zone of with a smaller band depth surrounding the south-pole, corresponding roughly with the southern curvilinear terrain.

The reasons for these differences are most likely the different approaches to the data. This study only used a small selection of the VIMS data, with data overlap in the mosaic generally being limited to 2-3 images at most, and generally less. The study by Combe processed a far larger data-set, which in turn helped with damping out noise effects without also affecting other parts of the data, such as resolution or general sharpness of the features, while methods like Gauss filters or averaging neighbouring pixels would affect these parameters. Likewise, the 3-sigma detection criteria which was used in this study was not used in the study by Combe et al., and likely not necessary to differentiate between real features and the result of noise in the study by Combe as noise effects had already been dealt with. That having been said, the positive detections of CO_2 by this study are not being contradicted by Combe's study, which suggests that this study's method has a risk of false negatives, but less so of false positives. This should be kept in mind when making conclusions about non-water ice species. The absence of a specie cannot conclusively be determined, but the presence of one can be made with a large degree of certainty.

8.2. Non-water ice species

There are a number of large-scale trends visible when combining the locations of the different non-water ice species, as shown in figure 8.1. The first is that Co, CO_2 and NH_3 all tend to be located in and

around the newer terrain of the leading and trailing hemispheres. Furthermore, most detections occur in and around the trailing hemisphere, though the only detections of CO are on the leading hemisphere.

Figure 8.1: This image shows the locations of the different non-water ice species. Ammonia is marked in blue, Carbon monoxide in red and carbon dioxide in green.

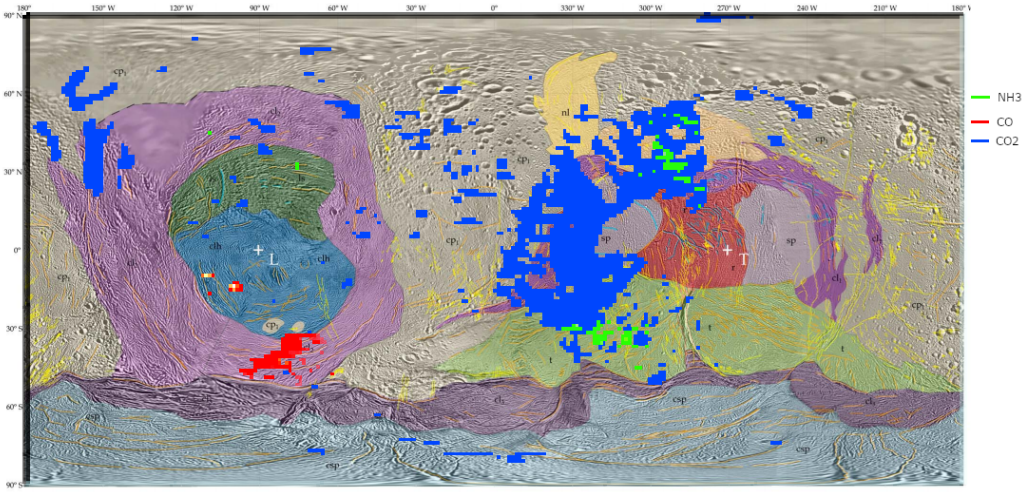

The absence of CO and NH_3 in the south-polar terrain matches what we know from the plumes, which are lacking CO and are light in NH_3[28], with the latter representing between 0.1% and 0.3% of the total plume mass. Given that the expected rate of accretion in the south-pole due to plume particles is very high, NH_3 and CO ices would get buried under the plume material that lacks these elements.

CO and NH_3 being mostly confined to newer terrain could be explained by a number of different factors. The first hypothesis would be that some factor, such as temperature or impacts by energetic particles, on the surface causes NH_3 and CO to disappear over time. The surface of Enceladus is generally at a temperature too high for pure CO ice to remain at the surface [44], but it could be trapped in smaller pockets within the water ice. Periods of higher temperature could result in the disappearance of these pockets, resulting in the CO sublimating into space. The presence of a warmer period in the past is suggested by the craters on Enceladus, all of which show a large degree of relaxation which is only possible if there had been a warmer period in Enceladus past [45].

Unlike CO, NH_3 should not be at risk of sublimating from the surface of Enceladus, yet it is still confined mostly to newer terrain. One possibility is that the effects of radiation causes NH_3 to be turned to N_2 and hydrogen [46]. This would explain why NH_3 is contained mostly to newer areas, as Nh_3 would disappear from older regions over time.

8.3. Crystallinity and crystal size

In this section the correlation between the location of the non-water ice features and the crystallinity and crystal size of the ice is discussed. Section 8.3.2 goes into detail on the correlation between crystallinity and the non-water ice species, while section 8.3.3 details the correlation between crystal size and the non-water ice species.

8.3.1. Crystallinity and crystal size

Figures 8.3 and 8.4 show the maps created for the crystal size and crystallinity of the Enceladus ice. There are a number of areas of interest on these maps, but for comparison the areas that are particularly noteworthy are those where the two maps show different structures. The degree of crystallinity and crystal growth are both linked to the input of heat, while bombardment by energetic particles can cause crystalline ice to become amorphous, and causes crystals to break apart. Because of this, old surface areas would be expected to have low crystal sizes and more amorphous ice, which are indicated by dark colors in figures 8.3 and 8.4, whereas newer areas are expected to have larger crystal sizes and more crystalline ice, indicated by lighter colors in the figures.

There are several areas that break this mold. One area that stands out is the large zone of higher crystal size in the south pole that is located in a fairly amorphous region, shown in figure 8.2. The south pole itself is considered very active area, with the relatively thin ice causing the temperature to be higher than in other areas of Enceladus, and the plumes contributing to a continual resurfacing. It is this combination of higher temperature and continual resurfacing that most likely leads to this combination of features. The higher temperature facilitates crystal growth, while the resurfacing process occurs by the accretion of flash-frozen plume material, which is amorphous in nature.

Figure 8.2: This image shows the crystallinity and crystal size for the area of high crystal size at the south pole.

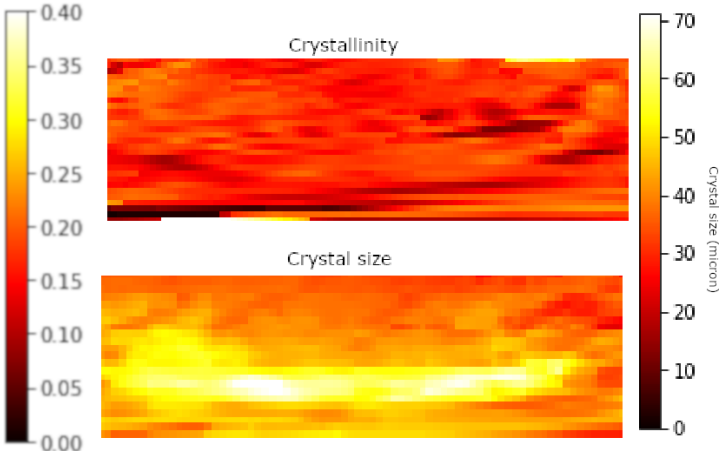

Figure 8.3: This figure shows the crystal size on Enceladus. The crystal size scale gives the crystal diameter in micron.

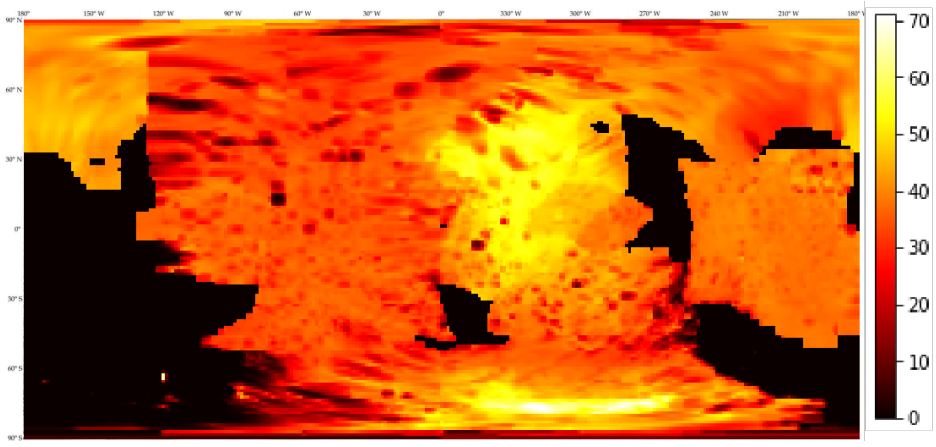

Another area that stands out is the area of higher crystal size but low or average crystallinity in the centre of the maps, shown in figure 8.5. The mix of circumstances is similar to that found at the south pole, but there should not be a high-temperature spot on Enceladus in that area, nor is there any evidence of accretion of plume material at the rate found on the south pole, as shown in figure 4.2 back in chapter 4. Despite this, the crystal size suggests that this must be a stretch of fairly young terrain. One possible explanation would be that that is a stretch of terrain that has only recently been exposed to the surface, but that raises further questions relating to the cause of such a change.

Last of all, there is the the cratered area at the right edge of the image. In the crystallinity map, the craters are neatly outlined. The map for crystal size shows that area to be far more uniform, and though there are lighter and darker spots, they do not neatly align with the craters visible in the crystallinity map. This is something that could be explained by the age of the craters. The amorphous crater floors would most likely not become less amorphous, while over time the crystallinity in the crater rim is reduced and the overall crystal sizes become roughly equal.

Figure 8.4: This figure shows the relative degrees of crystallinity for the IR mosaic of Enceladus. The pure black areas are areas not covered by the mosaic. The axis shows the ratio between the 1.65 and the 1.5 micron feature.

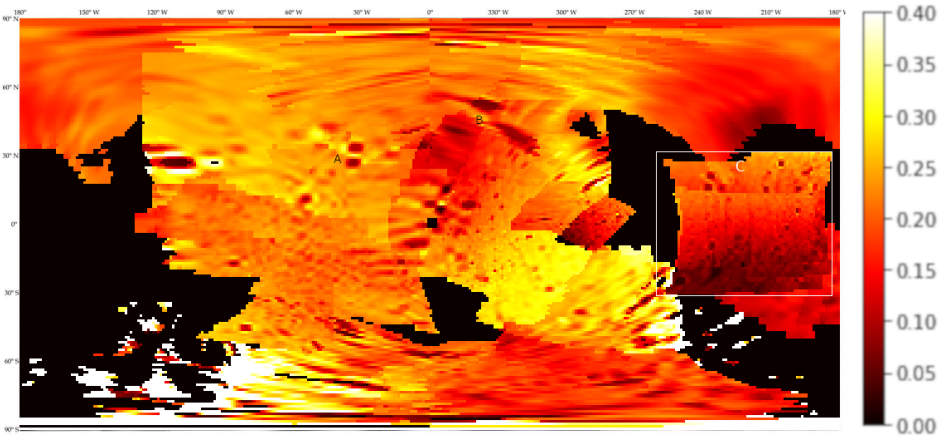

Figure 8.5: This image shows the crystallinity and crystal size for the area of high crystal size in the centre of the mosaic.

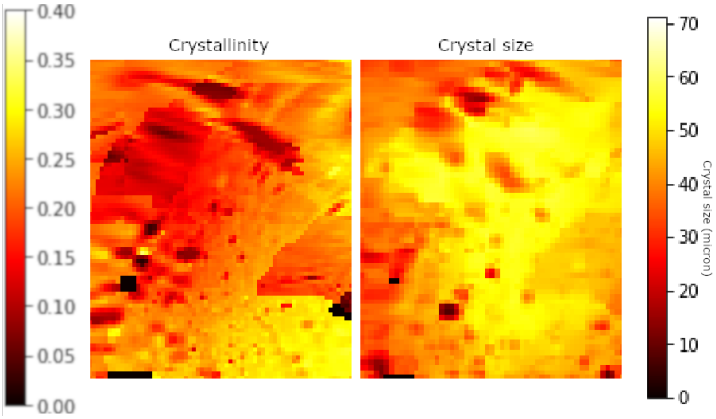

8.3.2. Crystallinity and non-water ice species

Figure 8.6 shows the locations of the different non-water ice species overlaid on the crystallinity map of Enceladus. Overall, there doesn't seem to be a direct correlation between crystallinity and CO. There seems to be some correlation between the locations of Ammonia and the more amorphous stripes at 280 west, 25 N. Given that NH_3 does not seem to specifically occur at lower or higher degrees of crystallinity in other locations, there is little evidence that the correlation is more than a coincidence.

CO_2 is spread out enough that no immediate correlation is in evidence. The detections in the south-polar area are near dark features which could be indicative of build-ups of newly accreted plume material. As the plume material would have some amount of CO_2 in them[47] it might cause these areas to be richer in CO_2 than other areas in the south.

8.3.3. Crystal size and non-water ice species

As in section 8.3.2, figure 8.7 does not clearly show a relations between crystal size and the presence of CO. There does seem to be some correlation between areas with lower crystal size and NH_3, particularly at the patches of NH_3 centered at 315 W, 15S. As these areas do not stand out in terms of crystallinity, it could be indicative of terrain that is older than usual in that area of Enceladus, suggesting that, for example, there hasn't been a recent accretion of new plume material.

CO_2 does show some relation to crystallinity, though not in a consistent way. There is a large detection of CO_2 in the bright central area, but in many other locations CO_2 conforms to areas of smaller crystal size. The presence of CO_2 in areas with smaller crystal size could be linked to CO_2 originating from the plumes, with newly accreted plume material consisting of very small crystals given the nature of the plumes. Temperature can cause these crystals to grow, which is why, despite having

Figure 8.6: This image shows the locations of the different non-water ice species with respect to the crystallinity. Ammonia is marked in blue, Carbon monoxide in red and carbon dioxide in green, while the degree of crystallinity is in gray-scale, with higher crystallinity resulting in brighter areas.

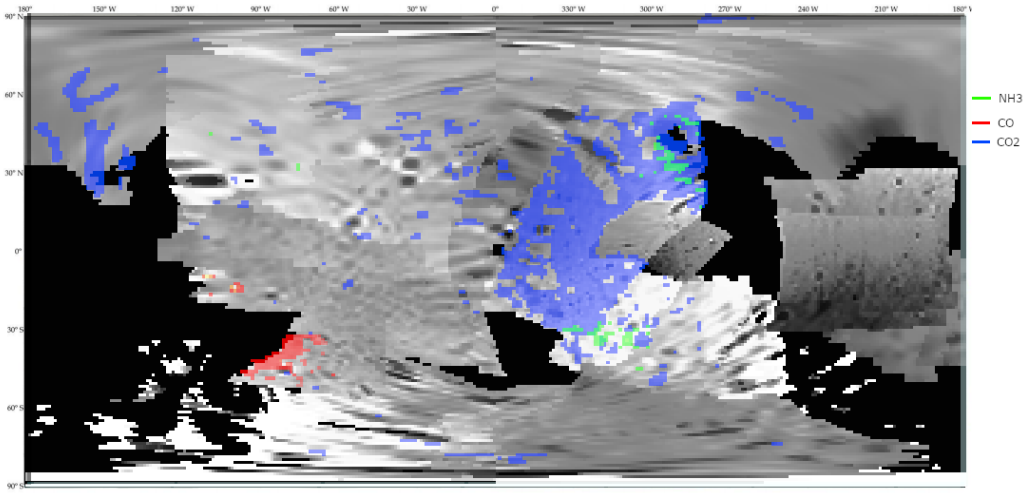

the highest rate of accreation from the plumes, the south pole tends to have high crystal sizes as it is one of the warmest area's on Enceladus.

Figure 8.7: This image shows the locations of the different non-water ice species with respect to the crystal size. Ammonia is marked in blue, Carbon monoxide in red and carbon dioxide in green, while the crystal size is in gray-scale, with larger crystals resulting in brighter areas.

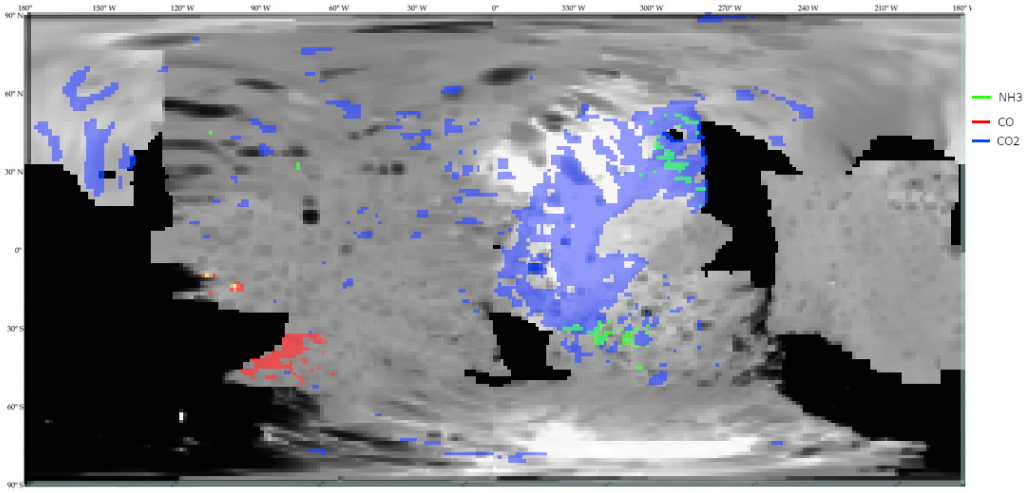

The detection of CO_2 in the bright zone adds to the peculiarity of that zone, as it goes against the expected locations for CO_2. The terrain itself is an unusually smooth zone just to the north of and surrounded by more textured terrain, so this could be very new terrain, with the presence of CO_2 ice being either due to a very recent deposit, or the peculiarities of the resurfacing process.

9

conclusion

This report covered research on the icy crust of Enceladus, focusing on two separate areas, being the presence of non-water ice species within the ice and the characterization of the water ice itself. The exact results of these approaches are detailed in chapters 6, 7 and 8. This chapter will summarize the conclusions drawn from these results, and present suggestions for further research based on the findings of this report.

On the topic of the presence of non-water ice species, previous research using VIMS data had found traces of CO and CO_2. Traces of these same elements have been found during the course of this study as well though CO_2 detections were less wide-spread, suggesting that the method in this study is prone to false negatives. The comparison with past studies does not show false positives, which suggests that the method is not prone to making detections where none should be made.

The same general pattern of crystallinity was observed as has been recorded in previous studies, with lower crystallinity in the south pole and the areas most affected by plume accretion, and higher crystallinity in other areas. Water ice tends to be amorphous if it is the result of gas or liquid-phase water flash-freezing, while slower freezing processes or increased temperatures after the freezing process allow for ice to become crystalline. This is why areas under a constant influx of new materials from the plumes tend to be more amorphous,as the plume materials are subjected to a flash-freezing process.

For crystal sizes, the opposite pattern, with high crystal sizes around the south pole and lower crystal sizes in the older cratered terrain was observed. Crystal sizes tend to increase in areas of higher temperature, while a bombardment by energetic particles will cause crystal sizes to decrease. Because of this, areas with higher temperature, such as the south pole, are expected to have higher crystal sizes than areas with lower temperatures.

When mapping the crystal sizes, one area with high crystal sizes around the equator stood out, as can be seen in figure 7.3. Crystal size is generally considered to be linked to terrain age, but part of this area has been classified as being part of the cratered terrain, which is generally considered to be among the oldest terrain on Enceladus. Visual inspection of a visual spectrum mosaic of Enceladus suggests that the terrain does look smoother than the surrounding areas, suggesting that the high crystal size area might be newer than previously thought, or alternatively some other effect is at play resulting in crystal growth in excess of crystal decline due to to weathering effects.

The degree to which craters stand out in some of the higher resolution VIMS images when observing crystal size is also noteworthy. Though these results are explained by the crater formation process, the clarity with which the rim and floor can be distinguished is remarkable, and could indicate a possible method for finding craters without having to rely on visual inspection.

In addition to the area with high crystal size and distinctive crates, one last thing of note have been discovered regarding the non-water ice species. First of all, some traces of NH_3 ice have been discovered on the Enceladus surface. Presence of ammonia had been previously theorized based on observations with earth-based IR telescopes, but none had been found in an initial survey of VIMS images, which focused mostly on the southern hemisphere. The traces of Ammonia are mostly in the more northern terrain, which has been studied less than the southern hemisphere.

So, to summarize; this study has found traces of both CO and CO_2, which had been detected on Enceladus before. The overall pattern of crystallinity and crystal size matches those that have

been found in previous studies as well. In addition to these, NH_3 has been detected, which had been theorized to be present based on measurements with earth-based IR telescopes, but had not been detected before using VIMS measurements. A previously unknown area of higher crystal size suggesting a rather young region has also been found. Finally, a number of craters where remarkably visible when observing their crystallinity.

The major target for further research is the area of high crystal-size around the equator. Its presence is rather unexpected and could be indicative of a recent resurfacing event or even previously unknown activity below the surface of this area. Combining more measurements and data from different instrument on Cassini, such as the CIRS IR spectrometer to gain a better understanding of local surface temperatures or the higher resolution cameras to better characterize the geological features of the area.

In addition, a more refined dataset could be used to further confirm and expand on the detections of ammonia and carbon monoxide. This would allow for more in-depth analysis of the reasons why ammonia is present in some locations on Enceladus, and not in others, while CO is interesting in that it can only remain on the surface in certain mixtures with water ice, as pure CO would evaporate.

Bibliography

[1] NASA, *Cassini trajectory,* (2019).

[2] J. R. Spencer, A. Barr Mlinar, L. Esposito, P. Helfenstein, A. Ingersoll, R. Jaumann, C. P. McKay, F. Nimmo, and J. Waite, *Enceladus: An active cryovolcanic satellite,* (2009) pp. 683–724.

[3] R. H. Brown, K. H. Baines, G. Bellucci, J.-P. Bibring, B. J. Buratti, F. Capaccioni, P. Cerroni, R. N. Clark, A. Coradini, D. P. Cruikshank, *et al.*, *The cassini visual and infrared mapping spectrometer (vims) investigation,* Space Science Reviews **115**, 111 (2004).

[4] C. A. Nixon, M. S. Kaelberer, N. Gorius, and T. C. I. Team, *User Guide to the PDS Dataset for the Cassini Composite Infrared Spectrometer (CIRS)*, NASA Goddard Flight center (2012).

[5] D. E. Jennings, F. Flasar, V. Kunde, C. Nixon, M. Segura, P. Romani, N. Gorius, S. Albright, J. Brasunas, R. Carlson, *et al.*, *Composite infrared spectrometer (cirs) on cassini,* Applied optics **56**, 5274 (2017).

[6] K. Lewicka, P. Siemion, and P. Kurcok, *Chemical modifications of starch: Microwave effect,* International Journal of Polymer Science **2015**, 1 (2015).

[7] E. N. Crow-Willard and R. T. Pappalardo, *Structural mapping of enceladus and implications for formation of tectonized regions,* Journal of Geophysical Research: Planets (2015).

[8] R. Mastrapa, M. Bernstein, S. Sandford, T. Roush, D. Cruikshank, and C. Dalle Ore, *Optical constants of amorphous and crystalline h2o-ice in the near infrared from 1.1 to 2.6 μm,* Icarus **197**, 307 (2008).

[9] R. Jaumann, K. Stephan, G. Hansen, R. Clark, B. Buratti, R. H. Brown, K. Baines, S. Newman, G. Bellucci, G. Filacchione, *et al.*, *Distribution of icy particles across enceladus' surface as derived from cassini-vims measurements,* Icarus **193**, 407 (2008).

[10] J.-P. Combe, T. B. McCord, D. L. Matson, T. V. Johnson, A. G. Davies, F. Scipioni, and F. Tosi, *Nature, distribution and origin of co2 on enceladus,* Icarus **317**, 491 (2019).

[11] H. Fraser and E. Van Dishoeck, *Surfreside: a novel experiment to study surface chemistry under interstellar and protostellar conditions,* Advances in Space Research **33**, 14 (2004).

[12] M. H. Moore, R. Ferrante, R. Hudson, and J. Stone, *Ammonia–water ice laboratory studies relevant to outer solar system surfaces,* Icarus **190**, 260 (2007).

[13] M. P. Bernstein, D. P. Cruikshank, and S. A. Sandford, *Near-infrared laboratory spectra of solid h2o/co2 and ch3oh/co2 ice mixtures,* Icarus **179**, 527 (2005).

[14] W. Grundy and B. Schmitt, *The temperature-dependent near-infrared absorption spectrum of hexagonal h2o ice,* Journal of Geophysical Research: Planets **103**, 25809 (1998).

[15] M. Ciarniello, F. Capaccioni, G. Filacchione, R. Clark, D. Cruikshank, P. Cerroni, A. Coradini, R. H. Brown, B. Buratti, F. Tosi, *et al.*, *Hapke modeling of rhea surface properties through cassini-vims spectra,* Icarus **214**, 541 (2011).

[16] P. A. Gerakines, W. Schutte, J. Greenberg, and E. F. van Dishoeck, *The infrared band strengths of h2o, co and co2 in laboratory simulations of astrophysical ice mixtures,* arXiv preprint astro-ph/9409076 (1994).

[17] R. B. Singer, *Near-infrared spectral reflectance of mineral mixtures: Systematic combinations of pyroxenes, olivine, and iron oxides,* Journal of Geophysical Research: Solid Earth **86**, 7967 (1981).

[18] G. B. Hansen and T. B. McCord, *Amorphous and crystalline ice on the galilean satellites: A balance between thermal and radiolytic processes,* Journal of Geophysical Research: Planets **109** (2004).

[19] W. U. Reimold and C. Koeberl, *Impact structures in africa: A review,* Journal of African Earth Sciences **93**, 57 (2014).

[20] D. L. MATSON, L. J. SPILKER, and J.-P. LEBRETON, *The cassini/huygens mission to the saturnian system,* Space Science Reviews (2002).

[21] ESA, *Cassini-huygens mission objectives,* (2019).

[22] F. Postberg, N. Khawaja, B. Abel, G. Choblet, C. R. Glein, M. S. Gudipati, B. L. Henderson, H.-W. Hsu, S. Kempf, F. Klenner, *et al.*, *Macromolecular organic compounds from the depths of enceladus,* Nature **558**, 564 (2018).

[23] e. a. Roger N. Clark, *The VIMS Wavelength and Radiometric Calibration 19, Final Report*, Tech. Rep. (NASA Planetary Data System, 2018).

[24] B. H. Stuart, *INFRARED SPECTROSCOPY: FUNDAMENTALS AND APPLICATIONS*, Analytical Techniques in the Sciences (John Wiley & Sons, ltd., 2004).

[25] G. W. Patterson, S. A. Kattenhorn, P. Helfenstein, and R. T. P. Geoffrey C. Collins, *Enceladus and the icy moons of saturn,* (University of Arizona, 2018) Chap. The Geology of enceladus.

[26] F. Spahn, J. Schmidt, N. Albers, M. Hörning, M. Makuch, M. Seiß, S. Kempf, R. Srama, V. Dikarev, S. Helfert, *et al.*, *Cassini dust measurements at enceladus and implications for the origin of the e ring,* Science **311**, 1416 (2006).

[27] S. kempf, U. Beckmann, and J. Schmidt, *How the enceladus dust plume feeds saturn's e ring,* Icarus (2010).

[28] W. B. McKinnon, J. I. Lunine, O. Mousis, J. H. Waite, and M. Y. Zolotov, *Enceladus and the icy moons of saturn,* (University of Arizona, 2018) Chap. The mysterious Origin of Enceladus: A Compositional Perspective.

[29] S. F. Newman, *Photometric and Spectral Analysis of the Distribution of Crystalline and Amorphous Ices on Enceladus as Seen by Cassini*, Ph.D. thesis, Massachusetts institute of Technology (2006).

[30] M. P. Bernstein, D. P. Cruikshank, and S. A. Sandford, *Near-infrared spectra of laboratory h2o–ch4 ice mixtures,* Icarus **181**, 302 (2006).

[31] F. Scipioni, P. Schenk, F. Tosi, E. D'Aversa, R. Clark, J.-P. Combe, and C. D. Ore, *Deciphering sub-micron ice particles on enceladus surface,* Elsevier (2017).

[32] J. Salmon and R. M. Canup, *Accretion of saturn's inner mid-sized moons from a massive primordial ice ring,* The Astrophysical Journal **836**, 109 (2017).

[33] R. Hyodo, S. Charnoz, K. Ohtsuki, and H. Genda, *Ring formation around giant planets by tidal disruption of a single passing large kuiper belt object,* Icarus **282**, 195 (2017).

[34] J. Spencer, J. Pearl, M. Segura, F. Flasar, A. Mamoutkine, P. Romani, B. Buratti, A. Hendrix, L. Spilker, and R. Lopes, *Cassini encounters enceladus: Background and the discovery of a south polar hot spot,* science **311**, 1401 (2006).

[35] B. Hapke, *Theory of reflectance and emittance spectroscopy* (Cambridge university press, 2012).

[36] T. H. Burbine, P. C. Buchanan, T. Dolkar, and R. P. Binzel, *Pyroxene mineralogies of near-earth vestoids,* Meteoritics & planetary science **44**, 1331 (2009).

[37] T. B. McCord, R. N. Clark, B. R. Hawke, L. A. McFadden, P. Owensby, C. M. Pieters, and J. B. Adams, *Moon: Near-infrared spectral reflectance, a first good look,* Journal of Geophysical Research: Solid Earth **86**, 10883 (1981).

[38] R. N. Clark, *A large-scale interactive one-dimensional array processing system,* Publications of the Astronomical Society of the Pacific **92**, 221 (1980).

[39] M. A. Craig, *Reflectance and Emission Spectroscopy: Curve Fitting Methods with Application to Impact Glasses and the Varying Grain Size of Planetary Analogue Minerals*, Ph.D. thesis, The University of Western Ontario (2016).

[40] J. H. Waite, M. R. Combi, W.-H. Ip, T. E. Cravens, R. L. McNutt, W. Kasprzak, R. Yelle, J. Luhmann, H. Niemann, D. Gell, *et al.*, *Cassini ion and neutral mass spectrometer: Enceladus plume composition and structure,* science **311**, 1419 (2006).

[41] S. Kempf, U. Beckmann, and J. Schmidt, *How the enceladus dust plume feeds saturn's e ring,* Icarus **206**, 446 (2010).

[42] P. A. Gerakines, J. Bray, A. Davis, and C. Richey, *The strengths of near-infrared absorption features relevant to interstellar and planetary ices,* The Astrophysical Journal **620**, 1140 (2005).

[43] P. Jenniskens, D. Blake, and A. Kouchi, *Amorphous water ice,* in *Solar System Ices* (Springer, 1998) pp. 139–155.

[44] H. J. Fraser, M. P. Collings, J. W. Dever, and M. R. McCoustra, *Using laboratory studies of co–h 2 o ices to understand the non-detection of a 2152 cm- 1 (4.647 μ m) band in the spectra of interstellar ices,* Monthly Notices of the Royal Astronomical Society **353**, 59 (2004).

[45] M. T. Bland, K. N. Singer, W. B. McKinnon, and P. M. Schenk, *Enceladus' extreme heat flux as revealed by its relaxed craters,* Geophysical Research Letters **39** (2012).

[46] R. Baragiola, M. Fama, M. Loeffler, U. Raut, and J. Shi, *Radiation effects in ice: New results,* Nuclear Instruments and Methods in Physics Research Section B: Beam Interactions with Materials and Atoms **266**, 3057 (2008).

[47] F. Postberg, R. N. Clark, C. J. Hansen, A. J. Coates, C. D. Ore, F. Scipioni, M. M. Hedman, and J. H. Waite, *Plume and surface composition of enceladus,* Enceladus and the Icy Moons of Saturn , 129 (2018).